PB-215 407

A MATHEMATICAL MODEL FOR PREDICTION OF CONCENTRATION-TIME PROFILES FOR DESIGN OF FLUID-BED ADSORBERS

Thomas M. Keinath, et al

Michigan University
Ann Arbor, Michigan

April 1968

DISTRIBUTED BY:

NTIS
National Technical Information Service
U. S. DEPARTMENT OF COMMERCE
5285 Port Royal Road, Springfield Va. 22151

WP-00706

PB 215 407
T-68-2

THE UNIVERSITY OF MICHIGAN

DEPARTMENT OF CIVIL ENGINEERING
Division of Sanitary and Water Resources Engineering

A Mathematical Model for Prediction of Concentration-Time Profiles for Design of Fluid-Bed Adsorbers

THOMAS M. KEINATH

and

WALTER J. WEBER, JR.

LIBRARY
FWPCA, Ohio Basin Region
4676 Columbia Pkwy. Cinti. O. 45226

Reproduced by
NATIONAL TECHNICAL
INFORMATION SERVICE
U S Department of Commerce
Springfield VA 22151

April 1968
Technical Publication
Research Project WP-00706
Federal Water Pollution Control Administration
United States Department of Interior

OFFICE OF RESEARCH ADMINISTRATION · ANN ARBOR

THE UNIVERSITY OF MICHIGAN
DEPARTMENT OF CIVIL ENGINEERING

A Mathematical Model for Prediction Of Concentration-Time Profiles For Design of Fluid-Bed Adsorbers

Thomas M. Keinath
and
Walter J. Weber, Jr.

Federal Water Pollution Control Administration
United States Department of Interior
Grant No. WP-00706
Washington, D.C.

TABLE OF CONTENTS

Page

ACKNOWLEDGMENTS ii

LIST OF TABLES vi

LIST OF ILLUSTRATIONS vii

NOMENCLATURE xi

I. INTRODUCTION 1

II. EXPERIMENTAL FACILITIES AND PROCEDURES OF INVESTIGATION. 9

Active Carbon. 9

Solute and Analytical Technique. 10

Batch System Experiments 15

Adsorption Isotherms 15

Non-Flow Kinetic Studies 16

Continuous Up-Flow Apparatus 17

Adsorption Columns 17

Automatic Rate Mechanism 18

Solution Feed Module 22

Composite Sampling System 23

III. THEORETICAL DEVELOPMENT 25

Material-Balance Relationships 30

Method of Second-Order Kinetics. 34

Mechanism and Rate of Molecular Transfer. . 45

Surface Reaction 45

External Diffusion 46

Preceding page blank

TABLE OF CONTENTS (continued)

Page

Internal Diffusion. 48

Fluid-Phase Pore Diffusion. . . . 49

Solid-Phase Pore-Surface Diffusion . 53

Combined External and Internal Diffusion 56

IV. HYDRODYNAMICS OF FLUID-PARTICLE SYSTEMS . . 59

General Considerations. 59

Single Particle Hydrodynamics 64

Drag Coefficient of a Sphere 68

Effect of Particle Shape on Drag Coefficient 71

Standard Drag Curve for a Sphere. . 72

Hydrodynamics of a Mutiparticle Fluidized-Bed System 75

Pressure Drop Analysis 76

Drag Force Analysis 79

V. MASS TRANSFER RELATIONSHIPS FOR SOLUTION OF THE BREAKTHROUGH EQUATIONS 95

Adsorption Equilibria 96

Adsorption Kinetics. 101

Film Diffusion Coefficients. 101

Pore Diffusion Coefficients. 111

VI. NUMERICAL PREDICTION OF CONCENTRATION-TIME PROFILES AND EXPERIMENTAL RESULTS 121

TABLE OF CONTENTS (continued)

Page

Correlation of Experiment Results and Calculated Curves 121

Flow Rate as a Variable 122

Particle Size as a Variable. 131

Effect of Expanded Bed Depth 138

Solute Concentration as a Variable . . 145

Reversibility 151

VII. SUMMARY AND PROJECTIONS. 154

LIST OF REFERENCES 163

LIST OF TABLES

Table	Title	Page
4-1	Hydrodynamic Properties For Calculation of Superficial Fluid/Terminal Particle Velocity Ratios.	82
4-2	Hydrodynamic Properties For Calculation of the Voidage Function.	90
5-1	Mass Transfer Parameters For Correlation of Film Diffusion Coefficients.	106
5-2	Physico-Chemical Properties of the Experimental Fluid-Bed Systems.	118

LIST OF ILLUSTRATIONS

Figure	Title	Page
2-1	Adsorption Spectrum for 2-sec-butyl-4,6-dinitrophenol.	13
2-2	Calibration Curve for 2-sec-butyl-4,6-dinitrophenol.	14
2-3	Schematic Diagram of Experimental Fluidized-Bed Apparatus.	19
2-4	Schematic Diagram of Flow Rate Control Module.	20
3-1	Diffusion Paths Within an Adsorbent Particle.	26
3-2	Basic Types of Possible Adsorption Isotherms.	29
3-3	Differential Volume Element for Fluidized Bed of Adsorbent.	31
3-4	Differential Spherical Shell of Adsorbent Particle.	50
4-1	Pressure-Drop/Flow Diagram for Typical Fluidization.	62
4-2	Flow Streamlines Surrounding a Submerged Sphere.	66
4-3	Drag Coefficients for Spheres Moving Relative to a Fluid.	73
4-4	Correlation of Void Ratio with Superficial Fluid/Terminal Particle Velocity Ratio.	84
4-5	Correlation of Voidage Function, $f(\epsilon)$, with Void Ratio, ϵ.	91
5-1	Isotherm for Adsorption of dinitro-o-sec-butyl phenol on Coal-Base Active Carbon.	97

LIST OF ILLUSTRATIONS (continued)

Figure	Title	Page
5-2	Correlation of the Mass Transfer Factor, j_d, with the Ratio of the Modified Reynolds Number to the Galileo Number.	104
5-3	Relationship Between α, the Pre-Exponential Coefficient for the j_d-Factor Correlation, and Expanded Bed Depth.	109
5-4	The Dependence of Mass-Transfer Rates for Pore Diffusion on the Mean Particle Diameter, d_p, of the Adsorbent.	113
5-5	Relationship Between Batch System Rates of Uptake and Initial Concentration of Solute.	115
6-1	Concentration- and Uptake-Time Profiles for a Flow Rate of 2 GPM/SQ.FT. in a 250-gram Fluid-Bed of 0.711-mm Carbon.	123
6-2	Concentration- and Uptake-Time Profiles for a Flow Rate of 4 GPM/SQ.FT. in a 250-gram Fluid-Bed of 0.711-mm Carbon.	124
6-3	Concentration- and Uptake-Time Profiles for a Flow Rate of 6 GPM/SQ.FT. in a 250-gram Fluid-Bed of 0.711-mm Carbon.	125
6-4	Concentration- and Uptake-Time Profiles for a Flow Rate of 7 GPM/SQ.FT. in a 250-gram Fluid-Bed of 0.711-mm Carbon.	126
6-5	Concentration- and Uptake-Time Profiles for a Flow Rate of 8 GPM/SQ.FT. in a 250-gram Fluid-Bed of 0.711-mm Carbon.	127
6-6	Concentration- and Uptake-Time Profiles for a Flow Rate of 10 GPM/SQ.FT. in a 250-gram Fluid-Bed of 0.711-mm Carbon.	128
6-7	Concentration-Time Profiles for Different Flow Rates (250-grams of 0.711-mm Carbon).	130

LIST OF ILLUSTRATIONS (continued)

Figure	Title	Page
6-8	Concentration- and Uptake-Time Profiles for a Flow Rate of 10 GPM/SQ.FT. in a 250-gram Fluid-Bed of 1.011-mm Carbon.	132
6-9	Concentration- and Uptake-Time Profiles for a Flow Rate of 10 GPM/SQ.FT. in a 250-gram Fluid-Bed of 0.503-mm Carbon.	133
6-10	Concentration- and Uptake-Time Profiles for a Flow Rate of 10 GPM/SQ.FT. in a 250-gram Fluid-Bed of 0.356-mm Carbon.	134
6-11	Concentration- and Uptake-Time Profiles for a Flow Rate of 10 GPM/SQ.FT. in a 250-gram Fluid-Bed of 0.273-mm Carbon.	135
6-12	Concentration-Time Profiles for Different Mean Particle Diameters (250-grams of Carbon; 10 GPM/SQ.FT. Flow Rate).	137
6-13	Concentration- and Uptake-Time Profiles for a Flow Rate of 10 GPM/SQ.FT. in a 350-gram Fluid-Bed of 0.711-mm Carbon.	139
6-14	Concentration- and Uptake-Time Profiles for a Flow Rate of 10 GPM/SQ.FT. in a 450-gram Fluid-Bed of 0.711-mm Carbon.	140
6-15	Concentration- and Uptake-Time Profiles for a Flow Rate of 10 GPM/SQ.FT. in a 550-gram Fluid-Bed of 0.711-mm Carbon.	141
6-16	Concentration- and Uptake-Time Profiles for a Flow Rate of 10 GPM/SQ.FT. in a 650-gram Fluid-Bed of 0.711-mm Carbon.	142
6-17	Concentration-Time Profiles for Different Depths of Expanded Bed (0.711-mm Carbon; 10 GPM/SQ.FT. Flow Rate).	144
6-18	Concentration- and Uptake-Time Profiles for an Influent Concentration of 25.8 moles/liter (250 grams of 0.711-mm Carbon; 10 GPM/SQ.FT.)	146

LIST OF ILLUSTRATIONS (continued)

Figure	Title	Page
6-19	Concentration- and Uptake-Time Profiles for an Inlfuent Concentration of 35.1 moles/liter (250-grams of 0.711-mm Carbon; 10 GPM/SQ.FT.).	147
6-20	Concentration- and Uptake-Time Profiles for an Influent Concentration of 46.3 moles/liter (250-grams of 0.711-mm Carbon; 10 GPM/SQ.FT.).	148
6-21	Concentration- and Uptake-Time Profiles for an Influent Concentration of [illegible].8 moles/liter (250-grams of 0.711-mm Carbon; 10 GPM/SQ.FT.).	149
6-22	Concentration-Time Profiles for Different Influent Concentrations (250-grams of 0.711-mm Carbon; 10 GPM/SQ.FT. Flow Rate.	150
6-23	Desorption-Time Profile for 250-grams of 0.711-mm Carbon Saturated with 185.2 millimoles DNOSBP (8 GPM/SQ.FT. Flow Rate).	152

NOMENCLATURE

ROMAN

Symbol	Description and Units
a	Effective area for mass transfer through the film surrounding the adsorben particle, (cm^2/cm^3).
a'	a/ρ, (cm^2/gram).
A	Pre-exponential factor for particle-size correlation of pore-diffusion controlled adsorption rates.
$\mathcal{A}$	Dummy variable.
A_p	Effective particle cross-sectional area normal to the direction of motion, (cm^2).
$A_{particle}$	External surface area of an arbitrarily shaped particle, (cm^2).
A_{sphere}	External surface area of a spherical particle having the same volume as the particle of arbitrary shape, (cm^2).
b	Langmuir equilibrium energy constant, (cm^3/mole).
b	Dummy Variable.
$\mathcal{B}$	Dummy Variable
C	Concentration of solute in bulk solution at a specified point in the column, (moles/cm^3).
$\mathcal{C}$	Dummy variable.
C_D	Drag Coefficient, (dimensionless).
C_o	Influent concentration of solute, (moles/cm^3).

NOMENCLATURE (continued)

Symbol	Description and Units
C_e	Concentration of solute in the fluid phase corresponding to a condition of equilibrium with the amount adsorbed by the solid phase, (moles/cm^3).
C_i	Internal or pore concentration of solute in the fluid phase, (moles/cm^3).
d_c	Diameter of cylindrical column, (centimeters).
d_p	Diameter of adsorbent particle, (centimeters).
D_G	Ratio of solid-phase and fluid-phase concentrations of solute at saturation, ($q_\infty \rho / C_o \epsilon$), (dimensionless).
D_l	Free-liquid diffusivity of solute, (cm^2/sec).
D_p	Intraparticle or pore diffusivity of the solute in the fluid phase, (cm^2/sec).
$f(\epsilon)$	Voidage function, (dimensionless).
F	Volumetric flow rate through column, (cm^3/min).
F_B	Buoyancy force of a fluid acting on a particle, (grams).
F_D	Drag force of a fluid acting on a constituent sphere in a multiparticle system, (grams).
F_{DS}	Drag force of a fluid acting on a single sphere situated in an infinite expanse of fluid, (grams).
F_G	Gravitational force acting on a particle, (grams).

NOMENCLATURE (continued)

Symbol	Description and Units
$F(\epsilon)$	Function of the void ratio, (dimensionless).
g	Gravitational acceleration term, (cm/sec^2).
g_c	Gravitational constant, (grams$_m$·cm/grams$_f$·sec^2).
G_{mf}	Minimum-fluidization mass flow velocity, (grams/cm^2/sec).
j_d	Mass transfer factor, $j_d = (k_f/\bar{V})(N_{sc})^{2/3}$, (dimensionless).
k	Rate factor for second-order, surface-reaction-controlled case, (cm^3/mole/min.).
k'	Rate factor for first-order, reverse surface-reaction controlled case, (cm^3/mole/min).
k_f	Mass transfer coefficient for the film-diffusion-limited case, (cm/min).
k_p	Mass transfer coefficient for the fluid-phase pore-diffusion-limited case, (cm/min).
k_s	Mass transfer coefficient for the solid-phase pore-diffusion-limited case, (cm/min).
L	Length of expanded bed, (cm).
L_o	Length of adsorbent bed in packed state, (cm).
m	Dummy variable
M	Molecular weight of solvent, (grams/mole).

NOMENCLATURE (continued)

Symbol	Description and Units
n	Dummy variable.
N_{Ga}	Galileo number, $N_{Ga} = d_p^3 \rho_1 (\rho_s - \rho_1) g/\mu^2$, (dimensionless).
N_{Re}	Reynolds number, $N_{Re} = d_p v_p \rho_1 / \mu$, (dimensionless).
N'_{Re}	Modified Reynolds number, $N'_{Re} = d_p v_p \rho_1 / \mu(1-\epsilon)$, (dimensionless).
$(N_{Re})_{mf}$	Reynolds number for minimum fluidization, (dimensionless).
N_{Sc}	Schmidt number, $N_{Sc} = \nu/D_1$, (dimensionless).
P	Pressure at any specified point in the column, (grams/cm^2); ΔP = pressure drop, (grams/cm^2/cm).
q	Amount of solute adsorbed per unit weight of adsorbent averaged over the entire particle at a specified time and position in the column, (moles/gram).
q_e	Concentration of solute in the solid-phase in equilibrium with the coexisting liquid phase at concentration C, (moles/gram).
q_i	Internal solid-phase concentration distribution of solute over the radius of the particle, (moles/gram).
q_∞	Saturation capacity, amount of solute adsorbed per unit weight of adsorbent in equilibrium with a solution of concentration C_o, (moles/gram).
Q	Ultimate capacity of the adsorbent, Langmuir "monolayer" capacity constant, (moles/gram).

NOMENCLATURE (continued)

Symbol	Description and Units
r	Equilibrium modulus, $r = 1/(1+bC_o)$, (dimensionless).
R	Radial distance from center of spherical particle, (cm).
R_p	Total radius of spherical particle (cm).
s	Column-capacity modulus, $s = \kappa v \epsilon / F$, (dimensionless).
t	Solution-capacity parameter for the kinetic case, $t = \kappa \cdot \tau / D_G$, (dimensionless).
T	Absolute temperature, (degree Kelvin).
v	Bulk volume of expanded bed, (cm^3).
v_p	Velocity of adsorbent particle in a stagnant fluid or velocity of fluid past a stationary particle, (cm/sec).
v_{p_o}	Terminal free fall velocity of adsorbent particle in a stagnant fluid, (cm/sec).
$(v_{p_o})_I$	Terminal particle velocity for Intermediate Law regime, (cm/sec).
$(v_{p_o})_N$	Terminal particle velocity for Newton's Law regime, (cm/sec).
$(v_{p_o})_S$	Terminal particle velocity for Stokes' Law regime, (cm/sec).
V	Total volume of solution passed through column, for $\tau > 0$, (cm^3).
V_p	Total volume of adsorbent particle, (cm^3).
V_o	Molal volume of solute molecule at normal boiling point, (cm^3/mole).

NOMENCLATURE (continued)

Symbol	Description and Units
$\bar{V}$	Superficial velocity of flow through column, (cm/min).
w	Dummy variable.
W_L	Vortex or wake length, (cm).
x	Distance variable in material balance relationship, (cm).
X	Association parameter for the solvent in the Wilke-Chang correlation, (dimensionless).
y	Distance variable in material balance relationship, (cm).
y	Dummy variable.
z	Distance variable in material balance relationship, (cm).
z	Dummy variable.
GREEK	
α	Pre-exponential factor for correlation of the j_d-factor with N'_{Re}/N_{Ga}.
β	Exponent for correlation of the j_d-factor with N'_{Re}/N_{Ga}.
γ	Intraparticle void ratio, (dimensionless).
δ_i	Activity distribution over radius of adsorbent particle, (number of active surface sites per unit volume of carbonaceous matter); δ = mean activity of entire particle of total radius R_p.
ϵ	Interparticle void ratio in expanded bed, (dimensionless).

NOMENCLATURE (continued)

Symbol	Description and Units
ϵ_{mf}	Interparticle void ratio for minimum fluidization, (dimensionless).
η	Variable of integration.
κ	General rate coefficient for the kinetic case, (min^{-1}).
κ_f	Rate coefficient for the film-diffusion-limited case, (min^{-1}).
κ_p	Rate coefficient for the fluid-phase pore-diffusion-limited case, (min^{-1}).
κ_s	Rate coefficient for the solid-phase pore-diffusion-limited case, (min^{-1}).
λ	Wavelength, (millimicrons).
μ	Absolute viscosity, (centipoise).
ν	Kinematic viscosity, (stokes).
ξ	Variable of integration.
ρ	Density of the adsorbent in the expanded bed, ($grams/cm^3$).
ρ_1	Density of solvent, ($grams/cm^3$).
ρ_s	Density of adsorbent, ($grams/cm^3$).
τ	Time from first entry of solution to column, (minutes).
ψ	Sphericity factor, $\psi = A_{sphere}/A_{particle}$, (dimensionless).

CHAPTER I

INTRODUCTION

Multiple use of surface waters has become commonplace as a result of the contiguous location of expanding urban and industrial complexes along major water courses. Nearly 40 percent of the Nation's population now indirectly uses water that has been used previously for domestic or industrial purposes. Direct reuse of reclaimed wastewater has been considered an attractive alternative in water source development, and has been instituted in several instances (61). With successive reuse of water, either directly or indirectly, undesirable organic compounds which are neither significantly affected by conventional waste treatment nor readily degraded subsequently in receiving waters (48) build up to concentration levels that may be esthetically distasteful or, in the limit, injurious to public health. This factor has become the prime deterrent to widespread application of direct recycle of wastewater effluents for human consumption.

The problems associated with dilatation of multiple reuse of surface waters have been compounded by the fact that both the quantity and complexity of treatment-resistant or persistent pollutants have increased in proportion to the expanding technology of the chemical industries.

Westlake and Gunther (69) have reported that the production of a categorical class of compounds developed primarily for use as pesticides has doubled decenially. The rapid expansion of production and proliferation of use of these toxic and extremely resistant materials (48) has resulted in continually increasing residual concentrations in surface waters. For example, levels as high as 0.094, 0.118, and 0.087 micrograms per liter have been reported for Endrin, Dieldrin, and DDT, respectively, in a preliminary survey of the national water quality network (28). While these concentrations of pesticides may not present acute toxicity hazards, they most likely are quite consequential in terms of potential chronic effects; trace levels of pesticides may cause serious gradual changes in the aquatic environment over a span of time.

Biological accumulation of pesticides, a characteristic of aquatic fauna and flora, has certainly magnified the problems created by such pollutants in streams. Certain lower species in the aquatic food chain have been observed to accumulate pesticides present in the water in even infinitesimal quantities. Higher forms that use these microfauna and microflora as a major source of food may then further accumulate or concentrate the pesticides to very high levels, until toxic proportions are ultimately reached in the upper trophic levels of the aquatic food chain. For example, a case has been reported (69) in which an insecticide was applied to a water at a dosage of 14 micrograms per liter to control gnats. It was later found that plankton had accumulated residues of 5 milligrams per kilogram of plant weight. Subsequent analyses of fish in the lake showed the presence of this insecticide at levels of 40 to 2500 milligrams per kilogram; high enough to cause a significant rate of mortality in a certain species of predatory shore bird feeding on the fish. Further, shellfish have been shown to be capable of biologically accumulating certain pesticides to extraordinary proportions within a short period of time. Oysters, for example, have achieved 90 percent extraction efficiency in laboratory studies in storing DDT at levels 70,000 times greater than the concentration in the surrounding water during 40-day exposures (5).

Although current levels of pesticides are 300 to 500 times lower than threshold toxicity concentrations (51), there is cause for justifiable concern where accumulation occurs in food chains, ultimately resulting in damage to some member of the chain and perhaps exposure of humans to high pesticide levels through consumption of the accumulator species, or of a subsequent predator, as food. Therefore, it is imperative that the concentrations of persistent pollutants such as pesticides in surface waters be maintained at as low levels as possible to prevent the risk of encountering toxic doses, to say nothing of possible accumulation and chronic effects in the human species itself.

The need for development of methods for the removal of perdurable pollutants such as pesticides from wastewaters prior to discharge to receiving waters is evident. The problem of removing such refractory contaminants is commonly complicated by the inordinantly small concentrations encountered, by the extreme range in the types and quantities of such pollutants present in a given waste, and by variations in types and concentrations occurring among different wastes. Because many persistent organic pollutants are surface active to some degree, the use of adsorptive processes employing materials such as activated carbon appears promising as a solution to the problem. Moreover, adsorption on active carbon is particularly suited for removal of trace concentrations of organic pollutants of diverse types (62).

Weber and Morris (64) have suggested that the optimum use of granular activated carbon as an adsorbent for treatment of waters and wastewaters is to be achieved by column-type operation. They have concluded that columnar operation has distinct advantages over batch treatment because rates of uptake are dependent on the concentrations of pollutants in the solution in contact with carbon. For column operation the carbon is continuously in contact with a fresh solution. Consequently, the concentration in the solution in contact with a given layer of carbon in a column is relatively constant. For batch treatment, conversely, the concentration of solute in contact with a specific quantity of carbon steadily decreases as adsorption proceeds, thereby decreasing the efficiency of the adsorbent for removing the solute from solution.

Studies on the kinetics of adsorption (64) have indicated the desirability of utilizing as small a size of adsorbent particle as conditions of efficient operation allow, so that high rates of adsorption may be attained. The adsorption process generally has been related to packed beds of the sorbent material. For wastewater treatment applications, however, packed-bed type operation commonly is beset with problems of clogging, severe head loss and air binding due to the presence of particulate matter and dissolved gases. The fluid-bed contacting technique, in contrast, is one method for taking advantage of small particle size and yet avoiding the shortcomings of the packed-bed system. Studies which have focused on the development of adsorption technology for wastewater-treatment applications have clearly demonstrated such marked advantages for a fluid-bed mode of operation (66).

Considerable effort has been directed to the identification and characterization of parameters significant to the performance of fluid-bed carbon adsorbers. Most recently, studies of complex multiple-solute systems have provided information on competitive interactions between representative types and classes of organic pollutants (60). These investigations have yielded useful information regarding general design and operating criteria for wastewater-treatment applications. There has remained, however, a definite need for the systematization of this information, and for the development of a quantitative design procedure for fluid-bed adsorbers.

Successful design of a fluid-bed separation process requires prediction of the concentration-time profile for the effluent. Such predictions can be made if the equilibrium distribution of solute between solid and solution phases and the nature of the mass transfer rate processes are known. Methods by which rate constants and mass transfer coefficients have been defined by previous investigators commonly have involved: 1) development of a model based on several assumptions regarding equilibrium and rate parameters; 2) assumption of a succession of incremental rate constants while generating a series of concentration-time profiles; 3) carrying out an experimental column study for any suitable system, subject to the nature of the assumptions involved; and, 4) determination of appropriate rate constants for the system by means of curve-matching techniques. It is to be noted that this approach is not truly predictive in nature, as it must resort to preliminary investigations of pilot-plant scale. Furthermore, previous researchers who have attempted exact mathematical solutions have required the use of restrictive - and often unrealistic - simplifying assumptions, thus limiting such models to systems conforming precisely to the suppositions involved.

The research reported herein has been directed toward the development and testing of a non-restrictive mathematical model for accurate description of mass transfer processes in columns of fluidized active carbon. This development has involved correlation of experimental kinetic and equilibrium data for agitated non-flow systems with those for continuous-flow fluid-bed systems. The objective has been to provide a model which will permit prediction of concentration-time profiles for systems of the latter type from measurements of selected adsorption parameters in critically designed non-flow systems. Measurements in simple non-flow batch experiments can of course be accomplished much more readily and with greater ease than can those in relatively complex and time consuming continuous flow column tests.

This development ultimately will be useful for the design and operation of adsorption systems. The engineer will thus be afforded the use of a method by which he will be able to directly determine the proper number of units and the design of a fluid-bed sorption apparatus. Also, he will be able to specify the operating conditions necessary to ensure that the effluent stream from a proposed adsorption installation will meet minimum quality standards. Further, preliminary pilot plant-scale investigations for determination of significant process parameters will be obviated. Development of such a predictive model, therefore, should represent a significant contribution to the technology and engineering design of adsorption systems.

CHAPTER 2

EXPERIMENTAL FACILITIES AND PROCEDURES OF INVESTIGATION

ACTIVE CARBON

The choice of active carbon as an adsorbent for treatment of wastewaters is a particularly expedient one, since this granular material provides large specific surface areas and, therefore, high capacities for adsorption. Activated carbons, characterized by large internal surface areas, are generally produced from carbonaceous raw materials such as wood, coal, sugar, nut shells and vegetable matter (49). Differences in the adsorptive characteristics of the various active carbons may be ascribed in part to the particular properties of the base material and to the inorganic impurities which may be incorporated in the carbonaceous matrix.

The production of active carbon involves first the formation of a char from the raw material. Carbonization is accomplished by heating in the presence of catalytic agents, producing a slightly-porous carbonaceous char. The char is then activated by treatment with oxidizing gases under carefully controlled conditions, resulting in the development of a porous structure with an extensive internal surface. Special properties may be imparted to the active carbon by pretreatment with certain reagents.

A coal-base active carbon, obtained from the Pittsburgh Activated Carbon Company (Type SGL), was used for all of the experiments. The carbon as received from the manufacturer was prepared for the studies by sieving into uniform particle size fractions with a set of United States Standard Sieves. Eight different size fractions, including 16/20 (particles passing a 16 mesh sieve and being retained on a 20 mesh sieve), 20/30, 30/40, 40/50, 50/60, 60/80, 80/100, and 100/200 mesh, having arithmetic mean diameters of 1.011, 0.711, 0.503, 0.356, 0.273, 0.213, 0.161 and 0.110-mm, respectively, were obtained. After separation, the sized samples were washed approximately twelve times in glass-distilled water to remove fines remaining from the sieving process. Subsequently, the carbon was dried in thin layers to constant weight at 110°C.

SOLUTE AND ANALYTICAL TECHNIQUE

A recognized pesticidel pollutant, 2-sec-butyl-4,6-dinitrophenol (DNOSBP), was used as a representative refractory solute for all the experiments. This aromatic compound, produced by four chemical firms, is sold commercially in 13 to 56-percent stock solutions as an alkanolamine salt of either the ethanol or isopropanol series. The commercial products are intended primarily for use as herbicides, acting as contact weed killers for most annual weeds and grasses. This group of herbicides also receives widespread use as a floor spray in fruit orchards (13,14).

The acute oral median lethal dose (LD_{50}) of DNOSBP to albino rats (standard measure of toxicity) has been determined to be in a range of 37 to 60 milligrams per kilogram of body weight (13). An LD_{50} of this magnitude may be classed as being extremely toxic on a relative toxicity scale ranging from super toxic (LD_{50}<5mg/kg.) to practically non-toxic (LD_{50}>15 grams/kg.).

DNOSBP, with a melting point of 28 to 30°C, exists as a reddish-brown liquid above the melting point and as a bright yellow solid below the melting point. It is nearly insoluble in distilled water, but is soluble in most organic solvents and oils. The molecular formula for this compound is $4,6,2\text{-}(O_2N)_2[CH_3CH_2CH(CH_3)]C_6H_2OH$, which may be represented structurally in two dimensions as,

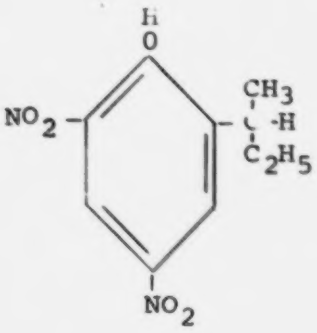

and has a formula weight of 240.22 grams per mole (13).

Purification of the commercially available DNOSBP, supplied by the Dow Chemical Company, was accomplished by double recrystallation in a distilled water-ethanol solution. Melted DNOSBP was mixed with an equal liquid volume of ethanol, heated to boiling, and then diluted with distilled water to the point at which the system became supersaturated. The solution was then refrigerated at 2°C until recrystallation was complete and the supernatant, containing the ethanol-soluble impurities, was decanted leaving the purified DNOSBP.

Analysis of DNOSBP was accomplished by UV-Visible spectrophotometry. The absorption spectrum of this adsorbate was determined on a Perkin Elmer (Model PE-202) continuous recording UV-Visible spectrophotometer. Maximum light adsorption was found at a wavelength of 375 millimicrons, as illustrated in Figure 2-1. The molar extinction coefficient was determined to be 14,000 liters/cm-mole from a calibration curve, plotted in Figure 2-2, taken at a wavelength of 375 millimicrons and a slit width of 0.03 millimeters on a Beckman Model DU-2 spectrophotometer.

Ten-millimolar stock solutions of DNOSBP were used in all experiments for both batch and columnar systems.

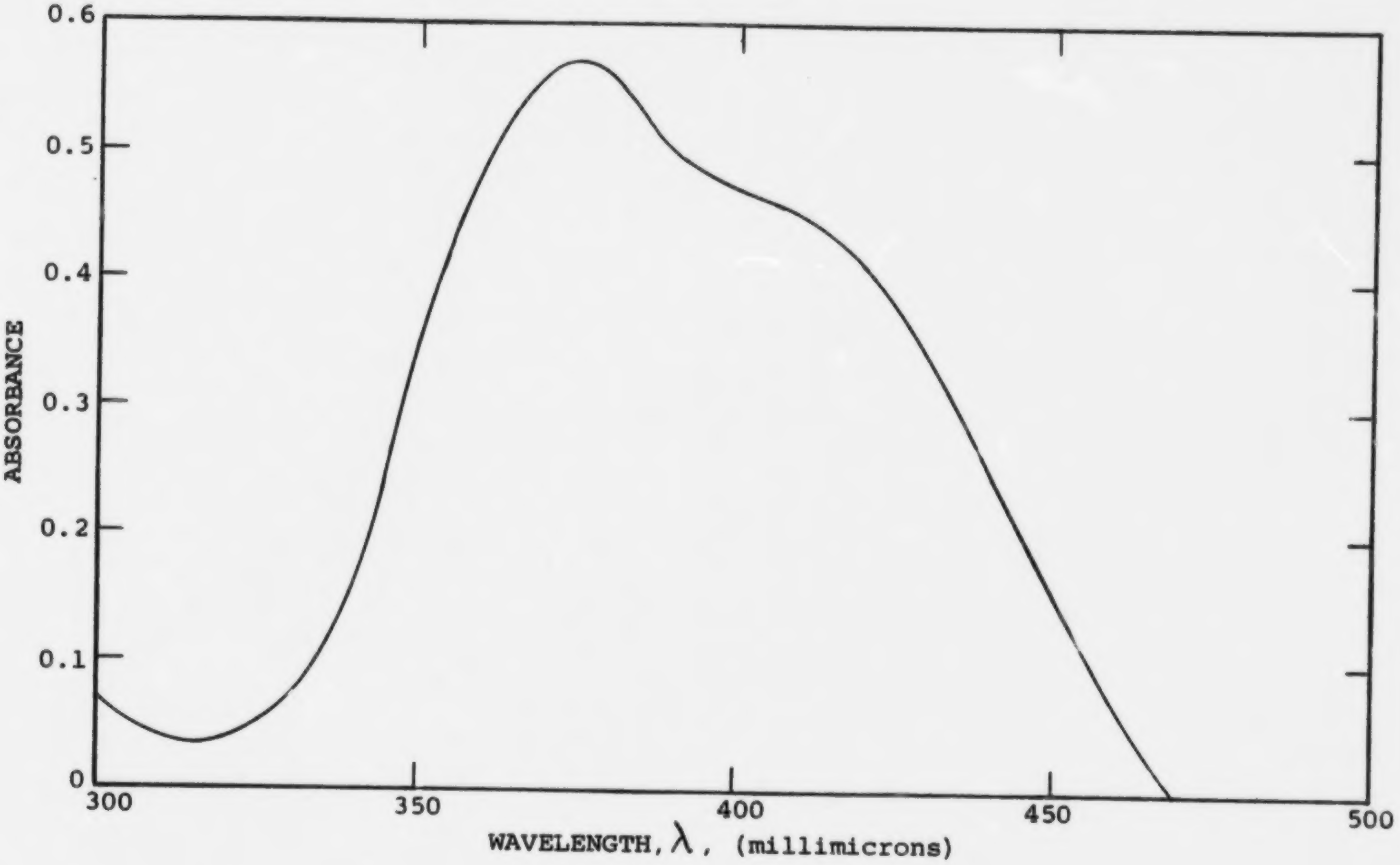

FIGURE 2-1. ABSORPTION SPECTRUM FOR 2-SEC-BUTYL-4,6-DINITROPHENOL

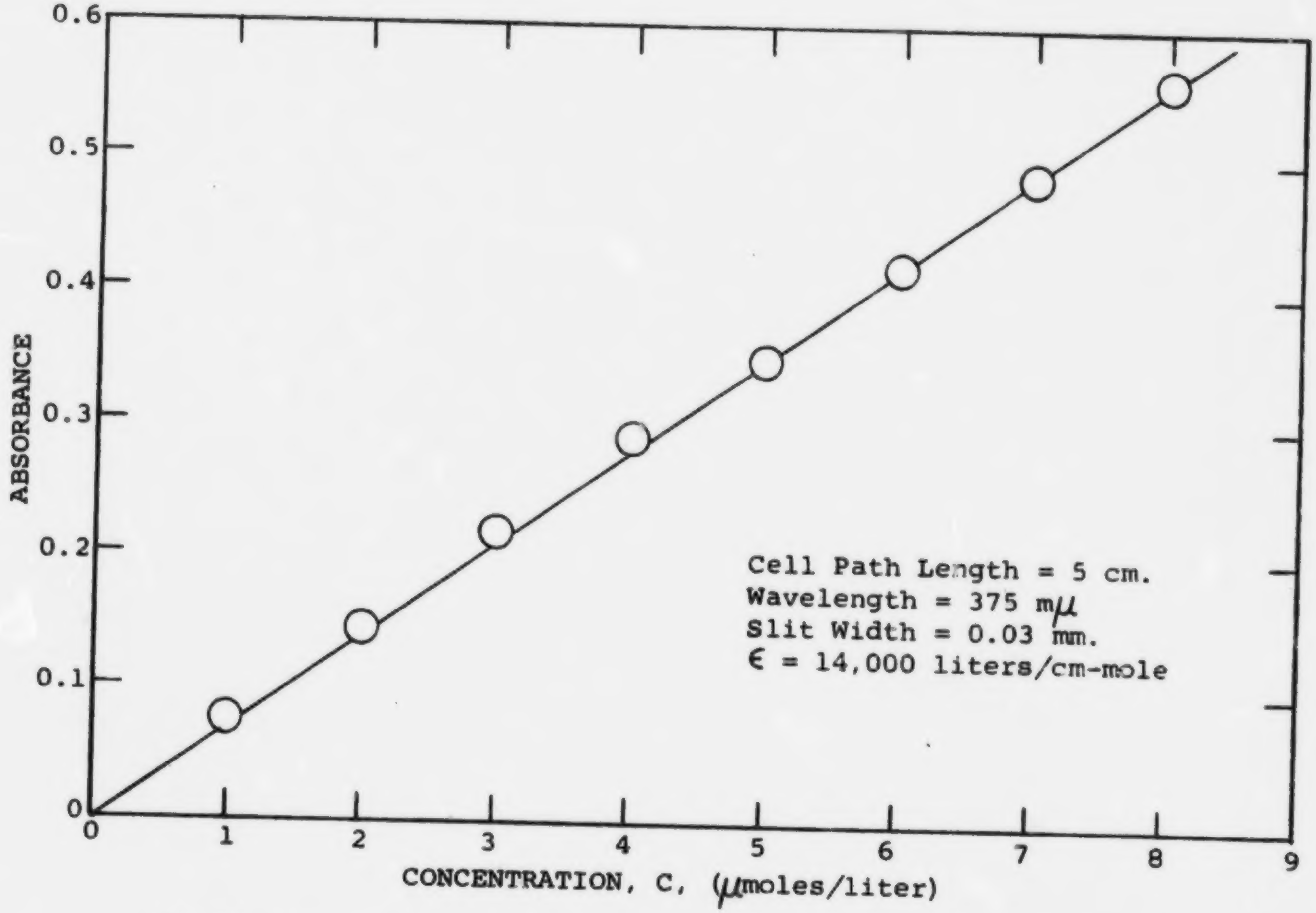

FIGURE 2-2. CALIBRATION CURVE FOR 2-SEC-BUTYL-4,6-DINITROPHENOL

Preparation of the solution was accomplished by adding KOH pellets to glass distilled water to produce a solution with pH=12, in which DNOSBP is considerably more soluble than in neutral solution. The solidified adsorbate was then added to the solution, which subsequently was heated until all of the solute had dissolved.

BATCH SYSTEM EXPERIMENTS

Adsorption Isotherms

A series of adsorption isotherms was established to evaluate appropriate equilibrium parameters for each of the specific systems investigated. This was accomplished by placing suitable, accurately weighed quantities of prepared carbon into 150-ml bottles and then adding 100-ml aliquots of a solution of the adsorbate in concentrations suitable for adequately defining the isotherms over the range of concentrations of interest for the column experiments. Also, several bottles were prepared without carbon to serve as blanks. A 10^{-3}-$\underline{M}$ carbonate buffer system was used to buffer the adsorbate solution at a pH of 10.2, which was comparable to the pH of the tap water used for the column experiments. Oscillating mechanical shakers provided continuous agitation of the sealed bottles during an equilibration period of four weeks, after which measurements of residual solute concentration were made to define the distribution of solute between solid and solution phases at equilibrium. Spectrophotometric analysis of the adsorbate was performed with a Beckman DU-2 subsequent to dilution of the samples to appropriate concentration levels with glass-distilled water buffered at pH=10.2 with a 10^{-3}-$\underline{M}$ carbonate system. The quantities adsorbed were computed from the differences between the concentrations of adsorbate measured for the blanks and for the reacted solutions.

During the equilibrium experiments the temperature was not specifically controlled but was allowed to vary with room temperature, which was monitored at $26 \pm 3^{\circ}$C. Since the heat of adsorption for DNOSBP on activated carbon, as determined by Weber and Gould (62), was found equivalent to -4190 calories per g-mole, the small temperature variations encountered represent insignificant differences in equilibrium values for adsorption.

Non-Flow Kinetic Studies

For each experiment on rates of adsorption, a 3-liter volume of adsorbate solution was prepared by diluting an appropriate volume of a 10^{-2}-$\underline{M}$ stock DNOSBP solution with distilled water buffered at a pH of 10.2 with a 10^{-3}-$\underline{M}$ carbonate buffer system; this was done directly in a 4-liter glass reaction vessel. The experimental solution was allowed to stand for a period of 12 hours to equilibrate at room temperature and to come to adsorptive equilibrium with the surfaces of the reaction vessel. Again, the temperature was not controlled, but the variation was much too small to influence the rates significantly.

Prior to introduction of an accurately weighed quantity of carbon to the vessel, an initial 10-ml sample of solution was removed and analyzed for concentration of solute with the Model DU-2. This gave an accurate check on the preparation of the solution and served as the reference concentration for the rate study. The carbon was then introduced into the vessel and was rapidly dispersed by a motor-driven polyethylene-coated stirrer operated at 1550 RPM; a speed for which the rate of adsorption is independent of the turbulence induced by mixing (64). Stirring was briefly interrupted at appropriate intervals while 10-ml samples were pipetted from the reaction vessel for analysis. Solute concentrations were then reduced, taking account of volume corrections, to yield rates of uptake for the rapidly agitated non-flow systems.

CONTINUOUS UP-FLOW APPARATUS

Adsorption Columns

The experimental system used for obtaining data with which to test the theoretical mass-transfer model is illustrated schematically in Figure 2-3. The adsorption columns consisted of Lucite cylinders, 2 inches in diameter and 6 feet in length. Each column was fitted at the base with a distribution chamber filled with 2-mm glass beads. This distribution chamber served to dissipate the velocity head at the influent section, thus ensuring steady-state, one-dimensional flow along the length of the column. A 140-mesh stainless steel screen supported the carbon in the column, and separated it from the glass beads in the distribution chamber. Samples of column effluent and total effluent were collected and analyzed at appropriate intervals to provide break-through and total solute uptake data, respectively, for the fluidized carbon columns.

Automatic Flow-Rate Mechanism

Flow to the columnar adsorbers from a constant-head feed tank was regulated by means of an automatic rate-controlling mechanism, diagramed in Figure 2-4, to provide precise control over flow despite changes in head loss during the long-term experiments. The automatic mechanism consisted of a 1/4-inch Hoke stainless steel needle valve coupled to a 100 inch-ounce Hurst reversible synchronous motor by a slotted aluminum chuck. This chuck, which was

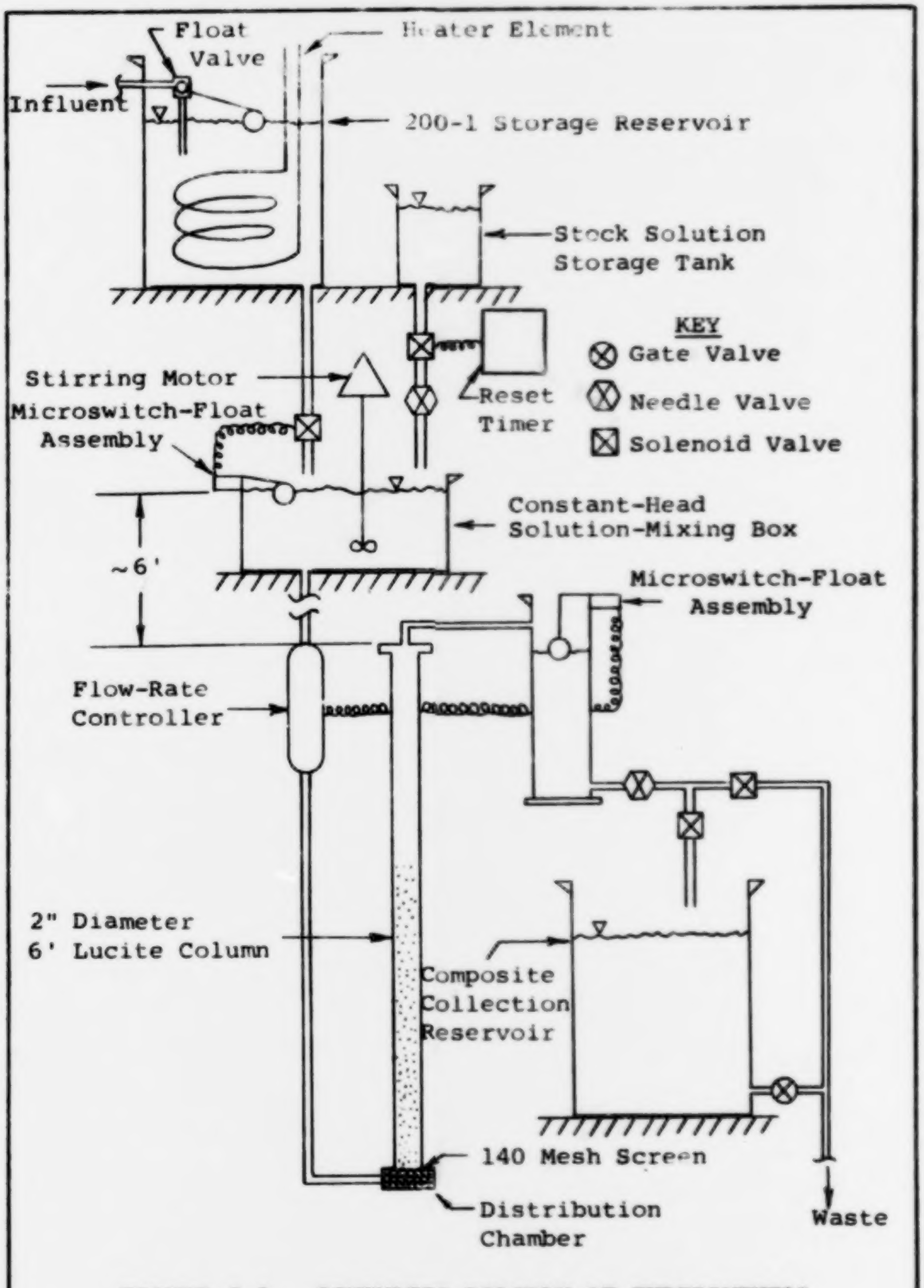
Float
Valve
Heater Element
Influent
200-1 Storage Reservoir
Stock Solution
Storage Tank
KEY
⊗ Gate Valve
Needle Valve
☒ Solenoid Valve
Stirring Motor
Microswitch-Float
Assembly
Reset
Timer
Constant-Head
Solution-Mixing Box
~6'
Microswitch-Float
Assembly
Flow-Rate
Controller
2" Diameter
6' Lucite Column
Composite
Collection
Reservoir
140 Mesh Screen
Distribution
Chamber
Waste

FIGURE 2-3. SCHEMATIC DIAGRAM OF EXPERIMENTAL FLUIDIZED-BED APPARATUS

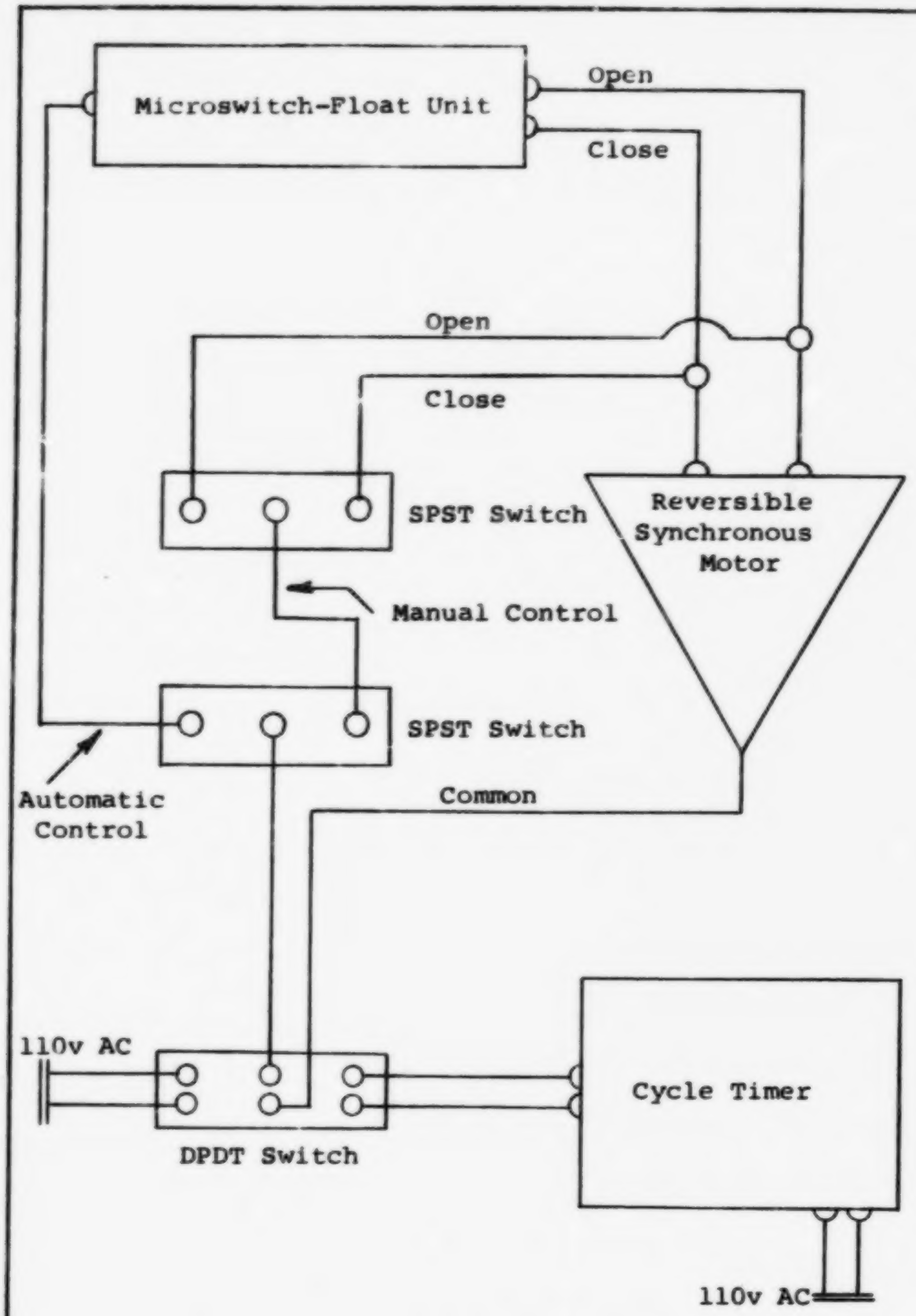
Microswitch-Float Unit
Open
Close
Open
Close
SPST Switch
Reversible Synchronous Motor
Manual Control
SPST Switch
Automatic Control
Common
110v AC
DPDT Switch
Cycle Timer
110v AC

FIGURE 2-4. SCHEMATIC DIAGRAM OF FLOW RATE CONTROL MODULE

attached to the motor, intermeshed with the stem of the needle valve and was positively linked to the valve by a stainless steel pin which was placed through a hole drilled through the valve stem. The valve stem, thus, rode up and down within the chuck as the needle valve was opened or closed.

The motorized needle valve was operated in response to an electrical signal derived from a microswitch-float assembly fitted to a 3-3/4-inch cast Lucite tube which served as a flow rate sensing device. This rate mechanism was operated by adjusting the needle valve in the effluent line of the 3-3/4-inch Lucite constant head reservoir to the desired flow. If the flow through the reaction column was greater than this preselected flow, the liquid level in the constant head cylinder would be elevated, subsequently orienting the microswitch-float unit in a raised position. This would close an electrical circuit causing the motor to rotate in a clockwise direction, thereby closing the needle valve and slightly decreasing the flow. Conversely, if the flow through the columnar adsorber was less than the preselected flow, the liquid level would drop; the lowered float assembly would then in turn close an electrical circuit, causing the synchronous motor to open the needle valve and increase the flow.

Because this rate mechanism had the tendency to overcompensate or "overshoot" in adjusting the flow rate, a cycle timer was installed in the circuit as shown in Figure 2-4. This timer, which had a variable on-off interval, was adjusted for a 2-second on period and a 58-second off period. This combination of the on and off intervals kept the "overshoot" to a minimum and maintained the flow rate at desired levels.

Either manual or automatic operation was possible for the synchronous motor-needle valve assembly. Manual control was generally used only for initial adjustment of the needle valve to the approximate rate of flow; the automatic mechanism was used from that point on.

Solution Feeding Module

A 200-l tap water storage reservoir, a 15-l container for the stock solution of solute, and an 8-l mixing tank which maintained a constant head for feed to the adsorption columns comprised the solution feed module. Tap water, which was passed through a carbon filter in the influent line, was admitted to the 200-l storage tank. This reservoir was fitted with a heating element and thermo-regulator which heated the solution to a constant temperature approximately equivalent to room temperature and allowed the water to equilibrate with the atmosphere. A mixing motor and stirrer eliminated any temperature gradients within the reservoir and facilitated evolution of dissolved gases. A ballcock and float assembly maintained the water surface at a constant level.

Carbon-filtered, temperature-equilibrated tap water was admitted to the solution mixing reservoir through a solenoid valve operated by a microswitch-float unit. Likewise, the stock solution of solute - 0.01 M DNOSBP - was introduced to the mixing tank through a solenoid valve which was controlled by a 15-second reset timer that was activated by a microswitch-float assembly. Thence, each time tap water was introduced into the tank an appropriate quantity of adsorbate was also added to maintain the desired concentration in the constant head reservoir. Mechanical stirring in the solution boxes ensured homogeneous, constant concentration solutions.

Composite Sampling System

Since the total throughput volume for any columnar experiment to complete exhaustion of the granular adsorbent was on the order of 10^4 to 10^5 liters, liquid storage limitations dictated that it was impossible to store the total volume treated during any one experiment. Instead, a representative composite sample was collected by means of the solenoid valve system shown in Figure 2-3, to describe the curve defining the quantity of solute adsorbed on the active carbon as a function of time. This was accomplished by collecting samples for a 3-second period during each minute of operation, and storing the composite in 200-l polyethylene containers.

CHAPTER 3

THEORETICAL DEVELOPMENT

The overall rate of adsorption of solute from an aqueous stream flowing through a fluidized bed of porous, activated carbon represents the combined effects of: 1) diffusion through the stagnant layer of fluid surrounding the particle (external or film diffusion; 2) diffusion within the voids of the particle (pore diffusion); 3) pore-surface diffusion (45,46,55); and, 4) adsorption on the internal pore surface (22). Pore surface diffusion is distinquished from pore diffusion in that it occurs on the solid side of the phase boundary. As indicated in Figure 3-1, solute may enter a particle of adsorbent directly from the exterior surface by movement in condensed or adsorbed form along the pore surfaces (identified as surface diffusion), or it may diffuse through the fluid phase held in the pores and then be deposited at a stationary location on the pore surface. In pore diffusion, the controlling mass-transfer process occurs before the phase change, but in solid diffusion it occurs afterward. Under different operating conditions, the same particle can exhibit either surface- or pore-diffusion behavior, favoring the former if the concentration level in the

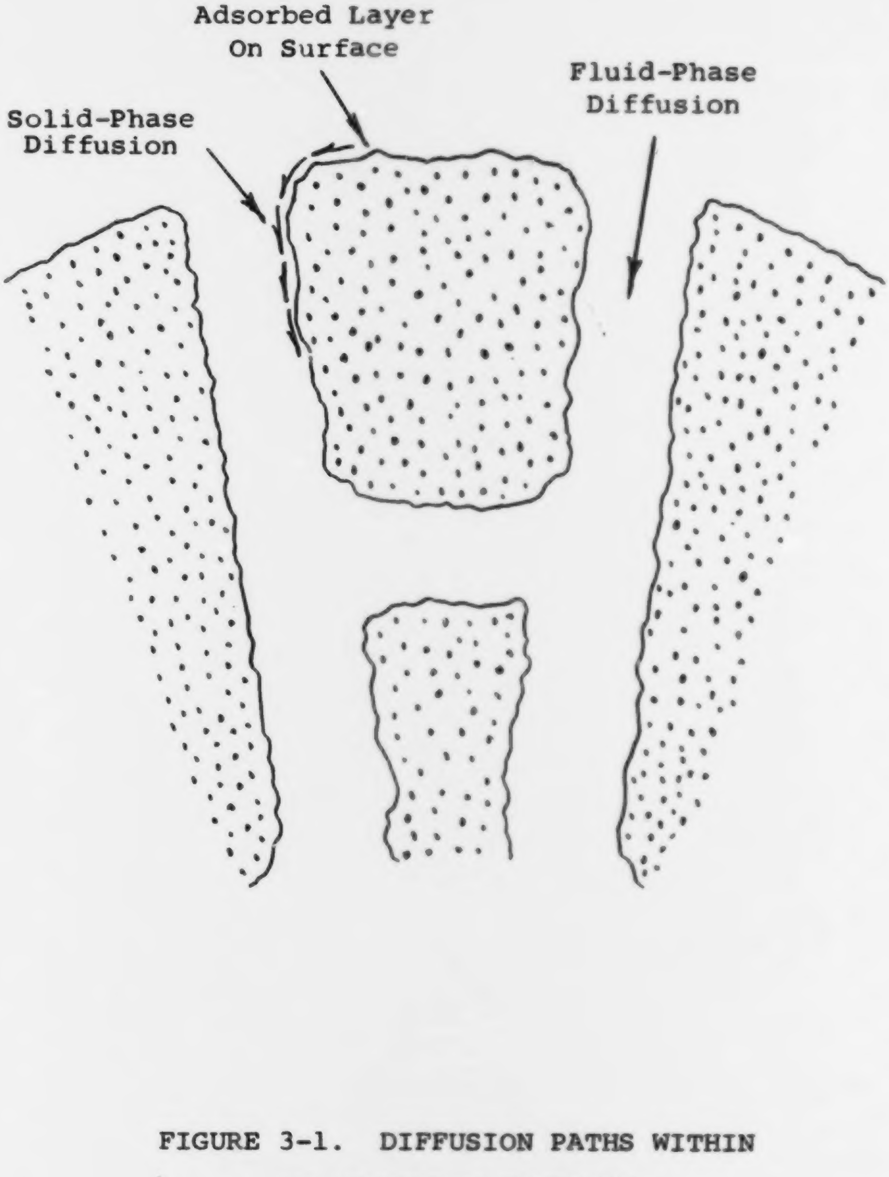
Adsorbed Layer
On Surface
Fluid-Phase
Diffusion
Solid-Phase
Diffusion

FIGURE 3-1. DIFFUSION PATHS WITHIN AN ADSORBENT PARTICLE

pore-fluid is low and the latter if this level is high (20). Of the two transport processes the more rapid one will control the overall rate of transport, because they act in parallel.

Most mathematical solutions for equations describing concentration-time profiles are limited to the special case in which only one of these four processes controls the overall rate of adsorption. Thomas (54), Rosen (45) and Kasten et. al.(26), for example, have presented solutions for systems in which intraparticle diffusion is the only significant resistance, and Furnas (15), Goldstein (17), and Klinkenberg (28) have provided solutions for systems in which either external diffusion or surface adsorption controls the rate of mass transport, while Vermeulen has presented a solution for the solid-diffusion case (57). Several investigators, including Rosen (46) and Amundson (2), have solved the more general case in which both external and pore diffusion resistances are significant, while Masamune and Smith (38) have presented a solution of the general three-resistance case in integral form. Unfortunately, however, each of these developments requires the use of simplifying assumptions relative to the equilibrium distribution of solute between solution and solid phases. Of the four basic types of isotherms, illustrated in Figure 3-2, most authors assume a linear distribution to represent equilibrium conditions, primarily because it is mathematically expedient to do so for ease of solution of the partial differential equations. Adsorption isotherms for compounds typical of wastewater pollutants, determined by Weber and Morris (65) and Weber and Gould (62), are generally of the favorable type and in some cases approach the condition of irreversibility. Certainly, therefore, these types cannot be approximated adequately by a linear type of isotherm.

The use of such mathematical models, developed on the premise that linear equilibrium exists, is thus severly restricted to a very narrow range over which the adsorption isotherm may be approximated by a linear segment without appreciable error. Conversely, the reaction-kinetics development of Thomas (53) allows the use of a generalized isotherm of the Langmuir type. The Langmuir isotherm provides for accurate definition of the favorable type of isotherm, but in the limit may also be utilized for description of the boundary conditions for irreversible and linear equilibria. The development of Thomas, therefore, appears specially suited for description of mass transfer processes for wastewater systems. Hiester and Vermeulen (23,58) have adapted the Thomas solution to packed bed adsorbers,

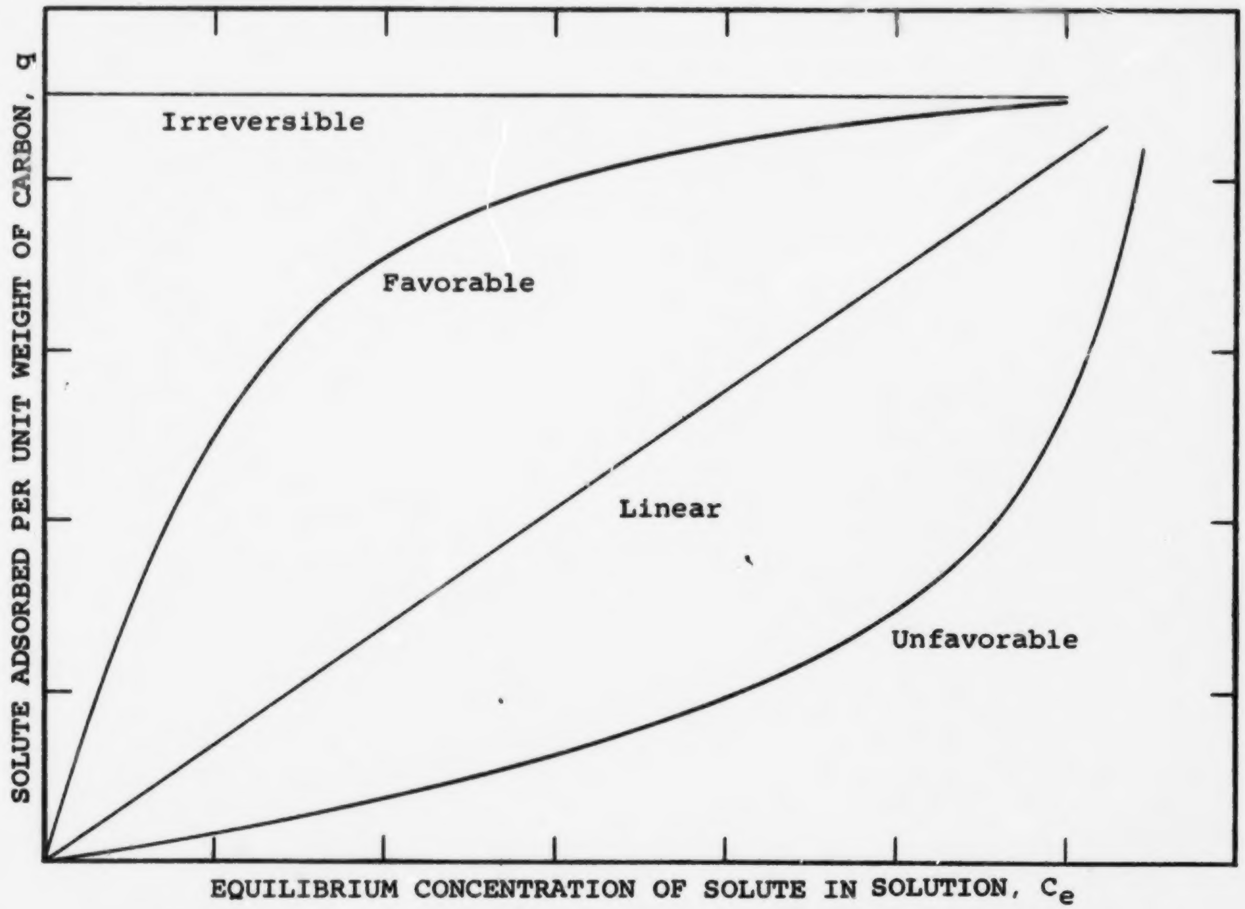

FIGURE 3-2. BASIC TYPES OF POSSIBLE ADSORPTION ISOTHERMS

and have presented methods for numerical solution of the equations for mass-transfer in such systems. The fundamental developments of Thomas and of Hiester and Vermeulen form the basis for the predictive model presented herein. The equations and pertinent assumptions will be outlined in the interest of providing a connected account of the theory. Appropriate revisions required to adapt the Hiester-Vermeulen equations to fluid-bed systems are included.

MATERIAL-BALANCE RELATIONSHIPS

Simply stated, the conservation of mass equation for an infinitesimal thickness of bed at a given cross-section in an adsorption column, diagrammed in Figure 3-3, expresses the fact that any loss of solute by the solution passing through that section must equal the gain of solute by the adsorbent contained within the section. It is assumed that axial diffusion in the bed, treated by Acrivos (1) and Aris and Amundson (3), is negligible with respect to convection and that concentration gradients in the radial direction, discussed by Lapidus and Amundson (2,30) are of minor import. Let the time from first entry of solution to the section be denoted by T, (minutes); the concentration of solute in the solution entering the section by C (moles/cm^3); the solid-phase or adsorbed quantity of solute averaged over the entire particle by q, (moles/gram); the bulk volume

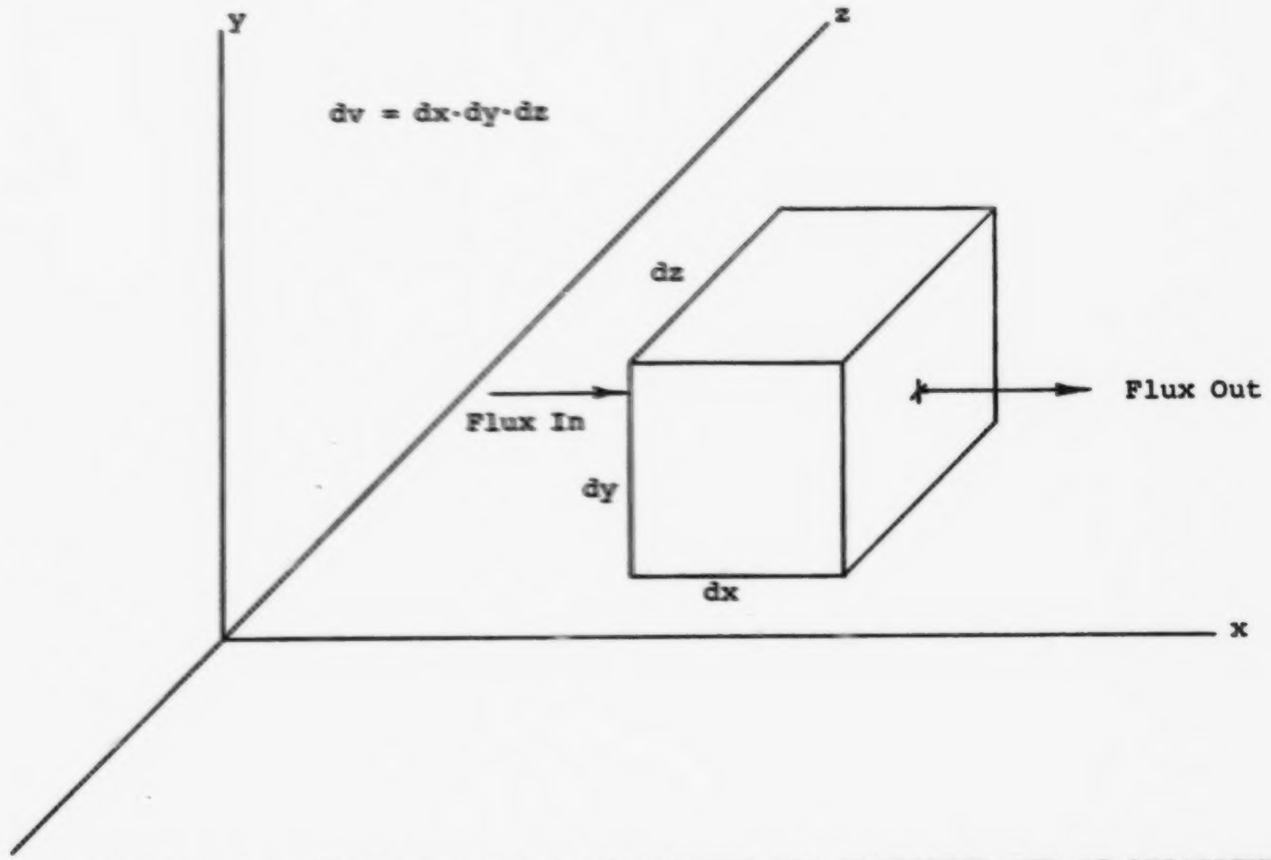
y
z
dv = dx·dy·dz
dz
Flux In
dy
dx
Flux Out
x

FIGURE 3-3. DIFFERENTIAL VOLUME ELEMENT FOR FLUIDIZED BED OF ADSORBENT

of expanded bed by v, (cm^3); the volume of influent solution fed to the column by V, (cm^3); the volumetric flow rate through column by F, (cm^3/min); the density of the adsorbent in the expanded bed by ρ, (grams/cm^3 of expanded bed); and, the interparticle void space of the expanded bed by ϵ, (dimensionless). The convective flow of mass into the differential volume element in time $\delta\tau$ then may be expressed by

$$C \cdot F \cdot \delta\tau \text{ - - - - - - - - - - - - - - } \tag{3-1}$$

the convective flow out of element by

$$(C+\frac{\partial c}{\partial v} \cdot dv) \cdot F \cdot \delta\tau \text{ - - - - - - - - - - - } \tag{3-2}$$

adsorption on the solid phase by

$$\rho \cdot \frac{\partial q}{\partial \tau} \cdot dv \cdot \delta\tau \text{ - - - - - - - - - - - - - } \tag{3-3}$$

and, accumulation of mass in the differential element by

$$\epsilon \cdot \frac{\partial c}{\partial \tau} \cdot dv \cdot \delta\tau \text{ - - - - - - - - - - - - - } \tag{3-4}$$

Summing over the differential volume element yields

$$C \cdot F \cdot \delta\tau - (C+\frac{\partial c}{\partial v} \cdot dv) \cdot F \cdot \delta\tau - \rho \frac{\partial q}{\partial \tau} \cdot dv \cdot \delta\tau = \epsilon \cdot \frac{\partial c}{\partial \tau} \cdot dv \cdot \delta\tau \text{ - - - - - - - } \tag{3-5}$$

which reduces to

$$\frac{\partial c}{\partial v} + \frac{\epsilon}{F}\frac{\partial c}{\partial \tau} + \frac{\rho}{F}\frac{\partial q}{\partial \tau} = 0 \quad \text{- - - -(3-6)}$$

or, for constant flow rate,

$$-\left(\frac{\partial c}{\partial v}\right)_V = \rho\left(\frac{\partial q}{\partial v}\right)_v + \epsilon\left(\frac{\partial c}{\partial v}\right)_v \quad \text{- - - - - - -(3-7)}$$

To simplify Equation 3-7 it is then convenient to replace the influent volume, V, by that volume, V-vϵ , which has passed through the cross section containing the adsorbent. By a fundamental property of derivatives for functions of functions or implicit functions (24)

$$-\left(\frac{\partial c}{\partial v}\right) = -\left(\frac{\partial c}{\partial v} \cdot \frac{\partial v}{\partial v} + \frac{\partial c}{\partial v}\cdot\frac{\partial v}{\partial v}\right) \quad \text{- - - - (3-8)}$$

or, upon substitution

$$-\left(\frac{\partial c}{\partial v}\right) = -\left[\frac{\partial c}{\partial v} \cdot \frac{\partial v}{\partial v} + \frac{\partial c}{\partial (V-v\epsilon)} \cdot \frac{\partial (V-v\epsilon)}{\partial v}\right] \quad \text{- (3-9)}$$

which yields

$$-\left(\frac{\partial c}{\partial v}\right)_V = \left(\frac{\partial c}{\partial (V-v\epsilon)}\right)_v - \left(\frac{\partial c}{\partial v}\right)_{V-v\epsilon} \quad \text{- - - - - (3-10)}$$

Equation 3-7 thus simplifies to

$$-\left(\frac{\partial c}{\partial v}\right)_{V-v\epsilon} = \rho\left(\frac{\partial q}{\partial (V-v\epsilon)}\right)_v \quad \text{- - - - - - - - - (3-11)}$$

Hiester and Vermeulen (23) have defined a dimensionless group involving v which is related simply to the time parameter T. This relationship, termed the column-capacity parameter, s, is defined as

$$s = \frac{K v \epsilon}{F} \quad - - - - - - - - - - - - - (3\text{-}12)$$

The term K in Equation 3-12 is a general rate coefficient which can be related to both the kinetic and diffusion rate developments.

METHOD OF SECOND-ORDER KINETICS

In accord with the original derivation of Thomas (53), the following schematic reaction scheme for physical adsorption can be considered.

$$\text{Sorbate} + \text{Sorbent} \underset{k}{\overset{k'}{\rightleftharpoons}} \text{Sorbate} \cdot \text{Sorbent} \; - \; (3\text{-}13)$$

Assuming a Langmuir-type adsorption equilibrium (62, 65) an expression for the rate of adsorption at the solid surfaces may be given as

$$\frac{d(\text{Sorbate} \cdot \text{Sorbent})}{dT} = \Big[k\,(\text{sorbate})(\text{sorbent}) - k'(\text{sorbate} \cdot \text{sorbent}) \Big]$$

or,

$$\frac{d(\text{Sorbate} \cdot \text{Sorbent})}{dT} = k \Big[(\text{sorbate})(\text{sorbent}) - (1/b)(\text{sorbate} \cdot \text{sorbent}) \Big] \; - \; (3\text{-}14)$$

where b, (k/k') is the Langmuir equilibrium constant relating to the energy of adsorption (in units of cm^3/mole), k is the rate factor for second-order surface-reaction-controlled kinetics (in units of cm^3/mole/min), and k' is the rate constant for the reverse of desorption reaction (cm^3/mole/min).

If the ultimate monolayer capacity of the adsorbent for the adsorbate is designated by the term Q (in units of moles/gram), then $q = Qbc/(1+bc)$, and $(Q-q)$ represents the unused capacity of the adsorbent. Substitution into Equation 3-14 yields

$$\frac{\partial q}{\partial T} = k\left[C(Q-q) - (1/b)q\right] \quad \text{- - - - - - - -(3-15)}$$

The saturation capacity, q_∞ , of the adsorbent is defined as that amount of solute which has been taken up when the adsorbent has attained equilibrium with the concentration of solute, C_o, in the influent solution. By setting $dq/dT = 0$ and $C = C_o$ in Equation 3-15, the saturation capacity is given as

$$q_\infty = \frac{QbC_o}{1+bC_o} \quad \text{- - - - - - - - - - - - - - -(3-16)}$$

Equation 3-15 may then be expressed more meaningfully in terms of the saturation capacity, q_∞ , rather than in terms of the Langmuir monolayer capacity, Q,

$$\frac{d(q/q_\infty)}{d\left[k\left\{1/(1/b+C_o)\right\}\mathcal{T}\right]} = \frac{C}{C_o} - \left[\frac{bC_o}{1+bC_o}\right]\frac{C}{C_o}\cdot\frac{q}{q_\infty} - \left[\frac{1}{1+bC_o}\right]\frac{q}{q_\infty} \quad - \text{(3-17)}$$

Equation 3-17 can be simplified by introduction of the dimensionless adsorption parameters, r, the equilibrium modulus,

$$r = \frac{1}{1+bC_o} = 1 - \frac{q_\infty}{Q} \quad \text{- - - - - - - - (3-18)}$$

and t, the solution-capacity modulus,

$$\begin{aligned} t &= k\left[\frac{1}{b} + C_o\right]\left[\mathcal{T} - \frac{v\,\epsilon}{F}\right] \\ &= k\left[\frac{1}{b} + C_o\right]\left[\frac{V - v\,\epsilon}{F}\right] \end{aligned} \quad \text{- - - - - - - - - (3-19)}$$

In column operation, $\mathcal{T}$ is the time measured from the first entry of saturating fluid into the column. This time must be corrected by subtracting the time, $v\,\epsilon/F$, required to fill the void space in the expanded bed. The correction, however, may be neglected if it is small relative to the total time required for saturation of the adsorbent. By substitution of C_o as defined in Equation 3-16 into Equation 3-19, the latter expression may be transformed to yield

$$t = k\,C_o\left[\frac{Q}{q_\infty}\right]\left[\frac{V - v\,\epsilon}{F}\right] \quad \text{- - - - - - - (3-20)}$$

Further, Equation 3-20 may be generalized by introducing the rate coefficient, K (refer to Equation 3-12), to yield (23)

$$t = \frac{K}{D_G} \cdot \frac{V - v\epsilon}{F} \qquad \text{- - - - - - - - - - (3-21)}$$

The term D_G in Equation 3-21 is a dimensionless coefficient which defines the limiting distribution of solute between solution and adsorbent phases,

$$D_G = q_\infty \rho \, / \, C_o \epsilon \qquad \text{- - - - - - - - (3-22)}$$

For the case of second-order kinetics, K and k are related by the expression

$$k \cdot \frac{Q}{q_\infty} = \frac{K\epsilon}{q_\infty \rho} \qquad \text{- - - - - - - - - - (3-23)}$$

By substitution of the dimensionless equilibrium and solution-capacity moduli r and t, respectively, Equation 3-17, written for any given cross-section of the column corresponding to a bulk volume, v, upstream, becomes (53)

$$\left[\frac{d(q/q_\infty)}{dt}\right]_v = \frac{c}{C_o}\left[(1 - q/q_\infty)\right] - r\,\frac{q}{q_\infty}\left[1 - \frac{c}{C_o}\right] \qquad \text{- - (3-24)}$$

Comparison of Equation 3-12 with Equations 3-20 and 3-23 shows that the column capacity parameter, s, may be related to the solution capacity modulus, t, by the expression

$$\frac{t}{s} = \frac{C_o(V - v\epsilon)}{q_\infty \rho\, v} = \frac{(V - v\epsilon)}{D_G v\epsilon} \qquad \text{- - - - - - - - (3-25)}$$

where $C_o(V - v\epsilon)$ is the total quantity of solute which was originally contained in that volume of solution which has passed through the column, and $\{q_\infty \cdot \rho \cdot v\}$ is equivalent to the total quantity of solute which has been retained by the adsorbent at the point of saturation; their quotient is thus a simple stoichiometric ratio.

Equation 3-11, the conservation of mass equation, may be simplified by multiplying the left and right elements by (C/C_o) and (q/q_∞), respectively, which yields

$$-\left[\frac{\partial(C/C_o)}{\partial v}\right]_{V-v\epsilon} = \frac{\rho q_\infty}{C_o}\left[\frac{\partial(q/q_\infty)}{\partial(V-v\epsilon)}\right]_v \text{ - - -(3-26)}$$

By substitution of the parameters v in terms of s (Equation 3-12 and $V-v\epsilon$ in terms of t (Equation 3-21) the above relation may be rewritten in the simple form

$$-\left[\frac{\partial(C/C_o)}{\partial s}\right]_t = \left[\frac{\partial(q/q_\infty)}{\partial t}\right]_s \text{ - - - - - - - - (3-27)}$$

The rate equation (Equation 3-24) and the conservation of mass equation (Equation 3-27) together provide a description of the mass transfer process sufficient to permit a mathematical solution. These equations may be integrated, subject to the appropriate boundary conditions, as described by Thomas (52).

Equation 3-27 ensures the existence of a function of s and t, f(s,t), such that

$$df = -(C/C_o)\,dt + (q/q_\infty)\,ds \text{ - - - - -(3-28)}$$

with

$$\begin{aligned} C/C_o &= -\partial f/\partial t \\ q/q_\infty &= \partial f/\partial s \end{aligned} \qquad \text{- - - - - - - - - - - - - - - - (3-29)}$$

The corresponding differential equation for the mass transfer process, governed by second order kinetics, becomes (52)

$$\frac{\partial^2 f}{\partial s\,\partial t} + A\cdot\frac{\partial f}{\partial s} + B\cdot\frac{\partial f}{\partial t} + C\cdot\frac{\partial f}{\partial s}\cdot\frac{\partial f}{\partial t} = 0 \quad \text{- (3-30)}$$

where

$$A = \frac{k'}{F}, \quad B = \frac{kQ}{F}, \quad C = -\frac{k}{F} \qquad \text{- - - - - - - - - - (3-31)}$$

Two additional constants are defined since they are required in the application of Equation 3-30, (52)

$$a = \frac{kC_o+k'}{F}, \quad b = \frac{1}{F}\,\frac{kk'Q}{kC_o+k'} \qquad \text{- - - - - - - - -(3-32)}$$

such that $AB = ab$

By making the substitution of a logarithmic expression including a new function of s and t, $\Phi(s,t)$, (52)

$$Cf = \ln\left[\exp - (Bs + At)\ \Phi(s,t)\right] \text{- - - -} \quad \text{(3-33)}$$

one obtains the linear equation

$$\frac{\partial^2 \Phi}{\partial s\,\partial t} = AB\,\Phi \qquad \text{- - - - - - - - (3-34)}$$

In the case of Equation 3-30 the expressions 3-29 yield the following formulae for the calculation of the concentrations

$$c = \frac{1}{C}\left[A - \frac{\partial \ln \Phi}{\partial t}\right]$$

$$q = -\frac{1}{C}\left[B - \frac{\partial \ln \Phi}{\partial s}\right] \quad \text{- - - - - - - - - - - (3-35)}$$

The boundary values are specified as

$$s = 0, \quad t \geq 0, \quad C/C_o = 1$$

$$s \geq 0, \quad t = 0, \quad q/q_\infty = 0 \quad \text{- - - - - - - - - - (3-36)}$$

The corresponding boundary conditions of Φ follow from Equation 3-35. Using the condition on the concentration in solution at the input of the column, one finds

$$\frac{\partial \ln \Phi(o,t)}{\partial t} = A - C \cdot C_o = \frac{kC_o + k'}{F}$$

or

$$\frac{\partial \ln \Phi(o,t)}{\partial t} = \partial$$

integrating

$$\Phi(o,t) = \exp(\partial \cdot t) \quad \text{- - - - - - - - - - (3-37)}$$

Similarly, from the equation determining q, one has

$$\frac{\partial \ln \Phi(s,o)}{\partial s} = B$$

or upon integration

$$\Phi(s,o) = \exp(B \cdot s) \quad \text{- - - - - - - - - (3-38)}$$

Thomas (52) applied the Riemann procedure which led directly to the solution of Equation 3-24 under the boundary conditions (Equation 3-37 and 3-38). Because of the symmetry of the differential equation the required Riemann function is $I_0(2\sqrt{A\cdot B\cdot(s-\xi)(t-\eta)})$, in which ξ and η are the variables of integration around the boundary. I_0 is the zeroth order Bessel function for purely imaginary argument. The solution for Φ is

$$\Phi(s,t) = I_0(2\sqrt{A\cdot B\cdot st}) + \int_0^s B\,e^{B\xi}\,I_0\left|2\sqrt{A\cdot B\cdot t(s-\xi)}\right|d\xi + \int_0^t a\,e^{a\eta}\,I_0\left|2\sqrt{a\cdot b\cdot t(t-\eta)}\right|d\eta \quad - - - - (3\text{-}39)$$

Solution of the above equation is facilitated by setting down properties of the integrals in Equation 3-39. Writing (52),

$$\Psi(y,z) = e^{y}\int_0^{y} e^{-w}\,I_0(2\sqrt{zw})\,dw$$

where w, y, and z are dummy variables, the solution is seen to be

$$\Phi(s,t) = I_0(2\sqrt{A\cdot B\cdot st}) + \Psi(B\cdot s,\ A\cdot t) + \Psi(a\cdot t,\ b\cdot s) \quad - - -(3\text{-}40)$$

After expanding the Bessel function in power series, rearranging the absolutely and uniformly convergent series, and integrating term-wise by parts (52), one finds

$$\Psi(y,z) = e^{y+z} - \sum_{0\le m\le n}^{\infty} \frac{y^m z^n}{m!n!} = \sum_{0\le n<m}^{\infty} \frac{y^m z^n}{m!n!} \quad - - - - - -(3\text{-}41)$$

Since,

$$I_0(2\sqrt{yz}) = \sum_{0}^{\infty} \frac{(yz)^n}{n!n!} = \sum_{0\le n\le m}^{\infty} \frac{y^m z^n}{m!n!} \quad - - - - - -(3\text{-}42)$$

one obtains the relation

$$\Psi(y,z) + \Psi(z,y) = e^{y+z} - I_0(2\sqrt{yz}) \text{ - - - - } (3\text{-}43)$$

On differentiation of the double series for Ψ one finds (52)

$$\frac{\partial \Psi(y,z)}{\partial y} = \Psi(y,z) + I_0(2\sqrt{yz}) \text{ - - - - - - } (3\text{-}44)$$

Making use of Equations 3-43 and 3-44 one finds

$$\frac{\partial \Psi(y,z)}{\partial z} = \Psi(y,z) - \frac{\partial}{\partial z} I_0(2\sqrt{yz}) \text{ - - - - -} (3\text{-}45)$$

Further, the limiting values of the integral are

$$\left.\begin{aligned} \Psi(0,z) &= 0 \\ \Psi(y,0) &= e^{y}-1 \end{aligned}\right. \text{ - - - - - - - - - - } (3\text{-}46)$$

By means of the preceding formulas the calculation of C from Equation 3-46 is easily carried out. The resulting equation is

$$\frac{C}{C_0} = \frac{I_0(2\sqrt{A\cdot B\cdot st}) + \Psi(\partial t, bs)}{I_0(2\sqrt{A\cdot B\cdot st}) + \Psi(Bs, At) + \Psi(\partial t, bs)} \text{ - -} (3\text{-}47)$$

In order to utilize the solutions advanced by Thomas for design calculations, Hiester and Vermeulen (23) have substituted the three dimensionless groups (r, s, and t) for the parameters used by Thomas and have expressed all of the solutions in terms of a function, J, for which calculation methods are readily available. The function $J(y,z)$ is related to Thomas' function $\Psi(y,z)$ in the following manner

$$J(y,z) = 1 - \left[\exp-(z+y)\right] \Psi(y,z) \text{ - - - - - - } (3\text{-}48)$$

which yields the following solution

$$\frac{C}{C_o} = \frac{J(rs,t)}{J(rs,t)+\left[\exp(r-1)(t-s)\right]\left[1-J(s,rt)\right]} \quad ---(3\text{-}49)$$

For evaluation of Equation 3-49, J(y,z) must be known very accurately. Thomas (53) has tabulated a solution after Onsager which reduces to

$$J(y,z) = \tfrac{1}{2}\left\{1-\mathrm{erf}(\sqrt{y}-\sqrt{z})+\frac{\exp-(\sqrt{y}-\sqrt{z})^2}{\sqrt{\pi}\left[\sqrt{z}+\sqrt[4]{yz}\right]}\right\} \quad -(3\text{-}50)$$

Substitution of Equation 3-50 into the relation for C/C_o yields the solution for the ratio of the concentration of solute in the effluent stream to the initial concentration in the influent stream in terms of the three dimensionless parameters r, s, and t. This equation, which enables one to numerically evaluate the quantity C/C_o, may be represented as

$$\frac{C}{C_o} = \left[\frac{\sqrt{\pi}\left[1-\mathrm{erf}(\sqrt{rt}-\sqrt{s})\right] \ \exp\ (\sqrt{rt}-\sqrt{s})^2-\left[\dfrac{1}{(\sqrt{rt}+\sqrt[4]{rst})}\right]}{\sqrt{\pi}\left[1-\mathrm{erf}(\sqrt{rs}-\sqrt{t})\right] \ \exp\ (\sqrt{rs}-\sqrt{t})^2+\left[\dfrac{1}{(\sqrt{t}+\sqrt[4]{rst})}\right]}+1\right]^{-1} \quad -(3\text{-}51)$$

Simplification of Equation 3-51 may be accomplished under certain conditions. If the absolute value of the argument $(\sqrt{y}-\sqrt{z})$ exceeds 7, the absolute value of the error function approaches unity and the approximations may be applied within 1% accuracy. Thus if

$$(\sqrt{y}-\sqrt{z}) > 7 \qquad \text{- - - - - - - - - - (3-53)}$$

then

$$\sqrt{\pi}\left[1-\mathrm{erf}(\sqrt{y}-\sqrt{z})\right]\ \exp(\sqrt{y}-\sqrt{z})^{2} = 1/(\sqrt{y}-\sqrt{z}) \text{- -(3-54)}$$

or, if

$$(\sqrt{y}-\sqrt{z}) < -7 \qquad \text{- - - - - - - - - - (3-55)}$$

then

$$\sqrt{\pi}\left[1-\mathrm{erf}(\sqrt{y}-\sqrt{z})\right]\ \exp(\sqrt{y}-\sqrt{z})^{2} =$$
$$2\sqrt{\pi}\exp(\sqrt{y}-\sqrt{z})^{2} \qquad \text{- - - - -(3-56)}$$

Either the numerator or the denominator of Equation 3-51 or in some cases both, may reduce by these means.

Also, as r tends toward zero, and s and t are large enough so that $(\sqrt{rt}-\sqrt{s})$ and $(\sqrt{rs}-\sqrt{t})$ each become less than -7, Equation 3-51 becomes

$$\frac{C}{C_o} = \left\{\exp\left[(\sqrt{rt}-\sqrt{s})^{2} - (\sqrt{rs}-\sqrt{t})^{2}\right]+1\right\}^{-1}$$

or

$$\frac{C}{C_o} = \left\{\exp\left[(r-1)(t-s)\right]+1\right\}^{-1} \qquad \text{- - - - - - (3-57)}$$

Conversely, as r becomes very large so that $(\sqrt{rt}-\sqrt{s})$ and $(\sqrt{rs}-\sqrt{t})$ are each greater than +7, Equation 3-54 may be used, and Equation 3-51 becomes

$$\frac{C}{C_o} = \left\{\left[(\sqrt{r}-\sqrt{t/s})\ /\ (r\sqrt{t/s}-\sqrt{r})\right]+1\right\}^{-1} \qquad (3\text{-}58)$$

These simplifying equations, used when the required conditions are satisfied, considerably shorten the computation time required and facilitate calculation of the S-shaped concentration-time profiles.

MECHANISM AND RATE OF MOLECULAR TRANSFER

As indicated previously, the overall rate of adsorption may be limited by film diffusion, pore diffusion, surface diffusion, or reaction with the solid surfaces of the adsorbent. The effective rate of adsorption evidently will in most instances be controlled chiefly by one or two resistances. Neglect of all but the rate-limiting resistance, or combination of all resistances into one effective step with a single rate parameter, are two alternative techniques by which one can considerably simplify the mathematical solution of the mass transfer equations.

It will be demonstrated that the diffusion equations for mass transfer are closely related to Thomas' kinetic equations and that numerical results suitable for design calculations can be obtained by way of this close relation ship. Even though the rate-limiting step may be one of film or pore diffusion, these operations may be described in terms of second-order kinetic processes; the materials adsorbed on the solid surfaces may be considered either to have become closely associated with the solid phase or to have undergone chemical reaction with it.

Surface Reaction

For purpose of this analysis it will be assumed that actual adsorption at the surface of the adsorbent is an extremely rapid process relative to the diffusion processes involved, thus, resistance due to this step may be neglected. The validity of this assumption has been adequately confirmed by the data of Vassiliou and Dranoff (56) and Weber and Morris (64) and by circumstantial evidence of Masamune and Smith (37).

External Diffusion

External diffusion or film transport is defined as the transfer of solute from bulk solution through the stagnant layer of fluid immediately adjacent to the external surfaces of the adsorbent. Film transport is governed by molecular diffusion and, in turbulent flow, by eddy diffusion, which controls the effective thickness of the laminar boundary layer. One may logically assume that the concentration of solute at the point in the hydrodynamic boundary layer immediately adjacent to the external surface of the particle is in equilibrium with the average solid-phase concentration on the internal surfaces. This condition may be stated algebraically as

$$\left[\frac{dq}{d\tau}\right]_f = k_f \, a\left(\frac{\epsilon}{\rho}\right) \, (C-C_e) \quad \text{- - - - - - - - - - -} \quad (3\text{-}59)$$

where k_f is the mass transfer coefficient for the case in which film diffusion is the rate-limiting step, (cm/min.); a, the effective area for mass transfer across the fluid film, (cm^2/cm^3); and C_e, the concentration of solute in the fluid phase in equilibrium with the coexisting solid-phase concentration, ($moles/cm^3$).

The net rate of surface reaction given in Equation 3-17 may be set equal to zero, which yields the following equilibrium relation:

$$C_e = \frac{qC_o}{q_\infty \cdot (1+bC_o) - bqC_o} \quad - - - - - - - - - - - (3\text{-}60)$$

If r is given by Equation 3-18, Equations 3-59 and 3-60 will combine to give

$$\left[\frac{dq}{d\tau}\right]_f = \frac{k_f\ a(\frac{\epsilon}{\rho})}{q_\infty\left[1+(r-1)q/q_\infty\right]}\left[C(q_\infty - q) - rq(C_o - C)\right] \quad - (3\text{-}61)$$

Equation 3-61 for the case in which film diffusion controls the rate of mass transport may be observed to have a form similar to the general rate expression set forth previously in Equation 3-17. An effective external-diffusion rate constant, K_f, may then be introduced, by reference to Equation 3-23, thus facilitating the use of Equation 3-51 for numerical solutions of the breakthrough curves. The rate constant, K_f, for external diffusion is given by the relationship (23)

$$\frac{K_f \epsilon}{q_\infty \cdot \rho} = k_f a \, \epsilon / q_\infty \cdot \rho \left[1 + (r-1)(q/q_\infty)_{av} \right] \quad - - - \; (3\text{-}62)$$

or

$$K_f = \frac{k_f a}{1 + (r-1)(q/q_\infty)_{av}} \quad - - - - - - - - - \; (3\text{-}63)$$

When the complete concentration-time profiles are to be calculated, the average value of $(q/q_\infty)_{av}$ may be taken as 0.5 if $r<1$, as shown by Vermeulen (58) for the favorable equilibrium condition; then,

$$K_f = \frac{2k_f a}{r+1} \;, \quad r < 1 \quad - - - - - - - - (3\text{-}64)$$

This rate coefficient, K_f, may then be used for numerical solution of Equation 3-51, which will yield adsorption curves for the external-diffusion-limited case.

Internal Diffusion

Internal diffusion controls the transfer of solute from the exterior of the porous adsorbent to the interior surfaces of the adsorbent particle (67). As discussed previously, two types of internal diffusion may operate within the pores of the particles; the contribution of each to the overall rate of internal diffusion being determined by the conditions of operation. The first, termed pore diffusion, occurs through the fluid phase contained in the pore spaces of the nonhomogeneous adsorbent particles. The second case, indicated by Glueckauf and Coates (16), is a two-dimensional diffusion along the pore boundaries of a particle consisting of impervious crystallites separated by pore spaces that are accessible to the solute. This type of internal diffusion is commonly called pore-surface diffusion. Of the two the more rapid will control the rate of transport, since they act in parallel.

Fluid-Phase Pore Diffusion

If one considers a differential spherical shell, illustrated in Figure 3-4, of radius R and thickness dR, then on equating inflow minus outflow by diffusion to the rate of accumulation in the shell, as outlined by Kasten and Amundson (25), there results

$$\gamma\left[(-D_p \cdot \frac{\partial c_i}{\partial R}) 4\pi R^2 dR\right] - \gamma\left[(-D_p \cdot \frac{\partial c_i}{\partial R}) 4\pi R^2 dR + \frac{\partial\left(-D_p \frac{\partial c_i}{\partial R} 4\pi R^2\right)}{\partial R} \cdot dR\right]$$

$$-\rho\left[\frac{\partial q_i}{\partial \tau} 4\pi R^2 dR\right] = \gamma\left[\frac{\partial c_i}{\partial \tau} 4\pi R^2 dR\right] \quad - - (3\text{-}65)$$

where the subscript i designates the interior of the particle. This reduces to

$$\frac{D_p}{R^2} \cdot \left[\frac{\partial\left(\frac{\partial c_i}{\partial R} \cdot R^2\right)}{\partial R}\right] - \frac{\rho}{\gamma} \cdot \frac{\partial q_i}{\partial \tau} = \frac{\partial c_i}{\partial \tau} \quad - - -(3\text{-}66)$$

and, upon differentiation, be expressed as

$$D_p \cdot \left[\frac{\partial^2 c_i}{\partial R^2} + \frac{2}{R} \frac{\partial c_i}{\partial R}\right] = \frac{\partial c_i}{\partial \tau} + \frac{\rho}{\gamma} \frac{\partial q_i}{\partial \tau} \quad - - -(3\text{-}67)$$

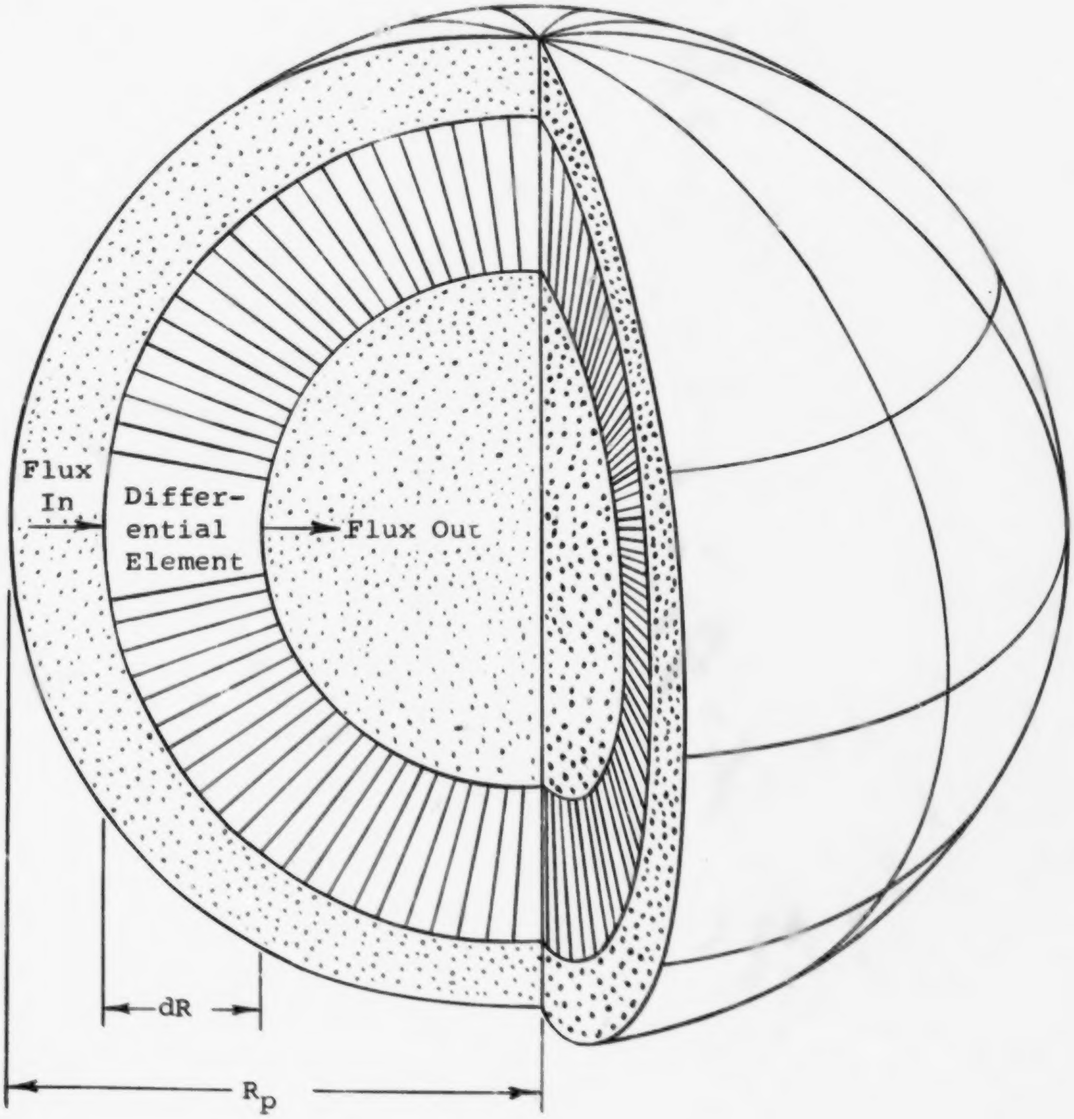
Flux In
Differential Element
Flux Out
dR
R_p

FIGURE 3-4

DIFFERENTIAL SPHERICAL SHELL OF ADSORBENT PARTICLE where D_p is the diffusivity of the solute in the fluid contained within the pore (cm^2/sec); γ is the intraparticle void volume (dimensionless); the remaining variables have been previously defined. The mean concentration of the entire particle, of total radius R_p, is

$$q = \frac{3}{R_p^3} \int_0^{R_p} q_i \, R^2 \, dR \quad - - - - - - - - - - -(3\text{-}68)$$

where q_i is the solid-phase concentration of solute at radius R.

Isotherms for pollutants commonly encountered in wastewaters frequently approach the condition of irreversibility. For this case the fluid-phase concentration of solute in the pores may be assumed negligible compared to the solid-phase value. Equation 3-67 then becomes

$$\frac{D_p}{R^2} \left[\frac{\partial \left(\frac{\partial c_i}{\partial R} \cdot R^2 \right)}{\partial R} \right] = \frac{\rho}{\gamma} \cdot \frac{\partial q_i}{\partial \tau} \quad - - - - - -(3\text{-}69)$$

Differentiation of Equation 3-68 gives

$$\frac{\partial}{\partial R} \left[\frac{dq}{d\tau} \right] = \frac{3R^2}{R_p^3} \left[\frac{\partial q_i}{\partial \tau} \right] \quad - - - - - - - - - -(3\text{-}70)$$

and combination of Equations 3-69 and 3-70 yields

$$\left[\frac{dq}{d\tau} \right]_p = \frac{3 D_p R^2 \gamma}{\rho \, R_p^3} \left[\frac{\partial c_i}{\partial R} \right] \quad - - - - - - - - (3\text{-}71)$$

This equation relates the rate of uptake to the radial concentration gradient of the solute within the particle. If the extent of saturation is averaged over the entire particle, then one may logically express the radial gradient in terms of the concentration difference $(C-C_e)$, where C is the bulk solution concentration (moles/cm^3) and C_e is the concentration of solute in the fluid-phase in equilibrium with the average solid-phase concentration on the internal surfaces of the adsorbent particle (moles/cm^3) (25). The rate of uptake may then be expressed algebraically as

$$\left[\frac{dq}{d\tau}\right]_p = k_p a \left(\frac{\gamma}{\rho}\right)(C-C_e) \qquad \text{- - - - - - - - (3-72)}$$

where k_p is the mass transfer coefficient for the case in which fluid-phase pore diffusion controls the rate of mass transport.

It is to be noted that Equation 3-72 is similar in form to the rate expression for the case where the rate step is limited by film diffusion (Equation 3-59). The difference between the two lies in the fact that in the film-diffusion-limited case a concentration gradient exists across a hydrodynamic boundary layer surrounding the particle; whereas, in the case in which fluid-phase pore diffusion limits the rate of uptake a concentration gradient across the external laminar boundary layer does not exist, but is set up strictly within the pores of the adsorbent particle.

Equation 3-72 may then be rearranged to a form similar to that of Equation 3-61 as follows,

$$\left[\frac{dq}{d\tau}\right]_p = \frac{k_p a \left(\dfrac{\gamma}{\rho}\right)}{q_\infty\left[1+(r-1)q/q_\infty\right]}\left[C(q_\infty - q) - rq(C_o - C)\right] \text{ - -(3-73)}$$

Again, this equation is seen to have a form similar to the rate expression for the case of second-order kinetics, Equation 3-17. By reference to Equation 3-23, a fluid-phase pore-diffusion rate parameter, $\mathcal{K}_p$, may be introduced. This is given by

$$\mathcal{K}_p = \frac{k_p a}{1+(r-1)(q/q_\infty)_{av}} \text{ - - - - - - - - -(3-74)}$$

If $r < 1$, the average value for (q/q_∞) may be approximated by 0.5, which simplifies Equation 3-74 to

$$\mathcal{K}_p = \frac{2k_p a}{r+1}, \quad r<1 \text{ - - - - - - - - (3-75)}$$

Concentration-time profiles for cases in which fluid-phase pore transport is rate limiting may be calculated by use of the rate coefficient, $\mathcal{K}_p$, and Equation 3-51, which gives a numerical solution for the mass transfer process in fluid-bed columns of activated carbon.

Solid-Phase, Pore-Surface Diffusion

An expression for the rate of solid-surface diffusion, a two-dimensional diffusion occurring after phase change along the surfaces of the pore boundaries, may be developed in a manner similar to that for the case in which fluid-phase pore diffusion is the rate-determining mechanism. The resulting relation is given by (38)

$$D_s \left[\frac{\partial^2 q_i}{\partial R^2} + \frac{2}{R} \cdot \frac{\partial q_i}{\partial R} \right] = \frac{\partial q_i}{\partial \tau} \quad \text{- - - - - -}(3\text{-}76)$$

where D_s is the solid-phase diffusivity of solute along the surfaces of the pores (cm^2/second). In the derivation of this relation the concentration of solute in the boundary layer surrounding the particle was assumed to be equivalent to that in the bulk solution in contact with the boundary layer. In additon, the degree of saturation of each particle is averaged over the entire particle.

Glueckauf and Coates (16) and Michaels (40) were the first to use the linear-driving-force relation as an approximation to Equation 3-76. In this connection the rate of approach to complete saturation is taken to be proportional to the difference between the extent of saturation at the outer surface of the particle and the average extent of saturation within the particle. This condition is given by

$$\left[\frac{dq}{d\tau} \right]_s = k_s a' \; (q_e - q) \quad \text{- - - - - - - -} \; (3\text{-}77)$$

where q_e is the local concentration of solute in the solid-phase that prevails at the outer surface and is assumed to be in equilibrium with the coexisting liquid phase at concentration C. The surface concentration of solute is given by the following relation, derived from Equation 3-24 for a zero net rate of reaction,

$$q_e = \frac{q_\infty C}{(1-r)C+rC_o} \quad \text{- - - - - - - - - (3-78)}$$

Substitution of this expression into Equation 3-77 yields

$$\left[\frac{dq}{d\tau}\right]_s = \frac{k_s a'}{(1-r)C+rC_o} \left[C(q_\infty - q) - rq(C_o - C)\right] \text{- - (3-79)}$$

Equation 3-79 for solid-surface diffusion, like the corresponding relationships for external diffusion and pore diffusion, (Equations 3-61 and 3-73, respectively), assumes the same form as that for the reaction-controlled case if the following approximate substitution is made

$$\frac{K_s}{q_\infty \rho} = \frac{k_s a'}{(1-r)C+rC_o} \quad \text{- - - - - - - - -(3-80)}$$

which upon substitution of Equation 3-22 for D_G and upon rearrangement yields,

$$K_s = \frac{k_s a' \ D_G}{(1-r)(C/C_o)_{av}+r} \quad \text{- - - - - - - (3-81)}$$

Again, if the entire adsorption wave is of interest, 0.5 C_o is a permissible value for C, and,

$$\kappa_s = \frac{2k_s a' D_G}{(r+1)} \qquad \text{- - - - - - - - - - - -(3-82)}$$

The rate coefficient for solid-surface diffusion, κ_s, may be used with Equation 3-51 for calculating concentration-time profiles for cases in which solid-phase diffusion along the surfaces of the pores is distinctly the rate-limiting step, just as κ_f and κ_r may be used to obtain numerical results for cases in which film transport and pore diffusion, respectively, are clearly rate-limiting.

Combined External and Internal Diffusion

For cases in which external (film) diffusion and internal (pore or solid-surface) diffusion occur in series at comparable rates, it has been shown (27) that the respective mass transfer coefficients, each measured individually under circumstances for which the alternative resistance is either absent or has been suppressed, may be added in the following manner

$$\frac{1}{\kappa} = \frac{1}{\kappa_f} + \frac{1}{\kappa_p} \qquad \text{- - - - - - - - - - - - (3-82)}$$

or,

$$\frac{1}{\kappa} = \frac{1}{\kappa_f} + \frac{1}{\kappa_s} \qquad \text{- - - - - - - - - - - - (3-83)}$$

Since pore diffusion and solid-surface diffusion occur in parallel, the more rapid of the two will limit the rate of internal diffusion. Only one of the two resistances, therefore, may enter into the series relationship governing combined external and internal diffusion, unless both occur at comparable rates. If pore diffusion is the limiting internal diffusion mechanism, Equation 3-82 is used to express the combined resistance; while Equation 3-83 is utilized to describe the overall rate coefficient, $\mathcal{K}$, for the case in which solid-surface diffusion is more rapid than pore transport.

Substituting for $\mathcal{K}_f$ and $\mathcal{K}_p$, Equations 3-63 and 3-74, respectively, into Equation 3-82 one obtains

$$\frac{1}{\mathcal{K}} = \frac{1+(r-1)(q/q_\infty)}{k_f a} + \frac{1+(r-1)(q/q_\infty)}{k_p a} \quad \text{- - (3-84)}$$

or, from Equations 3-64 and 3-75 for $r<1$,

$$\mathcal{K} = \frac{2}{(r+1)\left[\frac{1}{k_f a} + \frac{1}{k_p a}\right]} \quad \text{- - - - - - - - - (3-85)}$$

Similarly, Equation 3-83 upon substitution of Equations 3-63 and 3-81 transforms to

$$\frac{1}{\mathcal{K}} = \frac{1+(r-1)(q/q_\infty)}{k_f a} + \frac{(1-r)(C/C_0)+r}{k_s a' D_G} \quad \text{- - - - (3-86)}$$

or, from Equations 3-64 and 3-82 for $r<1$,

$$\mathcal{K} = \frac{2}{(r+1)\left[\frac{1}{k_f a} + \frac{1}{k_s a' D_G}\right]} \quad \text{- - - - - - -} \quad (3\text{-}87)$$

where $\mathcal{K}$ is the general rate coefficient for the kinetic case.

Equation 3-87 indicates that film diffusion will control the overall rate when $1/k_f a$ is larger than $1/k_s a' D_G$ because of the greater transport rate in the porous structure of the adsorbent. Since the value for $k_s a'$ is of the same order of magnitude as that for $k_f a$, solid-surface diffusion is predicted to become limiting as D_G approaches unity.

CHAPTER 4

HYDRODYNAMICS OF FLUID-PARTICLE SYSTEMS

GENERAL CONSIDERATIONS

The term, fluidization, is used to designate the fluid-solid contacting process in which a bed of finely divided solid particles is lifted and agitated by a rising stream of fluid. When a liquid passes upward through a bed of solid particulate matter, four general situations may exist depending upon the characteristics of the particles, the geometry of the bed, and the velocity of the fluid. These situations are: (1) fixed bed, (2) dense-phase fluidization, (3) two-phase fluidization, and (4) pneumatic transport (71).

In the fixed bed at low velocity, the passage of fluid up through the bed causes a relatively low pressure drop. The solid particles are essentially undisturbed and the fluid merely percolates through the void space in the bed. Further increase of the fluid velocity causes the bed to expand slightly resulting in greater and greater enlargements of the spaces among the granules. Eventually the pressure drop becomes equal to the weight of bed per unit area and the interparticle spaces become so large that no stable arrangment can exist, and the granules begin to circulate locally. Fluidization is considered to have begun at this point; i.e. incipient fluidization prevails with the creation of a quiescent fluidized bed in which the granular particles are free to circulate in random motion in all directions in a dense phase.

With a further increase in the rate of flow, the smaller particles of the bed are entrained with the fluid and form a dilute phase above the bed. This is a two-phase region. The larger particles form the dense lower phase, while the smaller particles comprise the dilute upper phase. The two-phase condition is relatively unstable and eventually most of the smaller particles are lost from the system. At still higher velocities, the entire bed is entrained with the fluid. This forms a dilute phase suspension termed pneumatic transport.

Dense phase fluidization may be further classified as either "aggregative" or "particulate". Aggregative fluidization is most commonly experienced in systems in which gas is used as the fluidizing medium. This type of fluidization is characterized by channeling or bubbling of fluid pockets through the bed, and slugging in piston-like fashion. Also, clustering and aggregation of particles frequently accompanies gas-phase fluidization. This phenomenon is due, in part, to various electrostatic

(7) and surface forces (29) that serve to bind particles to one another. Water vapor is also a common cause of aggregative fluidization (39,42). Such forces, however, are of minor consequence when the fluidizing medium is a liquid. Particles are thus freer to separate and to remain unattached. Dispersive or particulate fluidization, therefore, is a homogeneous-type of fluidization in which the particles are mono-dispersed in a fluid which is uniformly distributed in the bed. It is desired to make fullest use of the surface area of the granular-activated carbon for the adsorptive mass transfer processes considered in this thesis. Dispersive fluidization appears particularly well suited for this application, as it provides for intimate contact between the surfaces of the granular adsorbent and the supporting fluid.

The relationship between pressure drop and superficial fluid velocity in a bed of particulate matter has been given by Orr (41) and Frantz (11), and is illustrated in Figure 4-1. In the region A-B, the particles remain in the fixed-bed state and the pressure drop is a direct function of the fluid velocity. At point B, the particles become slightly suspended in the fluid stream and gain some freedom of movement. The deviation from linearity between B and C is indicative of movements and

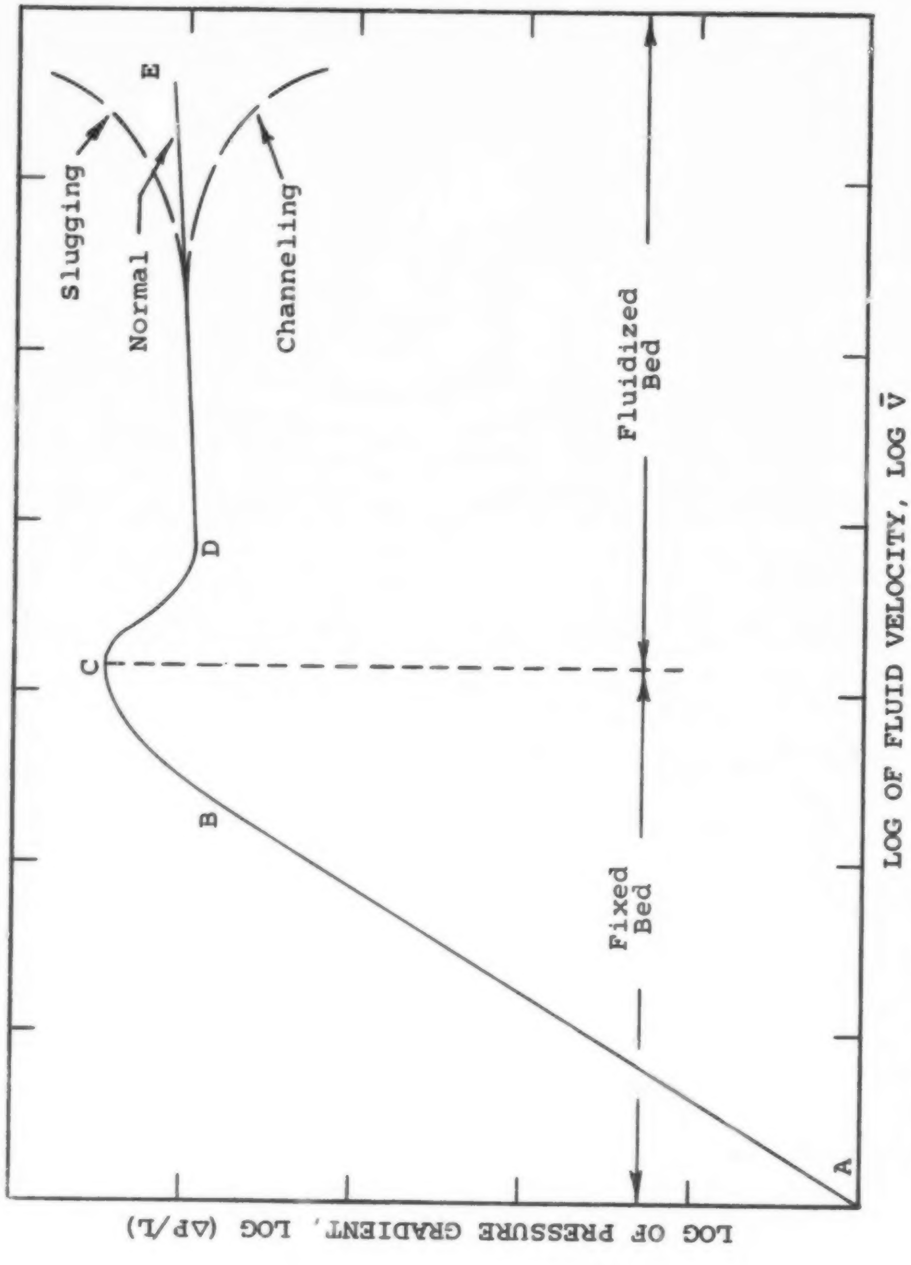

FIGURE 4-1. PRESSURE-DROP/FLOW DIAGRAM FOR TYPICAL FLUIDIZATION

rearrangements within the bed as the particles shift in order to offer the least possible area in the direction of flow. Little, if any, change in the bed's void fraction occurs up to point C. At C, the point of incipient fluidization, fixed-bed behavior terminates. Particles and clusters of particles begin to move continuously, although only a part of the bed may do so initially. Orr (41) has noted that a slight decrease in pressure loss often occurs as indicated between C and D as dynamic conditions develop. He postulates that this results as the particles separate from one another due to a compensation of the cohesive forces among the particles and subsequent decrease of particle interlocking and intermeshing. In a satisfactorily fluidized system, Leva (31) has found that the pressure gradient will rise slightly as the minimum at D is passed, but will not exceed that indicated by point C. In this region D-E, the bed is completely supported by the fluid stream, with the pressure drop approximately equal to the weight of bed per unit area.

If channeling occurs at higher velocities of flow, the pressure loss will not attain the value of C. Instead, the extent of the drop in the pressure gradient is an indication (32,33) of the channeling tendencies of the solids being fluidized. Conversely, if slugging occurs, the pressure loss will fluctuate, and in some instances may well exceed the value indicated by C. Leva (31) attributes the pressure-drop excess over the theoretical value to friction between the slugs of granular solids and the walls of the confining vessel. Pressure-drop fluctuations arise when solid slugs, rising in pistonlike manner between large fluid pockets, reach a certain height and then disintegrate, causing the granular matter to rain through the ascending fluid pocket in the form of smaller aggregates or as distinct particles. The heterogeneity of the fluid-solid distribution of a slugging bed thus, is responsible for oscillations in the pressure-drop velocity relationship.

SINGLE PARTICLE HYDRODYNAMICS

Preparatory to a treatment of the hydrodynamics of a dense-phase fluidized system it is desirable to consider first the motion of rigid single particles in a fluid stream. This is necessitated, since most considerations of multi-particle systems are based on relationships derived for description of the fluid dynamics of single particles moving in an infinite expanse of fluid. Furthermore, the analysis of single-particle dynamics lends itself quite readily to theoretical as well as experimental treatment and thus offers a firm reference point for the study of more complex multiparticle systems. A discussion of single particle motion in a fluid stream will thus ensue, followed by a theoretical consideration of a multiparticle, particulately fluidized system.

When a fluid flows around a submerged body, certain drag forces caused by skin friction and pressure differentials are exerted upon the body. A consideration of these drag forces created by the flow of fluid around a sphere, as depicted in Figure 4-2, is given by Zenz and Othmer (71). It is evident that at point A the fluid is decelerated (accompanied by an increase in pressure in accordance with Bernoulli's theorem); in passing from A to B, the fluid accelerates (resulting in a decreased pressure at point B) and simultaneously dissipates a portion of its energy to overcome the skin friction with the surface of the sphere; in flowing from B to C, the fluid again decelerates and should, accordingly, be accompanied by an increase in pressure to restore it to its original state. Since the fluid is real, its viscosity has caused energy dissipation as skin friction in flowing from A to B, and thus the energy required for restoring the full pressure increase in going from B to C is not available. The fluid must therefore follow a

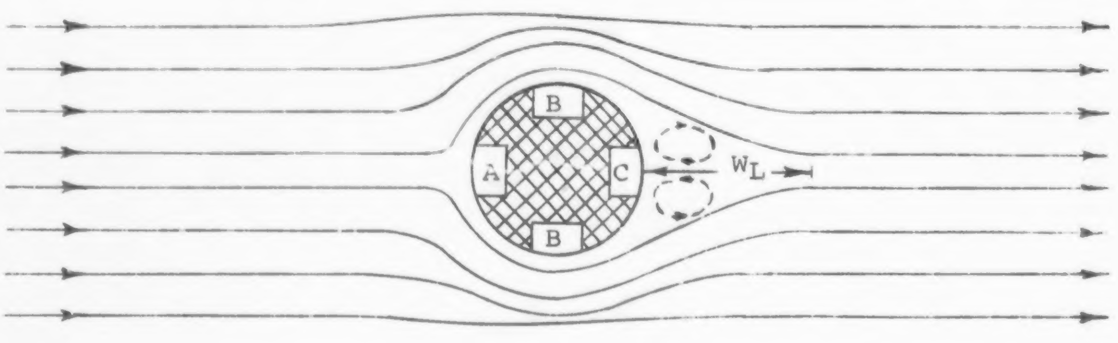

FIGURE 4-2

FLOW STREAMLINES SURROUNDING A SUBMERGED SPHERE flow pattern requiring less deceleration; which results in a separation of the streamlines from the downstream surface at point C. A portion of the fluid is thus drawn into the wake region by reverse flow to form a pocket of fluid termed a vortex. As the Reynolds number increases, the vortex or wake length, W_L, also increases. When the Reynolds number, defined by the diameter of the submerged body, the superficial fluid velocity, and the kinematic viscosity becomes great enough, the vortexes begin to interact and give rise to a turbulent wake. Because the separation of the fluid streamlines occurs in a region of high velocity, or low pressure, the pressure in the turbulent wake will also be low and, in fact, somewhat less than the initial fluid pressure even after subtracting the skin friction, depending on the location of the point of separation in the streamlines. The downstream surface of the submerged body is, therefore, subjected to a low-pressure region, whereas the upstream face of the sphere is subjected to a high-impact pressure. This differential exerts a pressure or form drag on the body in addition to the tangential shear of skin-friction drag. The sum of these drag forces, referred to as total drag, is conventionally expressed in terms of a drag coefficient, C_D, which is correlated with the Reynolds number.

Drag Coefficient of a Sphere

At high relative velocities, $5\times10^2 < N_{Re} < 2\times10^5$, the drag force on an isolated sphere moving in an infinite expanse of stagnant viscous fluid may be defined by Newton's equation

$$F_{DS} = 0.22\,\pi\left(\frac{d_p^{\,2}}{4}\right)\rho_1 v_p^{\,2} \quad \text{--------(4-1)}$$

where F_{DS} is the force exerted on the sphere, (grams); d_p is the diameter of the particle, (cm); ρ_1 is the density of the fluid, (grams/cm^3); and v_p is the velocity of the particle, (cm/sec). This relation accounts mainly for the inertia effect (50). At relatively low velocities, $N_{Re} < 2$, however, Stokes suggested that the inertial effects may be neglected. The resulting drag force obtained by use of his approximation for a symmetric flow field about a sphere is

$$F_{DS} = 3\,\pi\,\mu\, d_p\, v_p \quad \text{------------(4-2)}$$

where μ is the absolute viscosity of the fluid, (centipoise).

With the definition of the drag coefficient, C_D,

$$C_D = \frac{F_{DS}}{A_p\left(\frac{\rho_1 v_p^{\,2}}{2}\right)} \quad \text{------------(4-3)}$$

where A_p, the effective particle cross-sectional area, perpendicular to the direction of motion, is

$$A_p = \frac{\pi d_p^2}{4}$$

One then obtains, for Newton's relation, by use of Equation 4-1

$$C_D = 0.44 \text{ - - - - - - - - - - - - - - - - } (4\text{-}4)$$

and for the Stokes' law regime, using Equation 4-2

$$C_D = \frac{24}{\left(\frac{d_p v_p \rho_1}{\mu}\right)} = 24/N_{Re} \text{ - - - - - - - - - } (4\text{-}5)$$

where

$$N_{Re} = \frac{d_p v_p \rho_1}{\mu}$$

is the Reynolds number for a sphere based on its diameter. For intermediate values of Reynolds number, $2 < N_{Re} < 500$, Bird et. al., (4) relate that it is extremely difficult to make purely theoretical calculations for the drag coefficient, but that an empirical approximation of the form

$$C_D = \frac{18.5}{{N_{Re}}^{3/5}} \text{ - - - - - - - - - - - - - - - } (4\text{-}6)$$

frequently describes experimental data rather well. This indicates a lesser dependence on N_{Re} than in Stokes law.

For the case of free fall of spheres, the sum of the drag force (Equation 4-3) and the buoyancy force is equated to the force of gravity (12,21), which yields

$$F_{DS} = \frac{\pi}{8} C_D \rho_1 d_p^2 \, v_{Po}^2 = V_p \, (\rho_s - \rho_1) g$$

$$= \frac{\pi d_p^3}{6} (\rho_s - \rho_1) g \text{- -(4-7)}$$

where ρ_s is the density of the particle, (grams/cm^3); and g is the gravitational acceleration term, (cm/sec^2). The drag coefficient may then be written as

$$C_D = \frac{4}{3} \; \frac{d_p \, (\rho_s - \rho_1) g}{\rho_1 v_{Po}^2} \text{ - - - - - - - - - - - -(4-8)}$$

At high velocities, where $C_D = 0.44$, the solution for the particle velocity in Newton's regime is

$$\left(v_{Po}\right)_N = \left[3.03 \, \frac{d_p (\rho_s - \rho_1) g}{\rho_1} \right]^{\frac{1}{2}} .$$

$$500 < N_{Re} < 2\text{x}10^5 \text{ - - - - - - - - - - - - - -(4-9)}$$

and at low velocities, where $C_D = 24/N_{Re}$, the expression

$$\frac{24 \mu}{d_p v_{Po} \rho_1} = \frac{4}{3} \; \frac{d_p (\rho_s - \rho_1) g}{\rho_1 \; v_p^2}$$

may be solved for v_p to give the Stokes' law expression for the terminal velocity of a spherical particle

$$\left(v_{po}\right)_S = \frac{d_p^{\,2}(\rho_s-\rho_1)g}{18\mu}, \quad N_{Re} < 2 \text{ - - - - -(4-10)}$$

Similarly, for the intermediate regime, where C_D is aproximated by Equation 4-6, the particle velocity may be expressed as

$$\left(v_{po}\right)_I = \frac{0.153 d_p^{\,1.14}(\rho_s-\rho_1)^{0.71} g^{\,0.71}}{\rho_1^{\,0.29} \cdot \mu^{0.43}},$$

$$2 < N_{Re} < 500 \text{ - - - - - - - - - - - - - - -(4-11)}$$

Effect of Particle Shape on Drag Coefficient

For non-spherical particles of any arbitrary shape the diameter in Equation 4-8 is the diameter of the equivalent-volume sphere. By designating the surface area of an arbitrarily shaped particle, by $A_{particle}$; and the surface area of a spherical particle having the same volume as the particle of arbitrary shape, by A_{sphere}; then the shape factor, ψ, commonly termed the sphericity factor, may be defined by (31)

$$\psi = A_{sphere}/A_{particle} \text{ - - - - - - - - -(4-12)}$$

Since a spherical particle is a body that provides a given mass with the least surface area, values calculated by Equation 4-12 are always less than unity; with the more angular particles have smaller shape factors and the nearly spherical particles approaching unity. The drag coefficient equation (Equation 4-3) may be corrected for non-spherical particles by substituting $\psi \cdot d_p$ for d_p. This has the effect of increasing the drag coefficient, C_D, which in turn decreases estimated free-fall velocities calculated by use of Equations 4-9, 4-10, or 4-11. This prediction accords with observed tendencies reported by Zenz and Othmer (71), who indicate that the general tendency is for the shape and surface of irregular particles to influence the rate of fall in such a manner that a particle falls at a lower velocity than does a sphere of equivalent weight.

Standard Drag Curve for a Sphere

A standard drag curve, derived by Schlichting (47) from experimental data and presented by Soo (50) and Bird, et. al., (4), is shown in Figure 4-3. This curve is applicable to a single solid sphere moving at constant velocity in a stagnant, incompressible fluid, which is infinite in extent. The diagram shows that, by comparison to the standard curve, the Stokes regime applies for $N_{Re} \leq 2$ and the Newton's regime holds nearly for $5\text{x}10^2 < N_{Re} < 2\text{x}10^5$. Beyond $N_{Re} = 2\text{x}10^5$ (upper critical Reynolds number), a

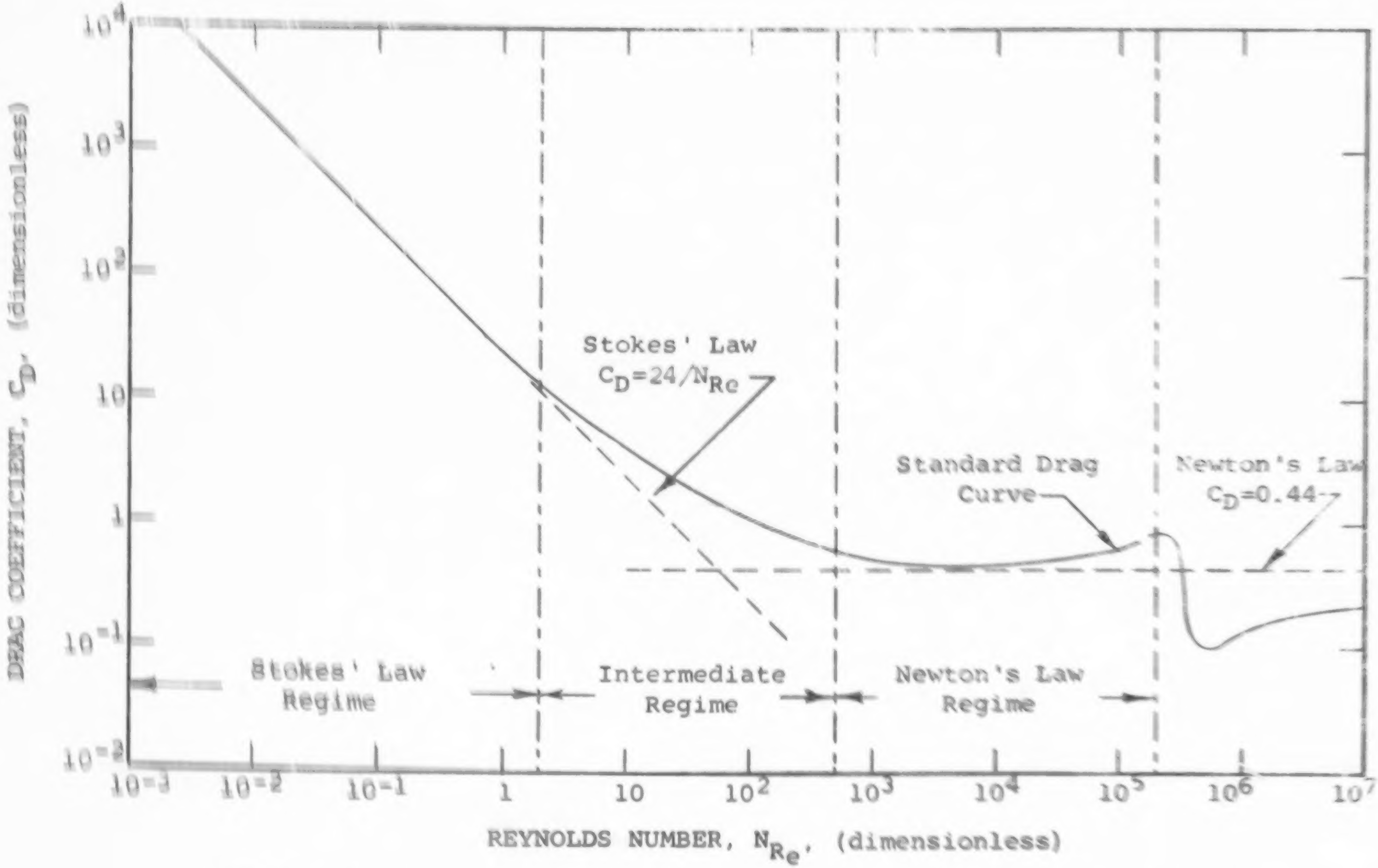

FIGURE 4-3. DRAG COEFFICIENTS FOR SPHERES MOVING RELATIVE TO A FLUID

sharp reduction in the drag coefficient occurs due to transition from laminar to turbulent boundary layers over the sphere.

It is seen that in the intermediate or transition zone, $2 < N_{Re} < 500$, accurate theoretical description of the flow field is not possible. This is due to the fact that in this region both inertial and friction effects contribute substantially to the total drag on the spherical body. Soo (50) explains the sequence of hydrodynamic conditions surrounding a sphere as N_{Re} is increased through this transition region. As inertial forces become significant, at $N_{Re}=10$, separation of the boundary layers occurs and the streamlines around the body curl up to form a stationary vortex ring at the downstream end of the sphere. A further increase of N_{Re} leads to growth of the vortex in size and strength. At $N_{Re}=100$, the vortex region extends to about 1 diameter behind the sphere. The contribution of inertial forces continues to increase at $N_{Re}=150$, at which point the vortex system begins to oscillate. In a laminar stream the vortices leave the body and form a wake at approximately $N_{Re}=500$. This Reynolds number, called the lower critical Reynolds number, constitutes the upper limit for the intermediate zone. As indicated previously, an empirical expression (Equation

4-6), termed the intermediate law, approximates the experimental standard drag curve in the hydrodynamic region encompassed by the Stokes' and Newton's regimes.

The standard drag curve, described by Equations 4-9, 4-10 and 4-11 and shown in Figure 4-3, applies only to an isolated particle in an infinite fluid medium and is independent of whether the particle is moving downward in a stagnant fluid or is being held in a nearly stationary position by a fluid moving upward. If a sphere, however, is falling in a cloud of other spheres, the drag coefficient is higher; the correction may be significant even when a cloud of spheres has a voidage as high as 99 percent (71). It is therefore imperative that the relationships, described above which correspond to a voidage of 100 percent, be adapted for application to multiparticle systems for accurate description of fluidized bed parameters.

HYDRODYNAMICS OF A MULTIPARTICLE FLUIDIZED-BED SYSTEM

Although the drag force of the fluid acting on an isolated sphere moving in an infinite expanse of stagnant fluid has been thoroughly studied and is well documented, the understanding of the drag force acting on each constituent particle in a multiparticle system has not yet achieved similar theoretical sophistication. This condition may be attributed to the fact that particle-particle interactions in the study of multiparticle hydrodynamics have been treated only qualitatively (71). No studies have, as yet, clearly delineated the effect of bed voidage on the drag forces acting on any randomly selected particle within the bed. For this reason all mathematical developments describing flow through beds of fluidized particles are semi-empirical in nature. Such equations may be derived from two basic analytical approaches; from a drag force consideration of a single particle moving in a stagnant fluid or from a pressure drop analysis extended from flow equations for fixed beds of particulate matter.

Pressure Drop Analysis

At the point of incipient fluidization, the pressure drop is given by

$$\frac{\Delta P \cdot g_c}{L_o} = (1-\epsilon_{mf})(\rho_s-\rho_l)g \quad \text{- - - - - - - - -} (4\text{-}13)$$

where L_o is the height of the adsorbent bed prior to expansion, (cm); g_c is the gravitational constant, $(\text{grams}_m \cdot \text{cm}/\text{grams}_f \cdot \text{sec}^2)$; ϵ_{mf} is the minimum fluidization voidage, (dimensionless). Since this is still at fixed bed conditions, the pressure drop can also be described from the correlation proposed by Ergun (10):

$$\frac{\Delta P \cdot g_c}{L_o} = \frac{150 \mu G_{mf}}{\rho_l \; d_p^2} \cdot \frac{(1-\epsilon_{mf})^2}{\epsilon_{mf}^3}$$

$$+ \frac{1.75 \; G_{mf}^2}{\rho_l \; d_p} \cdot \frac{(1-\epsilon_{mf})}{\epsilon_{mf}^3} \quad \text{-(4-14)}$$

where G_{mf} is the fluid mass velocity for minimum fluidization, (grams/cm^2/sec). Since the pressure drop of a fully fluidized bed may be considered to be approximately equivalent to the pressure gradient at the point of incipient fluidization (refer to Figure 4-1) one may, therefore, utilize Equation 4-14 for estimation of the head loss across a particulately fluidized bed. This estimate may subsequently be used for projection of power costs in scaled-up installations.

Correction for sphericity may be accomplished by substituting $\psi \cdot d_p$ for d_p in Equation 4-14, where ψ is defined by Equation 4-12. Combining the resultant equation with Equation 4-13, one obtains

$$N_{Ga} = \frac{1.75}{\psi \epsilon_{mf}^3} (N_{Re})^2_{mf}$$

$$+ \frac{150(1-\ _{mf})}{\psi^2 \; \epsilon_{mf}^3} \cdot (N_{Re})_{mf} \text{ - - - - - - - -(4-15)}$$

where N_{Ga}, the Galileo number, is defined by $d_p^3 \rho_l(\rho_s-\rho_l)g/\mu^2$.

Equation 4-15 is a dimensionless equation for the minimum fluidization velocity based on the pressure drop consideration and should be applicable for $(N_{Re})_{mf}$ up to 3000, which is the limiting value for application of Equation 4-14, as determined by Ergun (10).

Leva, Shirai, and Wen (34) reviewed the literature on the prediction of minimum-fluidization mass velocities. They stated that since values for the terms ψ and ϵ_{mf} often are not readily available, the correlation presented above, (Equation 4-15), is not convenient to use. Furthermore, the experimental methods for evaluation of voidage and shape factor are extremely complicated, and thus, elimination of the factors, ψ and ϵ_{mf}, should considerably improve the usefulness of Equation 4-15. These investigators, therefore, examined the relationship between ψ and ϵ_{mf}, utilizing fluidization data from the literature that represented a broad range of experimental conditions. From a correlation of these two parameters they found that voidage and sphericity are unique functions of the particle diameter and that two terms involving ψ and ϵ_{mf}, in Equation 4-15 can be approximated by

$$\frac{1-\epsilon_{mf}}{\psi^2\epsilon_{mf}^3} \simeq 11 \qquad \text{(4-16)}$$

and

$$\frac{1}{\psi\epsilon_{mf}} \simeq 14 \text{ ---------------(4-17)}$$

Substitution of Equations 4-16 and 4-17 into Equation 4-15, eliminates the parameters ψ and ϵ_{mf} and thereby yields

$$24.5(N_{Re})^2_{mf} + 1650(N_{Re})_{mf} - N_{Ga} = 0$$

or

$$(N_{Re})_{mf} = \left[(33.7)^2 + 0.0408 N_{Ga}\right]^{\frac{1}{2}} - 33.7 \text{ - - -(4-18)}$$

Leva et. al., (34) found good correlation between the minimum fluidization velocities calculated by use of Equation 4-18 and the corresponding experimental values. This equation may, therefore, be used for calculation of flow velocities at incipient fluidization, i.e., the minimum flow velocity required to just cause the particles to move relative to each other (point C in Figure 4-1). Unfortunately, however, this analysis cannot be extended for prediction of bed expansion during fluidization since the Ergun pressure drop equation which is limited for application to fixed beds, (Equation 4-14), was used in this analysis.

Drag Force Analysis

In particulate fluidization above the point of incipient fluidization, the particles are accelerated upward until the expanded bed of solids attains a state of stationary suspension such that the bed-fluid interface will remain at a constant height for a constant liquid velocity. At this point it is customarily assumed that the particles are uniformly distributed within the bed (31). Therefore, the forces of the fluid acting on each of the suspended particles must be in dynamic equilibrium; i.e. the sum of the drag force, F_D, and the buoyance force, F_B, must be equal to the gravitational force, F_G, acting in the opposite direction (refer to Equation 4-7). This condition may be represented as

$$F_D + F_B = F_G \quad \text{- - - - - - - - - - - - - -(4-19)}$$

However, although particles in a fluidized state are separated from each other by at least a film of liquid, there is mutual interference in the motion of densely associated particles, and the velocity of the concurrent liquid motion is considerably less than that computed by the equation derived on the assumption of free motion of particles in an infinite expanse of fluid. Since the mutual interference in the motion of the particles in a fluidized system should rapidly decrease with increased distances between particles (i.e. increasing void ratio), and inasmuch as this effect has not been theoretically delineated, Lewis and Bowerman (36) have proposed that the ratio of the steady-state liquid velocity through the fluidized bed to the terminal particle velocity can be related to a power function of the fraction voids, ϵ, in the fluidized bed of solids. This condition may be represented by the relation

$$\bar{V}/v_{po} = F(\epsilon) \text{ - - - - - - - - - - - - - - } (4\text{-}20)$$

in which $\bar{V}$ is the superficial fluid velocity in the cylindrical column and v_{po} is the terminal particle velocity as calculated either from Equation 4-9, 4-10 or 4-11 depending on which is applicable at the indicated Reynolds number.

Since the Reynolds number for the systems investigated in this study varies from 1.03 to 7.31 (Table 4-1), the Intermediate Law relationship (Equation 4-6) may be utilized for description of the particle dynamics for these experiments. The terminal particle velocity, $(v_{po})_I$, may therefore be calculated by use of Equation 4-7 and the velocity ratio (Equation 4-20) may be expressed as

$$\bar{V}/(v_{po})_I = F(\epsilon) \text{ - - - - - - - - - - - - - } (4\text{-}21)$$

Velocity ratios for the experimental columnar systems in

TABLE 4-1

HYDRODYNAMIC PROPERTIES FOR CALCULATION OF SUPERFICIAL FLUID/TERMINAL PARTICLE VELOCITY RATIOS

System	$\bar{V}$ (cm/sec)	d_p (cm)	N_{Re}	$(v_{p_o})_I$ (cm/sec)	$\bar{V}/(v_{p_o})_I$	ϵ
1	.136	.0711	1.03	3.84	.0354	.491
2	.272	.0711	2.06	3.84	.0709	.528
3	.407	.0711	3.08	3.84	.106	.574
4	.457	.0711	3.46	3.84	.119	.595
5	.544	.0711	4.12	3.84	.141	.614
6	.679	.0711	5.14	3.84	.176	.633
7	.679	.1011	7.31	5.71	.119	.553
8	.679	.0503	3.64	2.59	.262	.741
9	.679	.0356	2.57	1.74	.390	.795
10	.679	.0273	1.97	1.29	.525	.865

Notes:

A) Flow rate was studied as a variable in systems 1-6 and particle size in systems 7-10.

B) All experiments were conducted at 23°C.

C) ρ_s = 1.387 gm/cm^3, ρ_1 = 0.997 gm/cm^3, μ= 0.9358 centipoise.

which particle diameter and flow rate were studied as control variables were calculated and tabulated in Table 4-1. A plot of the bed voidage, ϵ, as a function of $\bar{V}/(v_{Po})_I$ is shown in Figure 4-4. With the exception of the left-most data point in the figure, rather good correlation is seen to obtain between the bed voidage and the velocity ratio. The point which lies in variance is that for which the flow rate was maintained at 8.15 cm/min., which, according to Lewis and Bowerman (36) is below the point of incipient fluidization, thereby causing the discrepancy.

The correlation, designated by the solid line in Figure 4-4, may be expressed by the relation

$$(\bar{V}/(v_{Po})_I)^{.256} = \epsilon$$

or

$$\bar{V}/(v_{Po})_I = \epsilon^{3.90} \text{ - - - - - - - - - - - - } (4\text{-}22)$$

which may be utilized for the purpose of predicting bed voidages and subsequently bed expansions, given the superficial fluid velocity, $\bar{V}$. Further it is of interest to note that this curve extrapolates at 100 percent voids to a value of $\bar{V}/(v_{Po})_I$ equal to 1; that is, as the void ratio approaches the condition of single particle dynamics,

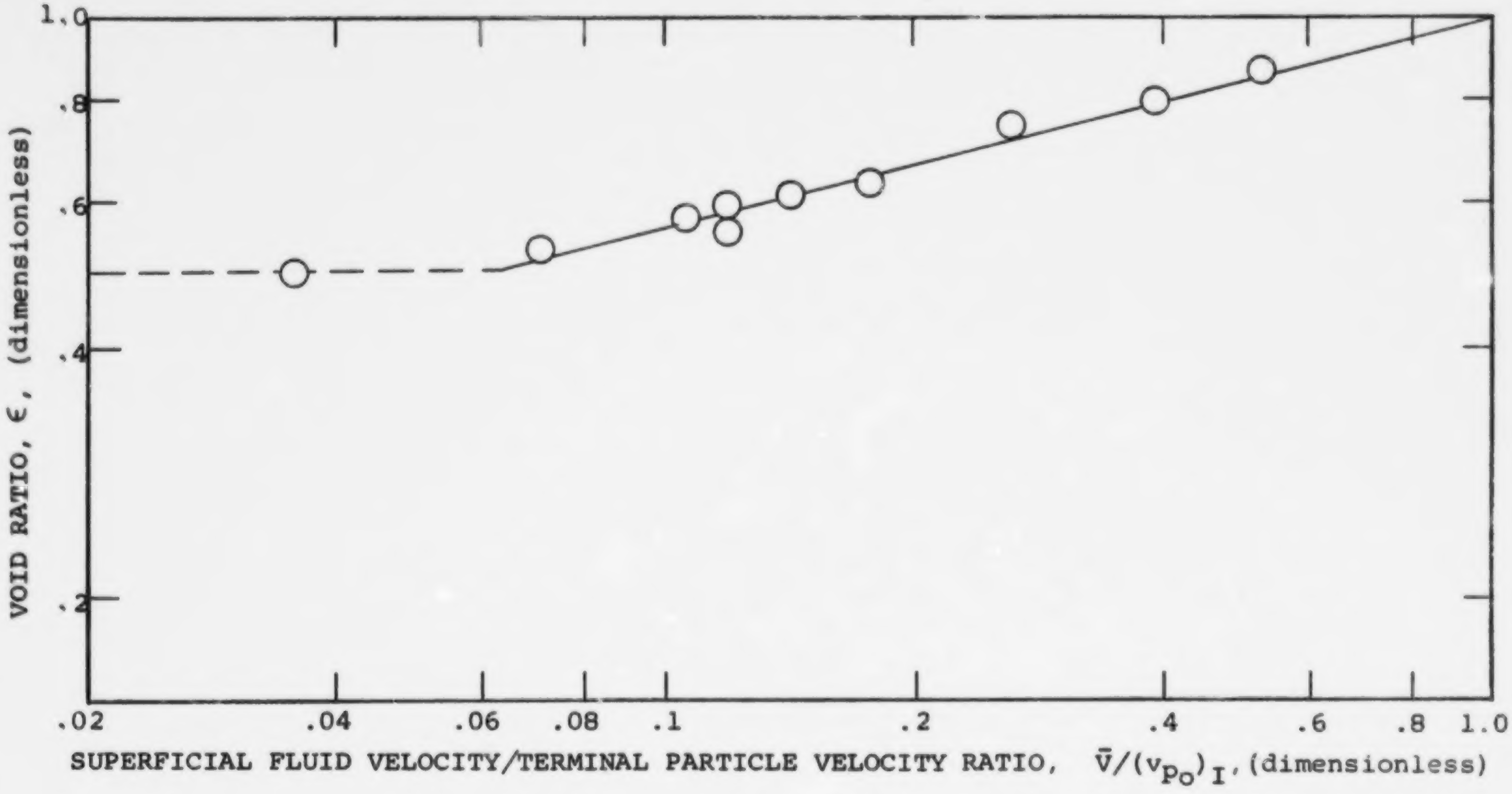

FIGURE 4-4. CORRELATION OF VOID RATIO WITH SUPERFICIAL FLUID/TERMINAL PARTICLE VELOCITY RATIO

the superficial fluid velocity, likewise, approaches the terminal velocity of a single particle as calculated by the Intermediate Law.

Another approach for predicting bed expansion has been forwarded by Wen and Yu (68). They proposed that the ratio of the drag forces,

$$F_D/F_{DS} = f\ (\epsilon) \text{ - - - - - - - - - - - - - - } (4\text{-}23)$$

should be proportional to a function of the bed void ratio. The drag force ratio, $f(\epsilon)$, termed the voidage function, was shown by these authors to have a unique trend of decreasing with increasing ϵ. Combination of Equations 4-19 and 4-23, therefore, yields

$$f(\epsilon)F_{DS} + F_B = F_G \text{ - - - - - - - - - - - - } (4\text{-}24)$$

Hence,

$$f(\epsilon) = \frac{F_G - F_B}{F_{DS}} \text{ - - - - - - - - - - - - - - -} (4\text{-}25)$$

The drag force, F_{DS}, acting on a single sphere in the intermediate flow region may be derived from Equations 4-3 and 4-6 and can be expressed as

$$F_{DS} = 2.31\pi d_p^{1.4} \rho_l^{0.4} \mu^{0.6} \bar{V}^{1.4} \text{ - - - -} (4\text{-}26)$$

Substitution for the gravitational and buoyance forces, defined by Equation 4-7, and the drag force (Equation 4-26) in Equation 4-25, the voidage becomes

$$f(\epsilon) = \frac{d_p^{1.6}(\rho_s-\rho_1)g}{13.86\rho_1^{0.4}\mu^{0.6}\bar{V}^{1.4}} \text{ - - - - - - } (4\text{-}27)$$

Examination of this relation along with that describing the particle terminal velocity (Equation 4-11) it is apparent that the voidage function may be given in the terms

$$f(\epsilon) = \left[\frac{1}{\bar{V}/(v_{po})_I}\right]^{1.4} \text{ - - - - - - - - - - - } (4\text{-}28)$$

This equation is seen to be very similar to Equation 4-21, which was set forth by Lewis and Bowerman (36). It is, therefore, evident that the velocity ratio analysis of Lewis and Bowerman (36) is essentially analogous to the drag force ratio analysis proposed by Wen and Yu. Proportionality between the two may be established by introduction of a power of 1.4. Equation 4-22 may then be substituted into Equation 4-28 to yield an expression for the voidage function as follows,

$$f(\epsilon) = \epsilon^{-5.45} \text{ - - - - - - - - - - - - - - } (4\text{-}29)$$

Combination of Equations 4-27 and 4-29 yields the expression

$$\epsilon^{5.45} = \frac{13.86\rho_1^{0.4}\mu^{0.6}\bar{V}^{1.4}}{d_p^{1.6}(\rho_s-\rho_1)g} \quad ------(4\text{-}30)$$

which, again, may be used for prediction of bed void ratios and expansions.

Both of the above analyses, that of Lewis and Bowerman (Equation 4-22) and that of Wen and Yu (Equation 4-30), made use of the Intermediate Law, which is appropriate for Reynolds numbers in the range of 2 to 500. For other flow conditions use may be made of either Stokes' Law or Newton's Law depending on the flow regime in which the experimental systems are operated. Wen and Yu (68), however, attempted to generalize the voidage function, described by Equation 4-25, such that it is applicable over a much broader range of particle Reynolds numbers than is covered by either of the three separate and distinct flow equations. This was accomplished by using the equation describing the drag force acting on a single particle

$$F_{DS} = \pi d_p^2 \rho_1 v_p^2 (3N_{Re}^{-1} + 0.45\ N_{Re}^{-0.313}) \quad - - - -\ 4\text{-}31)$$

to replace the theoretical relations describing the laminar, intermediate, and turbulent flow regions. This equation was derived by suitably combining the drag coefficients (Equations 4-4, 4-5 and 4-6) with the drag force equation (Equation 4-3). The first Reynolds number parameter defines the Stokes' Law region, while the intermediate and turbulent flow regimes are described by the second Reynolds number relation. Applicability of this drag force expression extends for Reynolds numbers from 0.001 to 1000.

Combining Equations 4-23 and 4-31 yields an expression for the drag force on a particle in a multiparticle system, which may be written as

$$F_D = f(\epsilon)\pi d_p^2 \rho_1 v_p^2 (3N_{Re}^{-1} + 0.45N_{Re}^{-0.313}) \text{ - -(4-32)}$$

Substitution for the buoyancy force, F_B, and the gravitational force, F_G, as defined by Equation 4-7, as well as the relation for the drag force (Equation 4-32) into the dynamic equilibrium expression (Equation 4-19), the voidage function, $f(\epsilon)$, for the entire flow regime, $10^{-3} < N_{Re} < 10^3$, becomes

$$f(\epsilon) = \frac{N_{Ga}}{18\, N_{Re} + 2.70 N_{Re}^{1.687}} \text{ - - - - - - (4-33)}$$

where N_{Ga} is the Galileo number, (dimensionless).

Because it was advanced that values of $f(\epsilon)$ should be proportional to a power function of the fraction of voids, ϵ, one may plot log $f(\epsilon)$ as a function of log ϵ to determine the relationship and the degree of correspondence between the parameters. Values of $f(\epsilon)$, as determined by Equation 4-33, are, therefore, plotted as a function of experimental fluidized bed void ratios in Figure 4-5. Parameters required for calculation of $f(\epsilon)$ and the experimentally determined values of ϵ for those systems in which flow rate or particle size were studied as variables are tabulated in Table 4-2.

Again, with the exception of the uppermost data point in Figure 4-5, excellent correlation is seen to obtain between the voidage function, $f(\epsilon)$, and the void ratio, ϵ. The linear trace in the figure illustrates that $f(\epsilon)$ is exclusively a function of ϵ which may be expressed as

$$f(\epsilon) = \epsilon^{-5.20} \text{ - - - - - - - - - - - - - } (4\text{-}34)$$

and thus

$$\epsilon^{5.20} N_{Ga} = 18 N_{Re} + 2.70 N_{Re}^{1.687} \text{ - - - - } (4\text{-}35)$$

or

$$\epsilon^{5.20} N_{Ga} = f(N_{Re}) \text{ - - - - - - - - - - - } (4\text{-}36)$$

Thus, by plotting $\epsilon^{5.20} N_{Ga}$ as a function of N_{Re}, a continuous curve may be obtained from which ϵ may be predicted

TABLE 4-2

HYDRODYNAMIC PROPERTIES FOR CALCULATION OF THE VOIDAGE FUNCTION

System	$\bar{V}$ (cm/min)	d_p (cm)	N_{Re}	N_{Ga}	$f(\epsilon)$	ϵ
1	8.15	.0711	1.03	1565	73.3	.491
2	16.3	.0711	2.06	1565	33.8	.528
3	24.4	.0711	3.08	1565	21.3	.574
4	27.4	.0711	3.46	1565	18.6	.595
5	32.6	.0711	4.12	1565	15.1	.614
6	40.7	.0711	5.14	1565	11.7	.633
7	40.7	.1011	7.31	4490	21.4	.553
8	40.7	.0503	3.64	554	6.19	.741
9	40.7	.0356	2.57	196	3.29	.795
10	40.7	.0273	1.97	89	2.02	.865

Notes:

A) Flow rate was studied as a variable in systems 1-6 and particle size in systems 7-10.

B) All experiments were conducted at 23°C.

C) $\rho_s = 1.387$ gm/cm^3, $\rho_1 = 0.997$ gm/cm^3, $\mu = 0.9358$ centipoise.

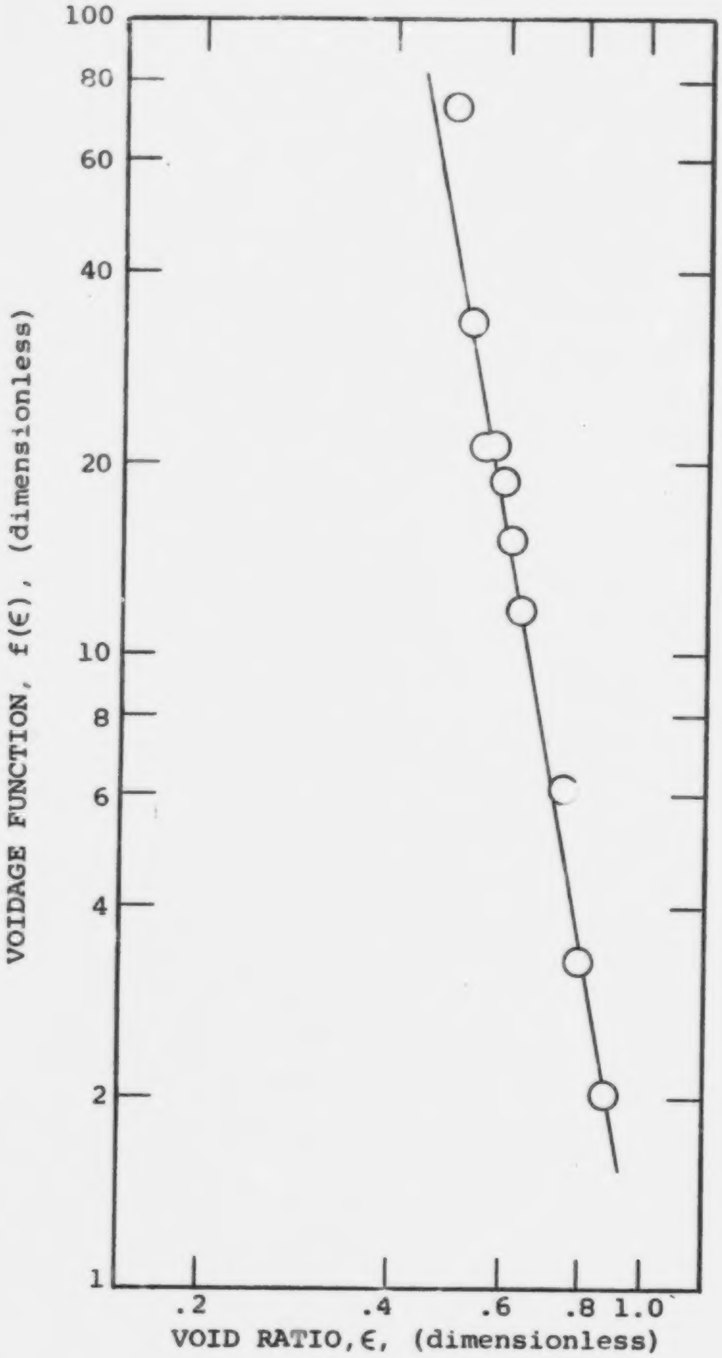

FIGURE 4-5. CORRELATION OF VOIDAGE FUNCTION, f(ϵ), WITH VOID RATIO, ϵ.

given N_{Ga} and N_{Re}.

Comparison of Equations 4-29 and 4-34 shows good correspondence between the two voidage functions. This indicates that the generalized drag force equation (Equation 4-31) adequately describes particle dynamics over the range of its limitation. Equation 4-35 may, therefore, be utilized for a generalized description of void ratios and bed expansions for flow velocities greater than the incipient fluidization velocity.

Wen and Yu (68) found that the voidage function, $f(\epsilon)$, varied as $\epsilon^{-4.7}$ for data, presented by numerous investigators, for fluidized systems consisting of spherical particles. Moreover, Lewis and Bowerman (36) and Richardson and Zaki (44), in other studies, calculated velocity ratio parameters, defined by Equation 4-21. As indicated previously, these may be related to the voidage function, $f(\epsilon)$, by Equation 4-28. Both found $f(\epsilon)$ to be a function of $\epsilon^{-4.65}$. The close agreement between the correlations of these three pairs of investigators and those set forth in this study corroborates the adequacy of these semi-theoretical approaches for prediction of bed expansions and void ratios. Further, the extreme range of experimental conditions for which the previous researchers obtained data exemplifies the generality of these methods. Their correlations included experimental evidence in which d_p ranged from 0.0015 to 0.636 cm., ρ_s from 1.06 to 11.25 gm/cm^3, ρ_l from 0.818 to 1.135 gm/cm^3, and μ from 1.0 to 15.01 centipoise.

The expressions describing $(N_{Re})_{mf}$ and ϵ, presented and discussed in this section, may be utilized in the mathematical model for prediction of concentration-time profiles. In addition, however, these parameters are invaluable when considering design of plant-scale installations. That is, one must be able to predict flow velocities at incipient fluidization, as defined by $(N_{Re})_{mf}$, such that the flow through the adsorbent bed may be maintained high enough for full fluidization to ensure that particulate matter suspended in the fluid stream will not be entrained in the bed and subsequently cause high head losses. Further, design of the height of the contacting unit is specified by the maximum anticipated bed expansion which may be calculated from the predicted void ratio, ϵ, for any given fluid-particle system.

Two additional parameters must be taken into account when considering scale-up procedures for fluidized-bed systems of this type. The ratio of the bed height, L, to column diameter, d_c, is occasionally of consequence in determining the quality of fluidization performance, particularly as it relates to the slugging or aggregative characteristics of a bed. Since a bed of granular particles that is particulately fluidized with a liquid is not subject to aggregation or slugging, this ratio, L/d_c, is of minor import in this application and may, therefore, be neglected when considering design of plant-scale installations.

The effect of the confining walls of the cylindrical column on multiparticle hydrodynamics must also be considered. This "wall effect", characterized by the ratio of d_c/d_p, affects the voidage of the system as this ratio becomes small. Leva (31) relates that this effect is negligible for values of $d_c/d_p > 16$. Because the ratio of the column diameter to particle diameter for the systems explored in this study varied from 50 to 200, the interference attributable to the confining walls may also be discounted.

CHAPTER 5

MASS TRANSFER RELATIONSHIPS FOR SOLUTION OF THE BREAKTHROUGH EQUATION

Numerical solution of the expression describing the concentration-time profile for any given system (Equation 3-51) requires specification of nine distinct parameters. For experimental purposes, the volumetric flow rate, F, may be set and maintained at some constant value. The influent concentration of solute, C_o, may be controlled, as was the case in this study, or may be monitored to determine a typical influent-concentration profile which may be used as an input parameter for the numerical solution. The latter situation is most likely to arise in plant-scale installations in which solute concentrations may fluctuate considerably. Several variables, including the density, porosity, and volume of the adsorbent bed in the expanded or fluidized state, relate to the hydrodynamic characteristics of the fluid-particle system. These may be determined from theoretical considerations, presented in the preceding chapter, for the fluidized state. The four remaining parameters which must specified to permit solution of the breakthrough equations include the two Langmuir equilibrium constants and the film and pore transfer coefficients. It is apparent that these four constants all relate to the interphase transfer of the solute and are, therefore, specific for any solute-solvent-adsorbent system. These parameters must be determined from experimental measurements, except in the case of the film transport coefficient, for which correlational methods are available. Evaluation of these coefficients can certainly be accomplished by measurements in columnar flow-through experiments. Because of the relatively elaborate nature of such test systems and the length of time required to obtain meaningful measurements, it is most advantageous to evaluate these parameters in simple, rapidly agitated non-flow systems. The objective of the present study has been to develop a procedure for predicting adsorption behavior in continuous-flow systems from measurements in batch systems; experimental evaluation of the required parameters has therefore been accomplished with systems of the latter type.

ADSORPTION EQUILIBRIA

An experimental isotherm has been determined for each of the five particle sizes of activated carbon used in the present studies over the appropriate range, of equilibrium concentrations. The data for each isotherm have been plotted in Figure 5-1. It is interesting to note that, although the mean particle diameter of the coal-base adsorbent varied from 0.273-mm to 1.011-mm no significant effect of particle

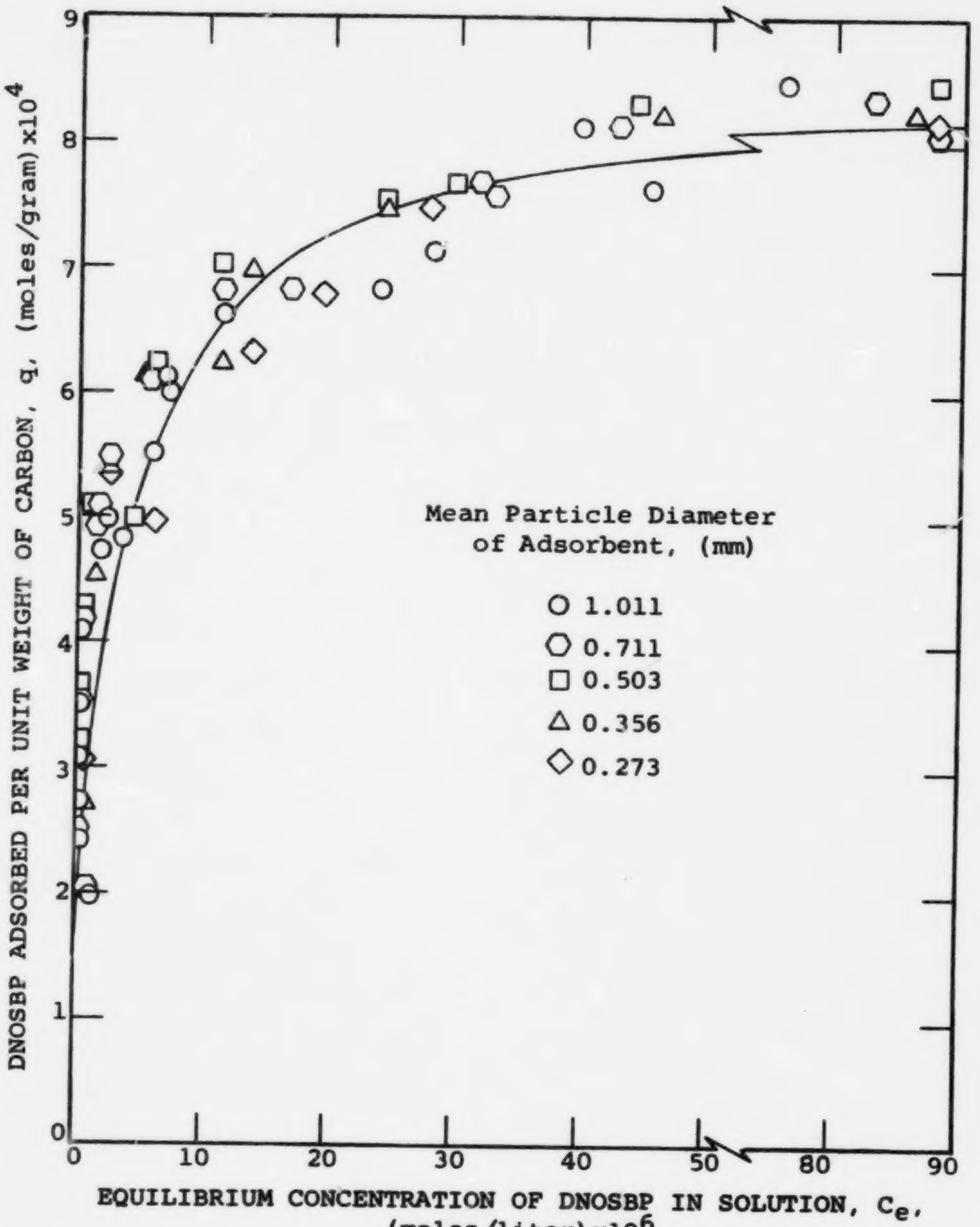

FIGURE 5-1. ISOTHERM FOR ADSORPTION OF DINITRO-O-SEC-BUTYLPHENOL ON COAL-BASE ACTIVE CARBON

size on equilibrium capacities for adsorption was discernable. The range of the uptake data for the several particle sizes may be observed to be no greater than that of the scatter for any single particle diameter. This result is in accord with theoretical expectations; i.e., if one assumes that the number of active surface sites per unit weight of adsorbent, is independent of particle size, even though the active surface area may be a function of the radial position with an adsorbent particle, and since the effective surfaces lie almost entirely within the interstices of the particle, one would not expect that the mean uptake of the solute per unit weight of adsorbent would vary with particle diameter. Further, experimental data of Dedrick and Beckman (8) confirms the above findings.

Earlier work of Weber and Morris (65) with a different type of active carbon, however, demonstrated a rather marked dependence of the ultimate capacity for adsorption on the particle size of the adsorbent. The difference in the findings of the present investigation and that of Weber and Morris regarding the dependence of capacity on particle size most likely arises from differences in the methods of preparing the carbon for study. In the latter case, carbon of a relatively large particle size was crushed by grinding prior to sieving, whereas for the present study the carbon was simply sieved without grinding.

It has been observed that a large quantity of fines (carbon dust) is produced during grinding operations. Approximately 50 percent of the total quantity of activated carbon that has been ground is pulverized to sizes smaller than 200 mesh for a single pass through a hammermill grinding apparatus. Also, because the abrasion resistance of the carbonaceous material of particles of active carbon decreases with increasing radial distance from the center of the particle, it appears reasonable that grinding quite probably has the effect of wearing away the exterior surfaces of the particle as opposed to splitting it into smaller ones. If the particles were, indeed, split into smaller ones, one would not expect that such large quantities of fines would be produced.

In the case in which smaller particles are presumed formed by the wearing away of the exterior surfaces of the original particles, one must postulate that the "activity", δ_i, (number of active surface sites per unit volume of carbonaceous matter) is an inverse function of the radial distance to explain the observations of Weber and Morris (65). These authors noted that the ultimate uptake capacity varied as $1/R_p^2$ for the small-pore gas-phase carbon they utilized. The mean activity, δ, of the entire particle of total radius, R_p, may be calculated by

$$\delta = 3/R_p^{3} \int_0^{R_p} \delta_i \, R^2 \, dR \quad - - - - - - - - - (5\text{-}1)$$

For the condition in which δ, a function of the ultimate uptake capacity, is proportional to $1/R_p^{2}$, δ_i must vary as $1/R^2$ to fully satisfy the above relationship. This inverse variation of the activity with the square of the radial distance, therefore, suggests that grinding by the proposed mechanism would certainly have the effect of producing smaller particles of greater activity, thereby increasing the specific number of active surface sites per unit volume of adsorbent in proportion to $1/R_p^{2}$.

The interpretation presented above explains the observations of Weber and Morris, but certainly, it is not conclusive. If grinding results by splitting the original particles to form smaller ones, the above explanation is not valid. One must then postulate that splitting has the effect of opening some tiny, sealed channels in the carbon particles which then become available for adsorption, thereby increasing the ultimate uptake capacity. This explanation is further supported by the fact that the particular carbon used by Weber and Morris has a relatively small average pore size, which suggests the probability of the existence of sealed channels. Neither of the two proposed explanations can, at this point, be proven conclusively. Both, therefore, must be considered as equally likely explanations for the observed dependence of ultimate uptake capacity on particle diameter.

Because particle size was observed to have no apparent effect on adsorption capacities for the carbon under study, a single isotherm has been fitted to the data for all particle sizes used. The Langmuir equation for adsorption equilibria,

$$q = \frac{QbC_e}{1+bC_e} \quad \text{- - - - - - - - - - - - - -} \quad (5\text{-}2)$$

requires specification of the ultimate adsorption capacity (Q) and the energy constant (b) to completely define the shape of the isotherm. Values of $Q = 8.469 \times 10^{-4}$ moles/gram and $b = 3.023 \times 10^{8}$ cm^3/mole have been determined from the equilibrium data plotted in Figure 5-1 for the present experimental systems. The solid line drawn through the data in Figure 5-1 is the calculated Langmuir isotherm to which these constants correspond.

ADSORPTION KINETICS

Film Diffusion Coefficients

The film diffusion coefficient is a measure of the resistance to transfer of solute from bulk solution through the hydrodynamic boundary layer to the outer surface of the adsorbent. No practicable method for determination of film diffusion coefficients in rapidly-agitated non-flow systems is available; as the description of the system (i.e. rapid agitation) implies, the hydrodynamic boundary layer is essentially eliminated and pore transport is the rate-controlling resistance. Fortunately, however, a correlational technique for determination of external diffusion coefficients is available.

Chu, et. al., (6) have been able to correlate a mass transfer factor $j_d = (k_f/\bar{V})(N_{Sc})^{2/3}$, with the modified Reynolds number, $N'_{Re} = d_p\bar{V}/\nu(1-\epsilon)$, for such diverse systems as liquid-solid and gas-solid fixed and fluidized beds, for a variety of different types of solutes and for numerous particulate solids of different size and geometric shape. Particle sizes ranged from 0.1 to several centimeters in diameter. In contrast, Resnick and White (43), using particulate solids smaller than 0.1 centimeter in diameter, have found that data for different particle sizes can not be adequately correlated by a simple plot of ln j_d vs. ln N'_{Re}. Rather, data for this range of particle sizes have been found to correlate well by plotting ln j_d vs. ln(N'_{Re}/N_{Ga}), where

$$N_{Ga} = \frac{d_p^{\,3}\,\rho_1(\rho_s-\rho_1)g}{\mu^2} \quad \text{- - - - - - - - -} \quad (5\text{-}3)$$

is the dimensionless Galileo number. The term ρ_l in Equation 5-3 represents the density of the liquid phase (grams/cm^3); ρ_s the density of the solid adsorbent (grams/cm^3); g the acceleration of gravity (cm/sec^2); and μ, the absolute viscosity of the fluid (centipoise). This correlation which accounts for particle size effects, may therefore be used for determination of the film diffusion coefficients for the present systems. One need only calculate the factor, N'_{Re}/N_{Ga}, which may be determined from the physical and hydrodynamic characteristics of the system, to obtain a value for j_d.

To illustrate the adequacy of the Resnick-White correlation for prediction of external diffusion coefficients, j_d-factors have been calculated and plotted in Figure 5-2 for each of the experimental columns for which either flow rate, particle size, or solute concentration was varied. Film transfer coefficients have been calculated for each column study by application of Equation 3-59 to the analysis of experimental measurements of initial values for q as a function of time; it had been established in previous studies (63) that film diffusion is indeed rate-limiting during the initial stages of a column test of this nature. Because no value for the bulk solution diffusivity, D_l, for DNOSBP was available in the literature, it has been

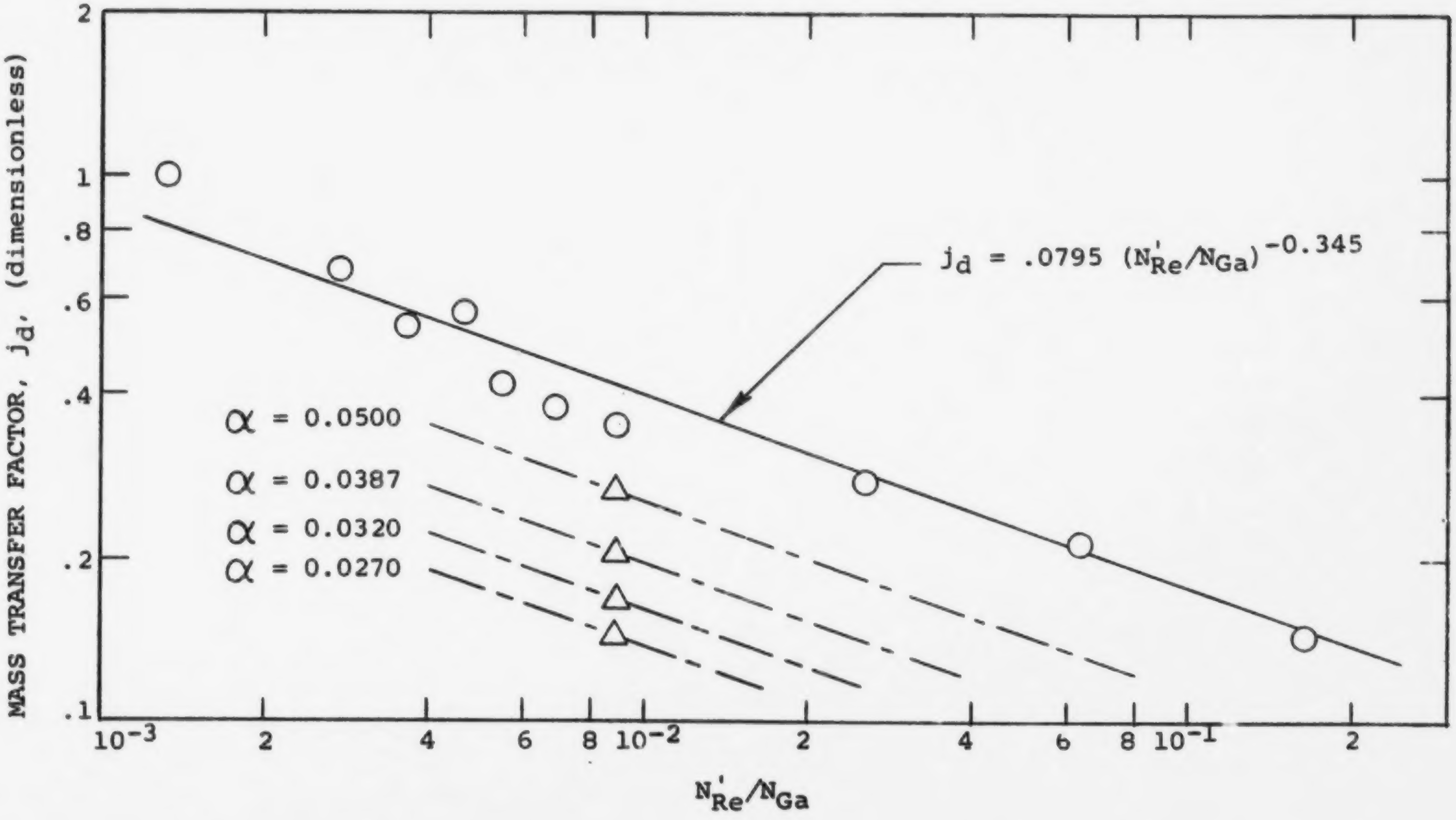

FIGURE 5-2. CORRELATION OF THE MASS TRANSFER FACTOR, j_d, WITH THE RATIO OF THE MODIFIED REYNOLDS NUMBER TO THE GALILEO NUMBER

necessary to calculate a value from the Wilke-Chang relationship for associated solvents (70)

$$D_1 = 7.4 \times 10^{-8} \left[\frac{T(X \cdot M)^{\frac{1}{2}}}{\mu V_o^{0.6}} \right] \text{ - - - - - - -(5-4)}$$

where D_1 is the coefficient for diffusion of the solute in bulk solution (cm^2/second); T the absolute temperature (^{o}K); X the association parameter for the solvent (for water, X = 2.0); M the molecular weight of the solvent (grams/mole); μ the absolute viscosity of the solvent (centipoise); and V_o the molal volume of the solute molecule. The bulk-solution diffusivity for DNOSBP, as calculated from Equation 5-4, is $D_1 = 6.21 \times 10^{-6}$ cm^2/sec. This value has been used for calculation of the Schmidt number, N_{Sc}, and subsequently for determination of the j_d-factor.

The data tabulated in Table 5-1 and plotted in Figure 5-2 indicate that the mass transfer factor is an adequate tool for description of the film diffusion coefficients over the experimental range of interest. The correlation may be described algebraically by an equation of the form

$$j_d = \alpha \left[N'_{Re} / N_{Ga} \right]^{\beta} \text{ - - - - - - - - - -(5-5)}$$

where α and β are constants. Values of $\alpha = 7.95 \times 10^{-2}$ and $\beta = -0.345$ have been obtained for the experimental studies of flow rate, particle size and solute concentra-

TABLE 5-1

MASS TRANSFER PARAMETERS
FOR CORRELATION OF FILM DIFFUSION COEFFICIENTS

System	k_f (cm/min)	$\bar{V}$ (cm/min)	j_d	N'_{Re}	N_{Ga}	N'_{Re}/N_{Ga}
1	6.49	8.15	0.995	2.07	1565	0.664
2	8.76	16.3	0.672	4.29	1565	1.315
3	10.92	24.4	0.560	7.25	1565	1.965
4	9.02	27.4	0.412	8.55	1565	2.21
5	9.84	32.6	0.377	10.65	1565	2.63
6	11.40	40.7	0.349	14.00	1565	3.26
7	17.10	40.7	0.527	16.35	4490	1.63
8	8.97	40.7	0.276	14.04	554	6.58
9	6.89	40.7	0.212	12.50	196	1.31
10	4.69	40.7	0.144	14.60	89	2.21
11	8.69	40.7	0.267	14.00	1565	3.28
12	6.66	40.7	0.205	14.00	1565	3.28
13	5.48	40.7	0.169	14.00	1565	3.28
14	4.69	40.7	0.144	14.00	1565	3.28

Notes:

A) Flow rate was studied as a variable in systems 1-6, particle size in systems 7-10, and bed depth in systems 11-14.

B) $j_d = (k_f/\bar{V})(N_{Sc})^{2/3}$

C) $N'_{Re} = N_{Re}/1-\epsilon$

tion, yielding

$$j_d = 7.95 \times 10^{-2} \left[N'_{Re}/N_{Ga} \right]^{-0.345} \quad \text{- - - (5-6)}$$

It is interesting to note, however, that the j_d factors for experimental columns in which depth of bed has been studied as a variable, designated by the triangular symbols in Figure 5-2, are not correlated by the relationship given in Equation 5-6. Rather, j_d decreases regularly with increasing depths of expanded bed. Resnick and White (43) also have noted an effect of bed height on the mass transfer factor for gas-fluidized systems in which bed heights, measured at rest, less than 1 inch were utilized. They, however, could not quantify the effect because of the variability of the data available to them and the experimental error involved in the tests from which the data derived. For the present experiments, the variation of the j_d-factor with bed depth is too regular and of such magnitude that it cannot be explained on the basis of experimental error.

For correlating differences in the mass transfer factor resulting from variations in bed depth, it has been assumed that the constant, β, is independent of expanded bed depth (i.e. the variation of j_d with N'_{Re}/N_{Ga} as a function of flow rate, particle size, and influent concentration is the same for any bed depth as for the bed depth of 44.8 centimeters which corresponds to the correlation of Equation 5-6. Based on this assumption, the parameter, α, has been plotted as a function of 1/L (L is the expanded bed depth in centimeters) to define the dependence of the j_d-factor on bed depth. With the exception of the point corresponding to a bed depth of 44.8-cm., good correlation may be noted in Figure 5-3, the resulting relationship being $\alpha = 3.15/L$. The expression for the j_d-factor (Equation 5-5), generalized to include the effect of bed depth, thus takes the form

$$j_d = \frac{3.15}{L}\left[\frac{N'_{Re}}{N_{Ga}}\right]^{-0.345} \qquad \text{-------(5-7)}$$

This equation apparently is applicable for values of 1/L less than 1.8×10^{-2}, corresponding to bed depths greater than 55.5 centimeters.

The effect of bed depth on the mass transfer factor is doubtlessly associated with the end effects at the influent section of the cylindrical column. The observed variation of α with 1/L in Figure 5-3 may be explained if one assumes that the end effects are such as to increase the mass transfer factor and that the zone of influence of this effect is limited to a finite distance in the vicinity of the influent section. One would then expect a decrease

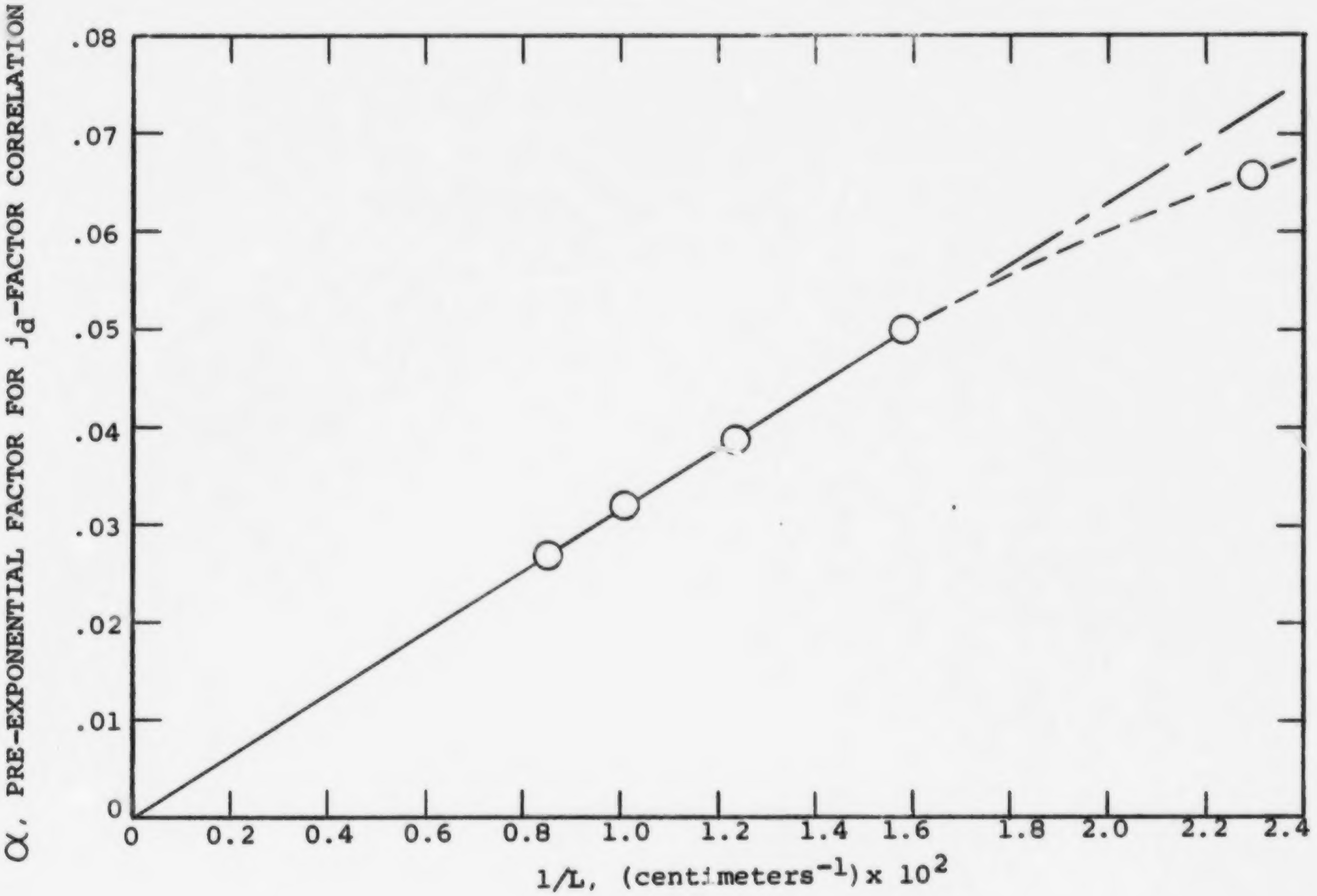

FIGURE 5-3. RELATIONSHIP BETWEEN α, THE PRE-EXPONENTIAL COEFFICIENT FOR THE j_d-FACTOR CORRELATION, AND EXPANDED BED DEPTH

in the j_d-factor with increasing bed depth; the end effect would have a decreasing influence on the mass transfer factor, averaged over the total bed depth, with increasing depth of bed. For depths of expanded bed greater than those in which the mass transfer factor is influenced by the end effects, j_d would vary linearly as 1/L, while the dependence of the mean j_d-factor on 1/L would become curvilinear and asymptotically approach the value for j_d at the influent section for bed depths in the zone of influence. This type of dependence of j_d on 1/L is indeed noted in Figure 5-3; i.e. for bed depths greater than 55.5 centimeters j_d varies linearly as 1/L and for L less than 55.5 centimeters the variation between j_d and 1/L becomes curvilinear. It is apparent, therefore, that the zone of influence extends over approximately 55.5 centimeters.

It is not possible to provide a qualitative definition of the specific nature of the observed end effect on the basis of the available data. However, it is surmised that the effect arises due to a non-uniform velocity profile at the influent section. This then suggests that the design of the influent distribution section would affect the entrance velocity profile thereby altering the effect of bed depth. Further experimental investigations are required, therefore, to provide sufficient data for interpretation of those effects.

If the observed effect of bed depth on film-diffusion-controlled mass transfer rates is confirmed by larger-scale column tests, this factor may have significant impact on the design of plant-scale fluid-bed contacting systems. The preliminary data relative to the effect of bed depth obtained in the course of the present study suggest that it may be more desirable to design a fluid-bed reactor in a stage-wise fashion, maintaining bed depths in each stage as small as practicable, than it would be to design a single contractor with a depth of bed equivalent to the sum of the depths in the individual stages. In this manner one would capitalize on the beneficial end effects. Further, there is some indication that influent distributor design may be of considerable import in the overall mass transport process. The existing evidence is certainly not conclusive, however, and no definite projection of these observations should be advanced until the nature of the specific end effect has been more fully delineated.

Pore Diffusion Coefficients

Previous investigators (67) have indicated that pore transport is the rate-limiting step for removal of organic solutes from dilute aqueous solution by porous active carbon in rapidly agitated non-flow systems. Measurements of adsorption in such systems thus provide a means for determination of pore diffusion coefficients and values for the corresponding transfer coefficients required for solution of Equation 3-51.

For systems in which pore transport is rate limiting, data obtained from rate experiments for values for the amount of solute adsorbed per unit weight of adsorbent should increase linearly with the square-root of time (64). Such a dependence has been observed for the rate studies used for evaluation of pore-diffusion transfer coefficients in the present experiments. In this case, however, an equivalent plot of the square of the quantity adsorbed as a function of time has been used for normalization of the data; apparent adsorption rates then have been obtained from the slopes of such plots.

Several hundred kinetic experiments with batch systems have been carried out to define the effect of particle size and the initial solute concentration on rates of uptake for the pore-diffusion case. Relative to the particle size dependence, Hiester and Vermeulen (23) and Griffin and Dranoff (19) have found rates of uptake to vary inversely with $d_p^{1.6}$. The data presented in Figure 5-4 illustrate a rather good correlation with the reciprocal of $d_p^{1.4}$, for six different initial concentrations of solute; in

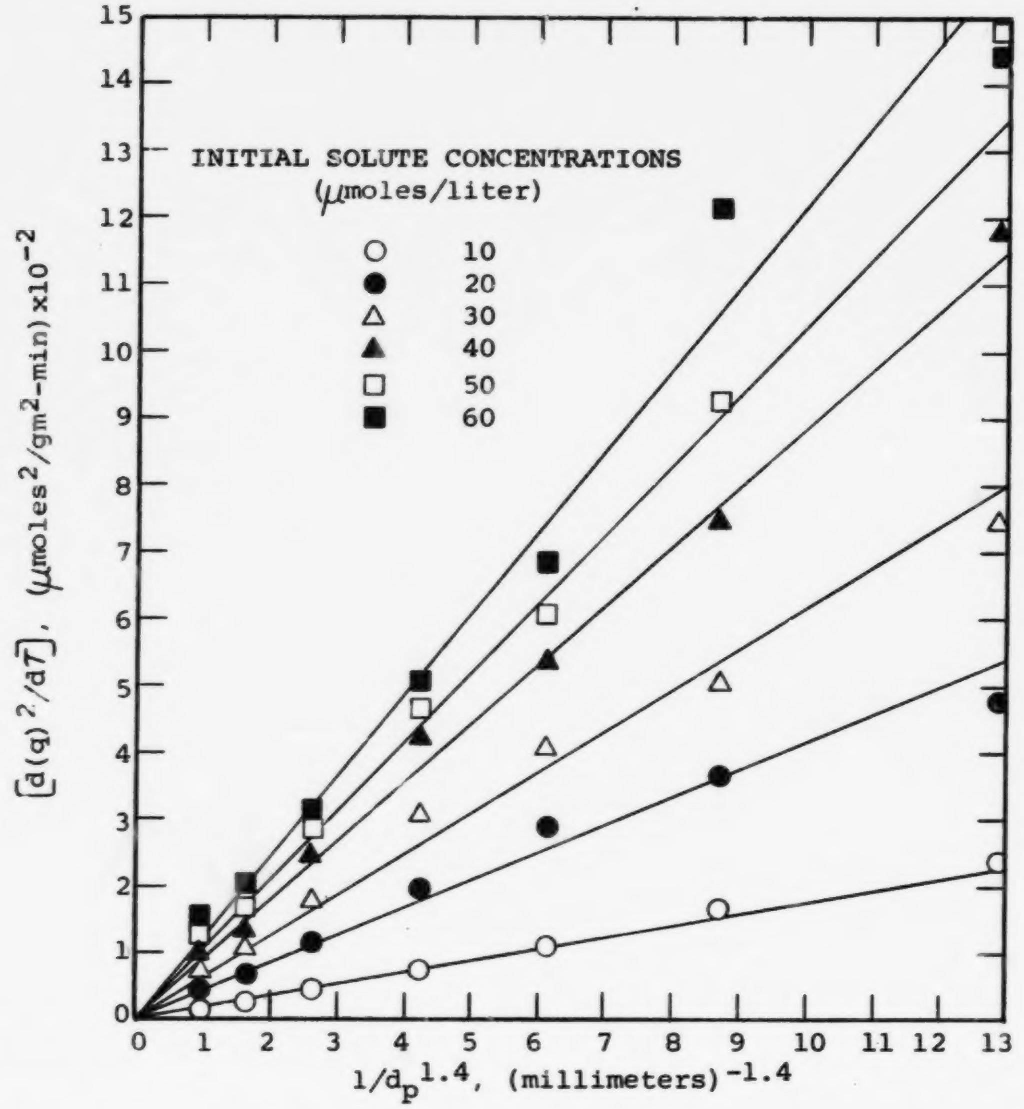

FIGURE 5-4. THE DEPENDENCE OF MASS-TRANSFER RATES FOR PORE DIFFUSION ON THE MEAN PARTICLE DIAMETER, d_p, OF THE ADSORBENT

reasonable agreement with the results of Hiester and Vermeulen and Griffin and Dranoff. The particle size dependence was determined by taking the slope of a plot of $\ln(d(q)^2/d\mathcal{T})$, vs. $\ln d_p$ for the experimental data. An equation of the form

$$d(q)^2/d\mathcal{T} = A/d_p^{1.4} \qquad \text{--------- (5-8)}$$

may be used to describe the relationship between adsorption rates and particle size. Each of the data points, shown in Figure 5-4, represents an average of approximately eight separate and distinct rate experiments.

Because initial solute concentration was the only variable for each of the six linear correlations given in Figure 5-5, the pre-exponential factor, A, of Equation 5-8 should then be strictly a function of C_o. In studies of Weber and Morris (64), rate of uptake was found to be directly proportional to initial solute concentration. Therefore, one might expect A to vary linearly with C_o. The plot of A vs. C_o, given in Figure 5-5, confirms the behavior anticipated. The empirical relationship between the two variables is

$$A = 2.08\ C_o \qquad \text{----------- (5-9)}$$

Substitution of Equation 5-9 into Equation 5-8 yields a generalized correlation relating pore-diffusion adsorption rates with particle size and initial concentration,

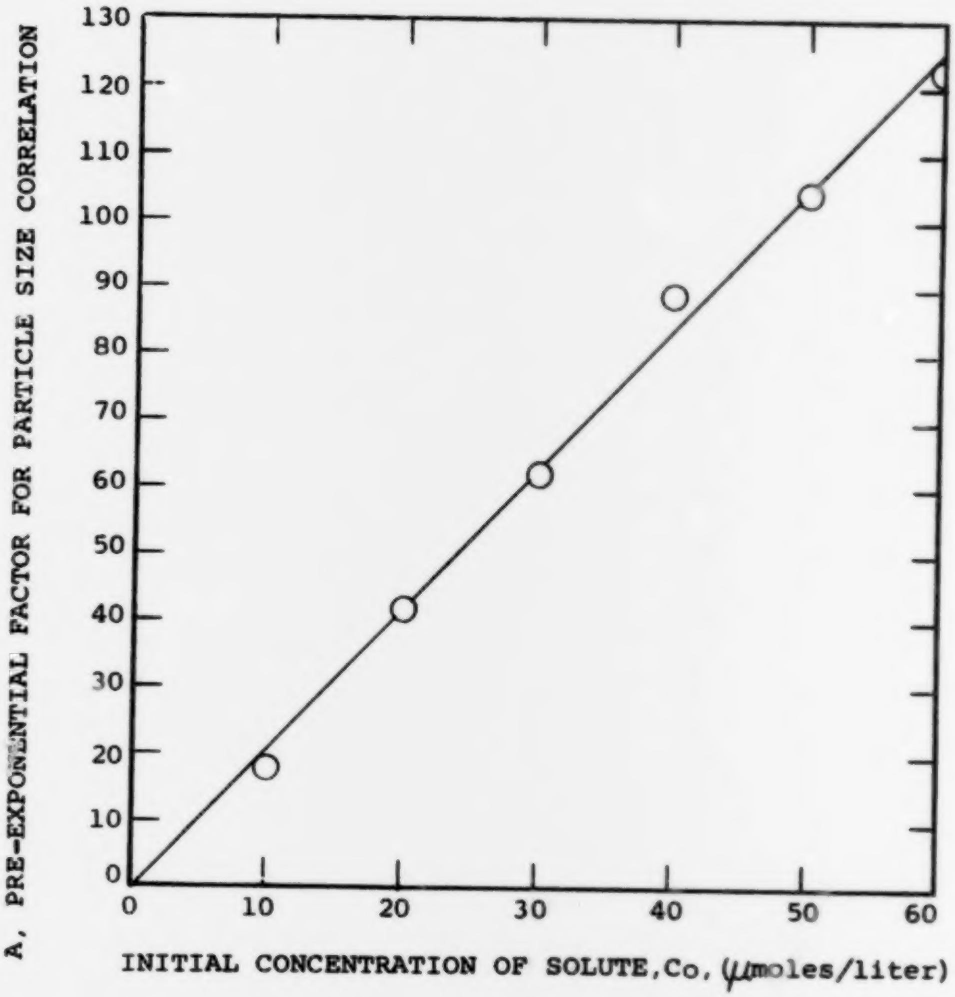

FIGURE 5-5. RELATIONSHIP BETWEEN BATCH SYSTEM RATES OF UPTAKE AND INITIAL CONCENTRATION OF SOLUTE

$$d(q)^2/d\tau = 2.08\ C_o/d_p^{1.4} \quad \text{- - - - - - -} \quad (5\text{-}10)$$

Equation 5-10 may then be used in conjunction with either Equation 3-72 or Equation 3-77, depending on whether fluid-phase pore diffusion or pore-surface diffusion is the more rapid of the two limiting internal resistances, for determination of appropriate values for the internal diffusion transfer coefficient required for numerical solution of the breakthrough equations. For the present systems the transfer coefficient, k_p, determined by Equation 3-72, is approximately 60 times the magnitude of the corresponding parameter, k_s, for the two-dimensional pore-surface diffusion case. The latter transfer coefficient was calculated by Equation 3-77. Because values of the distribution coefficient, D_G, range from 10^3 to 10^5, the rate parameter for the pore-surface diffusion case of second-order kinetics, κ_s, conversely, was found to be 2 to 4 orders of magnitude greater than κ_p, as determined by Equations 3-82 and 3-75, respectively. Pore-surface diffusion, therefore, is considered to be the limiting internal resistance for the systems investigated. It is to be noted, however, that the choice of the limiting internal rate mechanism is dependent upon the particular mathematical model utilized and that the use of another model with a different set of assumptions might indicate that pore diffusion is the internal rate determining step. It is imperative, therefore, that the use of any limiting internal mechanism is always referred to the mathematical model by which it was designated. Values of k_s used in the numerical calculations are tabulated in Table 5-2, along with values for other parameters pertinent to the solution of the equations.

Combined External and Internal Diffusion

As noted previously, Equation 3-87 may be used for calculation of the general rate coefficient, K, for the kinetic case. It indicates that external or film diffusion will be the principal rate limiting mechanism for cases in which the term $1/k_f a$ is significantly greater than the term $1/k_s a' D_G$ and that internal or pore-surface diffusion will become the controlling resistance as D_G approaches unity. For the present experiments, values for D_G have been found to range from 10^3 to 10^5. It is apparent, therefore, that film diffusion is the primary rate controlling mechanism for adsorption in the experimental fluid-bed systems. For the present experiments the resistance due to pore-surface diffusion was ,nevertheless, included in the calculations in order to preserve the generality of the solution; although, it could have been neglected without appreciably affecting the shape of the calculated profiles. In experimental systems in which D_G is small, however, it

TABLE 5-2

PHYSICO-CHEMICAL PROPERTIES OF THE EXPERIMENTAL FLUID-BED SYSTEMS

System	v (cm^3)	C_o(moles/ (cm^3)x10^9	ϵ dimensionless	ρ (gms/cm^3)	L (cm)	$k_f a$ (min^{-1})	$k_s a'$ (min^{-1})
1	656	16.0	0.491	0.381	32.4	2.05	9.95
2	707	16.6	0.528	0.354	34.9	2.57	8.86
3	784	15.7	0.574	0.319	38.7	2.89	8.40
4	824	16.3	0.595	0.304	40.6	2.27	7.90
5	864	16.3	0.614	0.290	42.6	2.36	7.53
6	909	16.0	0.633	0.275	44.8	2.59	7.18
7	744	15.5	0.553	0.337	36.8	4.10	6.58
8	1288	15.8	0.741	0.194	63.6	1.81	7.02
9	1641	16.5	0.795	0.152	81.3	1.24	8.34
10	2415	16.0	0.865	0.104	119.5	0.86	6.96
11	1270	16.0	0.633	0.275	62.8	1.98	7.18

TABLE 5-2 Continued

12	1632	15.9	0.633	0.275	81.0	1.52	7.24
13	2000	15.6	0.633	0.275	99.0	1.25	7.27
14	2362	15.6	0.633	0.275	117.0	1.07	7.30
15	909	25.8	0.633	0.275	44.8	2.52	4.90
16	909	35.1	0.633	0.275	44.8	2.46	4.68
17	909	46.3	0.633	0.275	44.8	2.49	3.97
18	909	56.8	0.633	0.275	44.8	2.74	3.55

NOTES:

A) Flow rate was studied as a variable in systems 1-6; particle size in systems 7-10; bed depth in systems 11-14; and solute concentration in systems 15-18.

B) All studies were carried out at flow rates of 10 gal/min/sq.ft. except for systems 1-5, for which flow rates of 2, 4, 6, 7, and 8 gal/min/sq. ft., respectively, were maintained.

C) Each system contained 250 grams of activated carbon except systems 11-14, in which 350, 450, 550, and 650 grams, respectively, were used.

D) Sizes of the granular adsorbent for systems 7-10 were 1.011, 0.503, 0.356, and 0.273-mm, respectively, while 0.711-mm carbon was used for all other systems.

is necessary to include the effect of pore transport on the overall process for accurate prediction of the breakthrough curves.

CHAPTER 6

NUMERICAL PREDICTION OF CONCENTRATION-TIME PROFILES AND EXPERIMENTAL RESULTS

CORRELATION OF EXPERIMENTAL RESULTS AND CALCULATED CURVES

Eighteen fluid-bed studies have been conducted to test the agreement between the experimental data derived therefrom and the concentration-time profiles numerically calculated from the predictive model presented in Chapter 3. The coal-base carbon and single-solute solutions of DNOSBP have been used for all studies. Table 5-2 lists the salient properties for each of the eighteen systems studied. These were derived from correlations of the hydrodynamic (v, ϵ, ρ, and L) and mass-transfer parameters (C_o, $k_f a$, and $k_s a'$) presented in Chapters 4 and 5, respectively.

Flow rate, particle size of adsorbent, depth of expanded bed, and influent solute concentration have been studied as control variables. For purposes of illustrating the validity of the predictive model, plots of the experimental data and the corresponding curves calculated by Equation 3-38 are presented together in Figures 6-1 through 6-6, 6-8 through 6-11, 6-13 through 6-16, and 6-18 through 6-21. In addition, the calculated concentration-time profiles for each control variable are provided on summary plots to illustrate the respective effects of these variables over the ranges investigated (Figures 6-7, 6-12, 6-17, and 6-22). Further, uptake-time profiles are provided to give the solid-phase concentrations at any point of time.

Flow Rate as a Variable

Column studies 1 through 6 represent experiments in which the effects of flow rates on concentration-time profiles have been investigated. Each of the six experimental columns contained 250-grams of 0.711-millimeter carbon; influent concentrations of solute were maintained at 15.7 to 16.5 μmoles/liter. Expanded bed depths ranged from 32.4 centimeters at 2 GPM/SQ.FT. to 44.8 centimeters at 10 GPM/SQ.FT.

Data for the fluid-bed systems 1 through 6, with flow rates of 2, 4, 6, 7, 8, and 10 GPM/SQ.FT. are plotted in Figures 6-1 through 6-6, respectively, along with the concentration-history curves calculated by the predictive mass transfer model. Good agreement may be noted between the calculated S-shaped curve—typical for fluid-bed mass transfer systems—and the experimental data. Although, for the higher flow rates, some scatter in the data is noted for values of C/C_0 greater than 0.8. The uptake

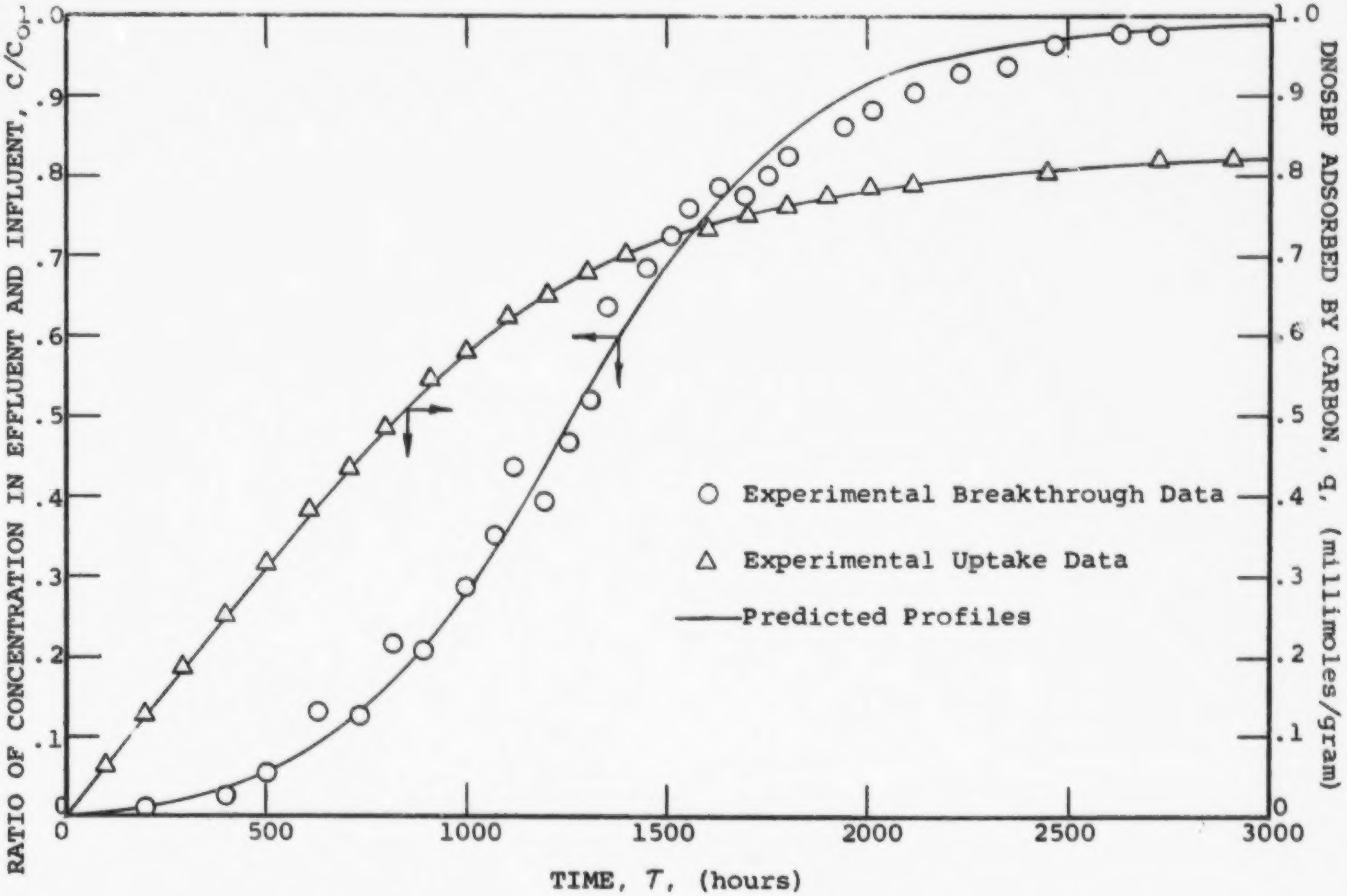

FIGURE 6-1. CONCENTRATION- AND UPTAKE-TIME PROFILES FOR A FLOW RATE OF 2GPM/SQ.FT. IN A 250-GRAM FLUID-BED OF 0.711-MM CARBON

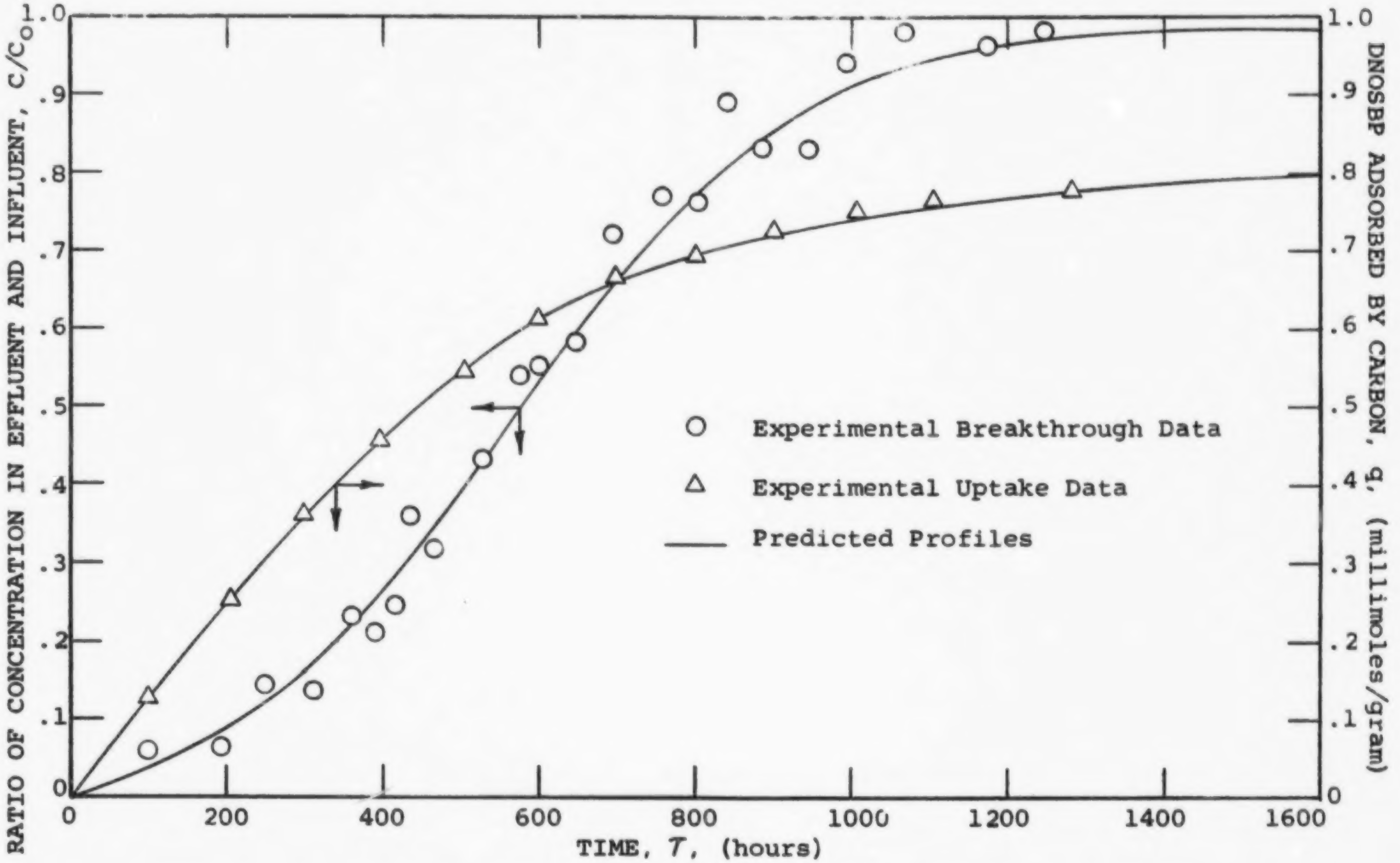

FIGURE 6-2. CONCENTRATION- AND UPTAKE-TIME PROFILES FOR A FLOW RATE OF 4 GPM/SQ.FT. IN A 250-GRAM FLUID-BED OF 0.711-MM CARBON

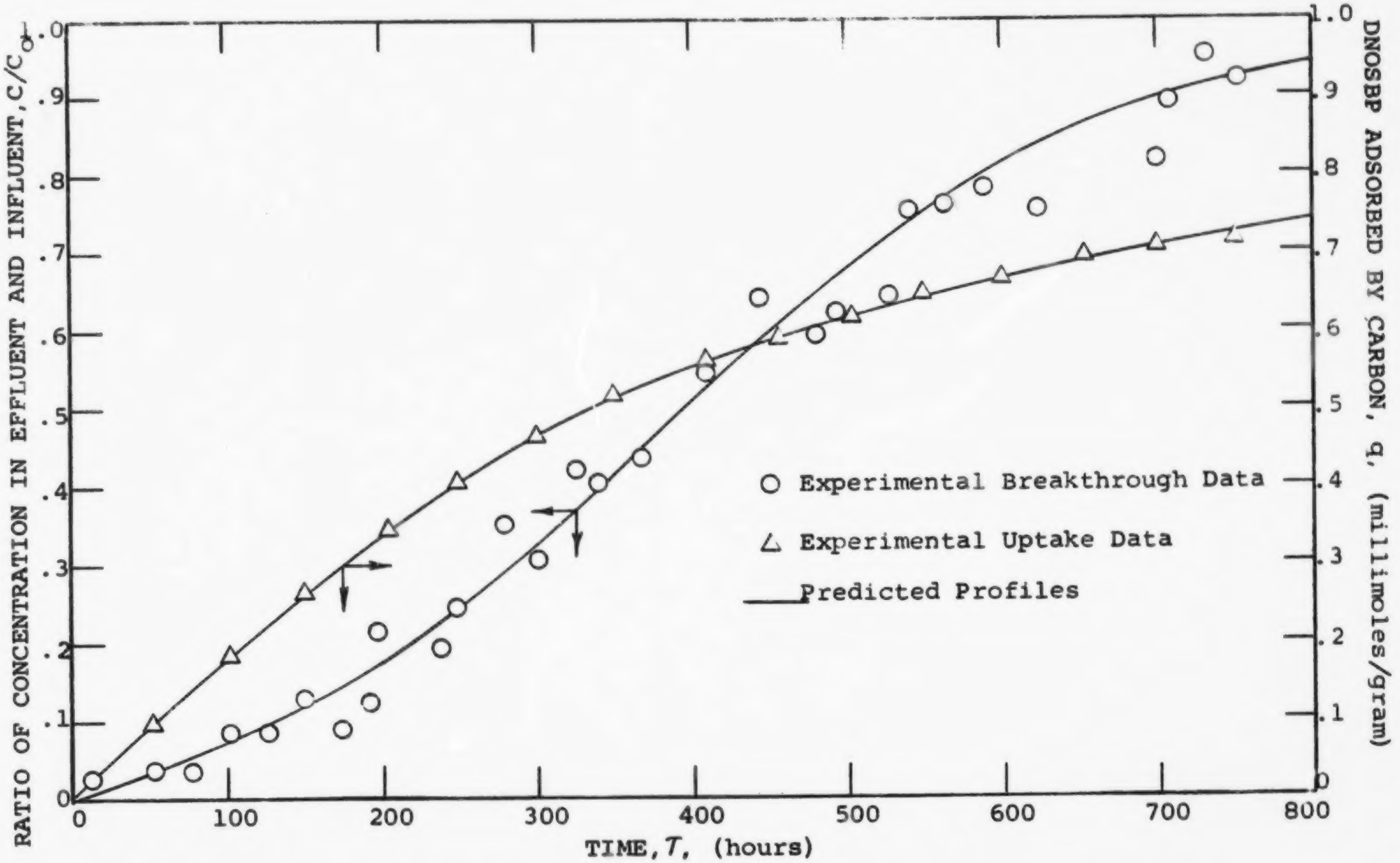

FIGURE 6-3. CONCENTRATION- AND UPTAKE-TIME PROFILES FOR A FLOW RATE OF 6 GPM/SQ.FT. IN A 250-GRAM FLUID-BED OF 0.711-MM CARBON

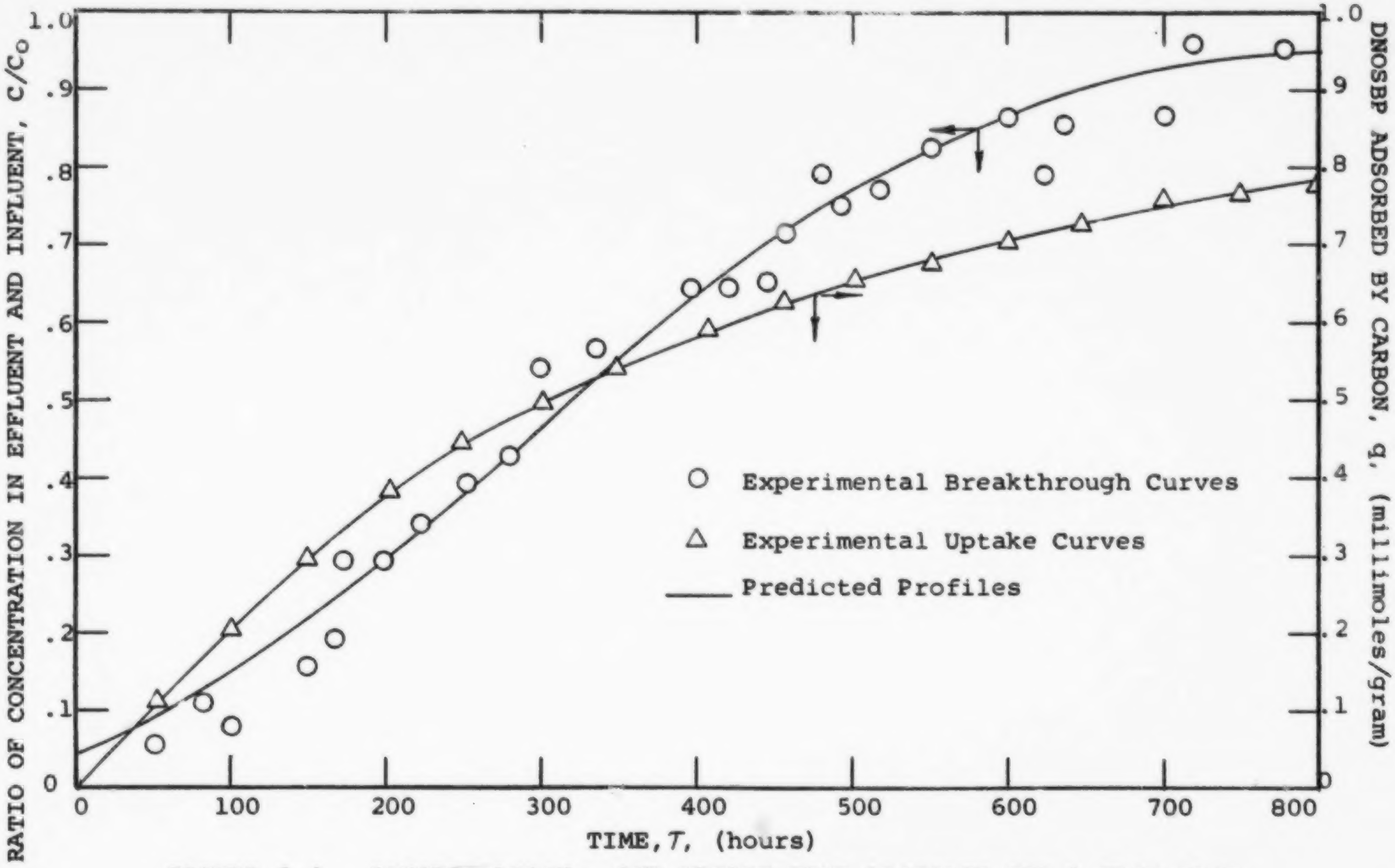

FIGURE 6-4. CONCENTRATION- AND UPTAKE-TIME PROFILES FOR A FLOW RATE OF 7 GPM/SQ.FT. IN A 250-GRAM FLUID-BED OF 0.711-MM CARBON

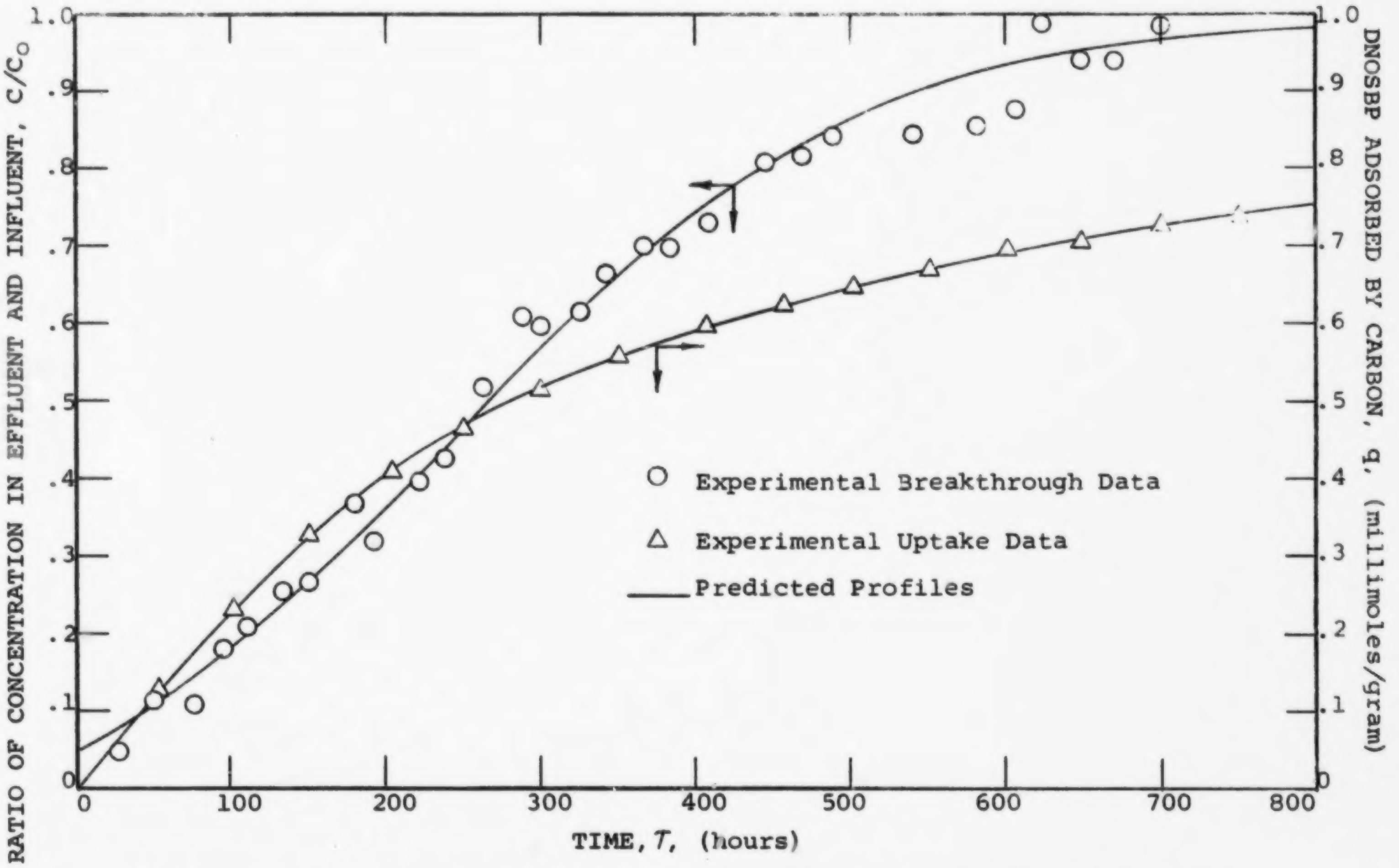

FIGURE 6-5. CONCENTRATION- AND UPTAKE-TIME PROFILES FOR A FLOW RATE OF 8 GPM/SQ.FT. IN A 250-GRAM FLUID-BED OF 0.711-MM CARBON

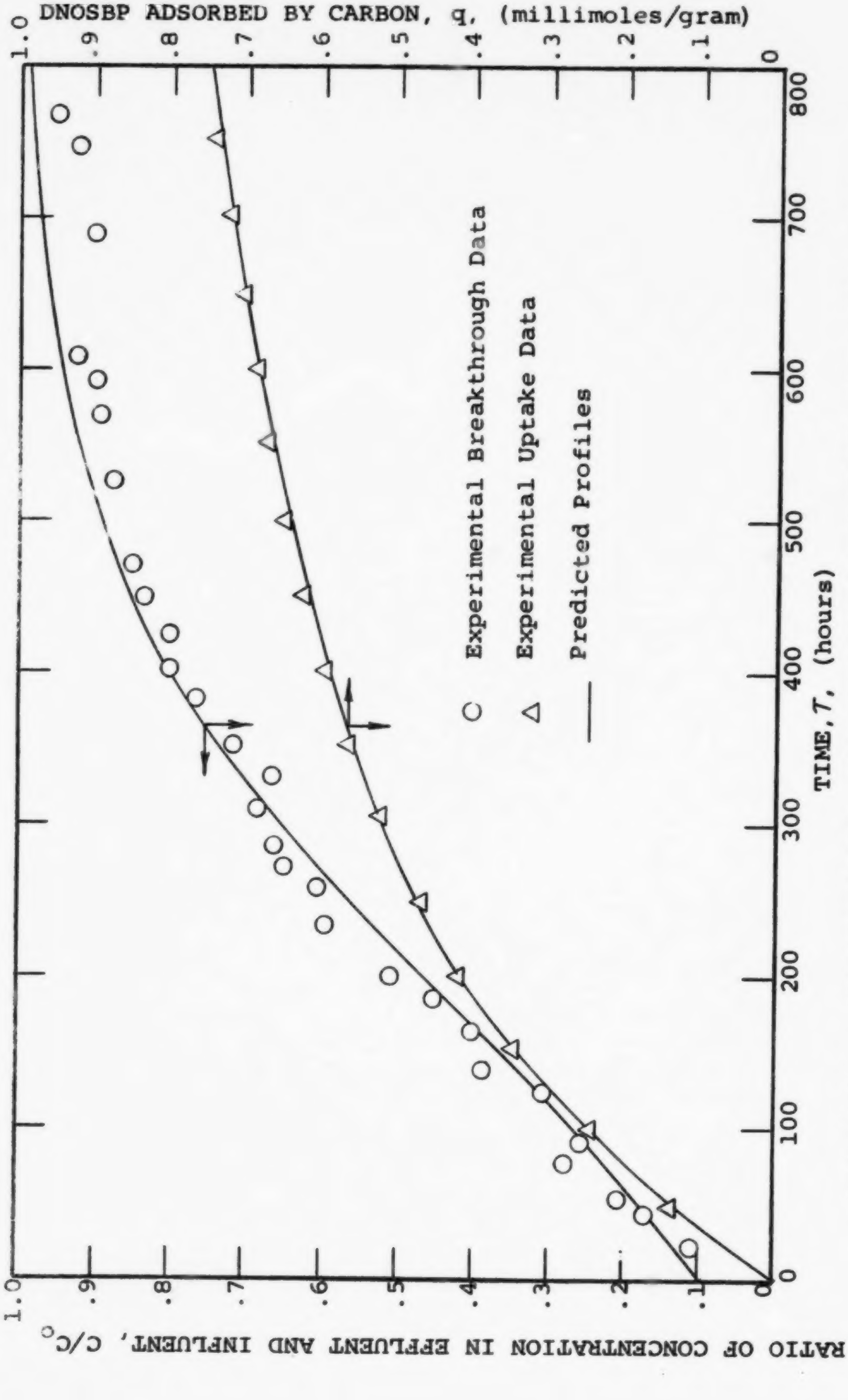

FIGURE 6-6. CONCENTRATION- AND UPTAKE-TIME PROFILES FOR A FLOW RATE OF 10 GPM/SQ. FT. IN A 250-GRAM FLUID-BED OF 0.711-MM CARBON

curves for the six studies appear to be approaching an ultimate saturation value of approximately 800 micromoles/gram. This corresponds to an uptake value of 19.2 percent by weight of the granular material at the point of complete exhaustion of the activated carbon. Further, if one considers a columnar fluid-bed installation and arbitrarily selects a shut-off breakthrough point of C/C_o equivalent to 0.3, increasing efficiency in the use of adsorbent is achieved for lower flow rates. In a complete economic analysis, however, many other factors, which must be considered, will dictate the optimum rate of flow.

The effect of flow rate on the concentration-time profile over the experimental range of this control variable is illustrated by the numerically derived curves presented in Figure 6-7. It may be observed in Figure 6-7 that the slope of the breakthrough portion of the concentration-time profile becomes steeper with increasing flow rate. The incremental change in slope becomes smaller, however, as the flow velocity increases. Concentration-time profiles in the higher velocity regions therefore show only minor differences in breakthrough pattern or shape, the difference between consecutive curves being primarily a simple displacement on the time axis. Because film-diffusion is the principal rate-limiting mechanism, these

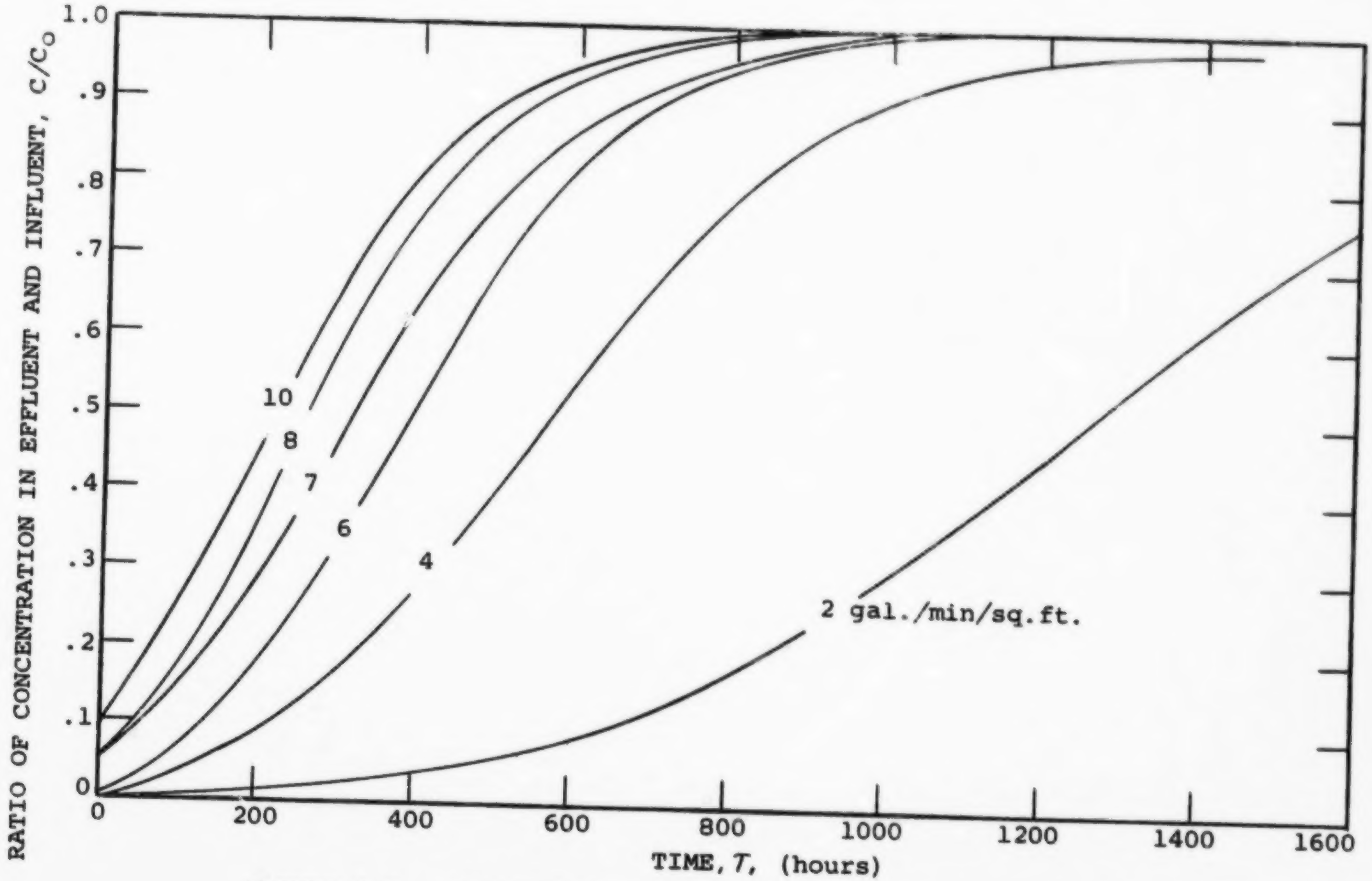

FIGURE 6-7. CONCENTRATION-TIME PROFILES FOR DIFFERENT FLOW RATES
(250-GRAMS OF 0.711-MM CARBON)

observations may be explained on the basis that an increase in flow rate results in a compression or reduction of the surface film, thereby decreasing resistance to mass transfer and increasing the mass transfer rate. Hydrodynamic considerations indicate that the thickness of the surface film is inversely proportional to the cube-root of the flow velocity for rigid spherical particles in fluid-bed systems (35). This implies that changes in the mass transfer rate with flow rate are considerably greater in low-velocity regimes than in high-velocity regimes. Incremental changes in the slope of the breakthrough curve consequently become smaller as the flow velocity increases.

Particle Size as a Variable

Five experiments (Systems 6-10) have been carried out with different particle sizes—250 grams of 0.711, 1.011, 0.503, 0.356 and 0.273-mm., respectively—at flow rates of 10 gal/min/sq.ft. with an initial concentration of solute of 16.0 ± 0.5 micromoles/liter. Expanded bed depths ranged from 36.8 centimeters for the 1.011-mm carbon to 119.5 centimeters for the 0.273-mm carbon.

Values of C/C_o are plotted as a function of time in Figures 6-6 and 6-8 through 6-11 for systems 6 through 10, respectively. Good correlation between the experimental data and the corresponding numerically-generated profile

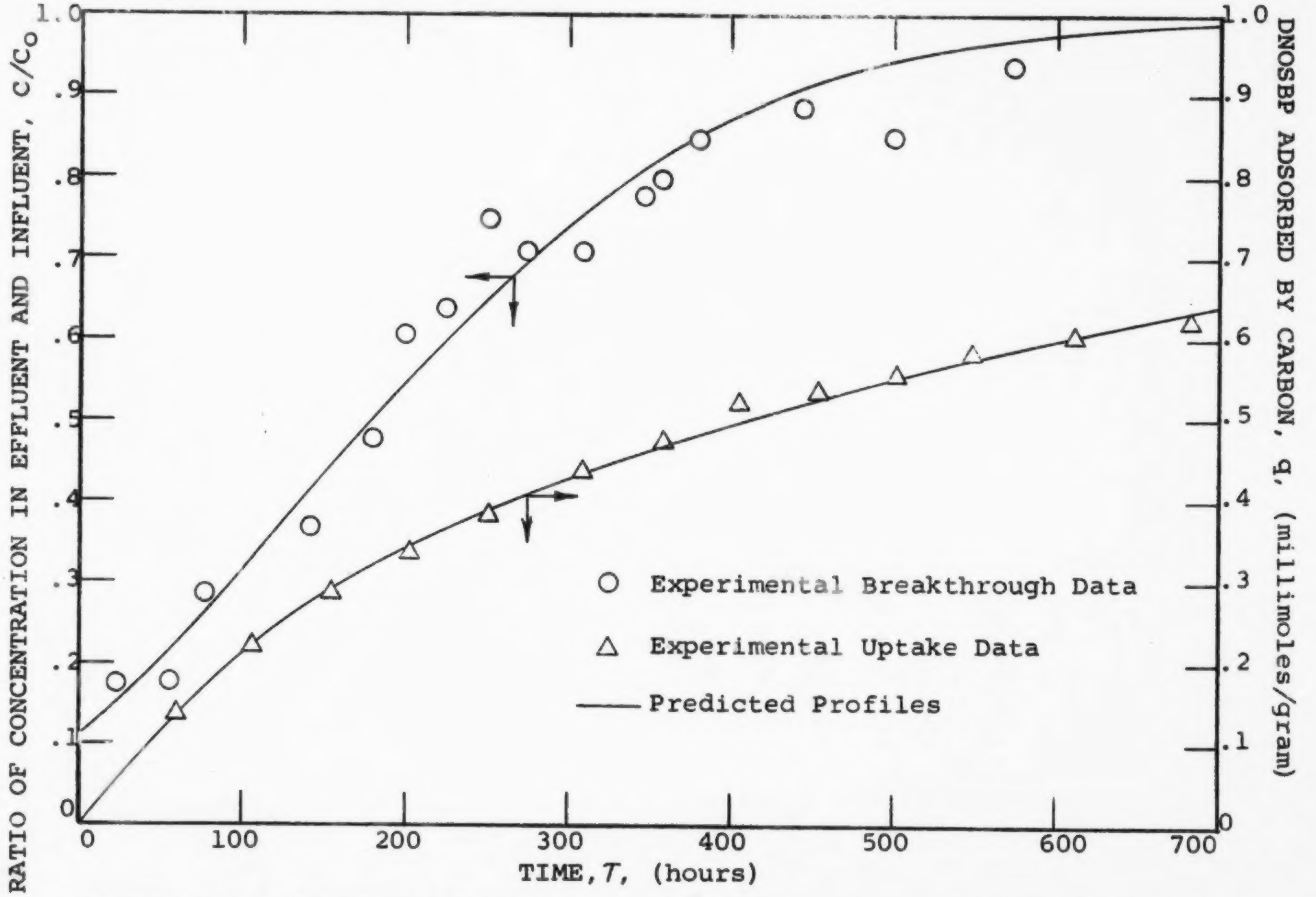

FIGURE 6-8. CONCENTRATION- AND UPTAKE-TIME PROFILES FOR A FLOW RATE OF 10 GPM/SQ. FT. IN A 250-GRAM FLUID-BED OF 1.011-MM CARBON

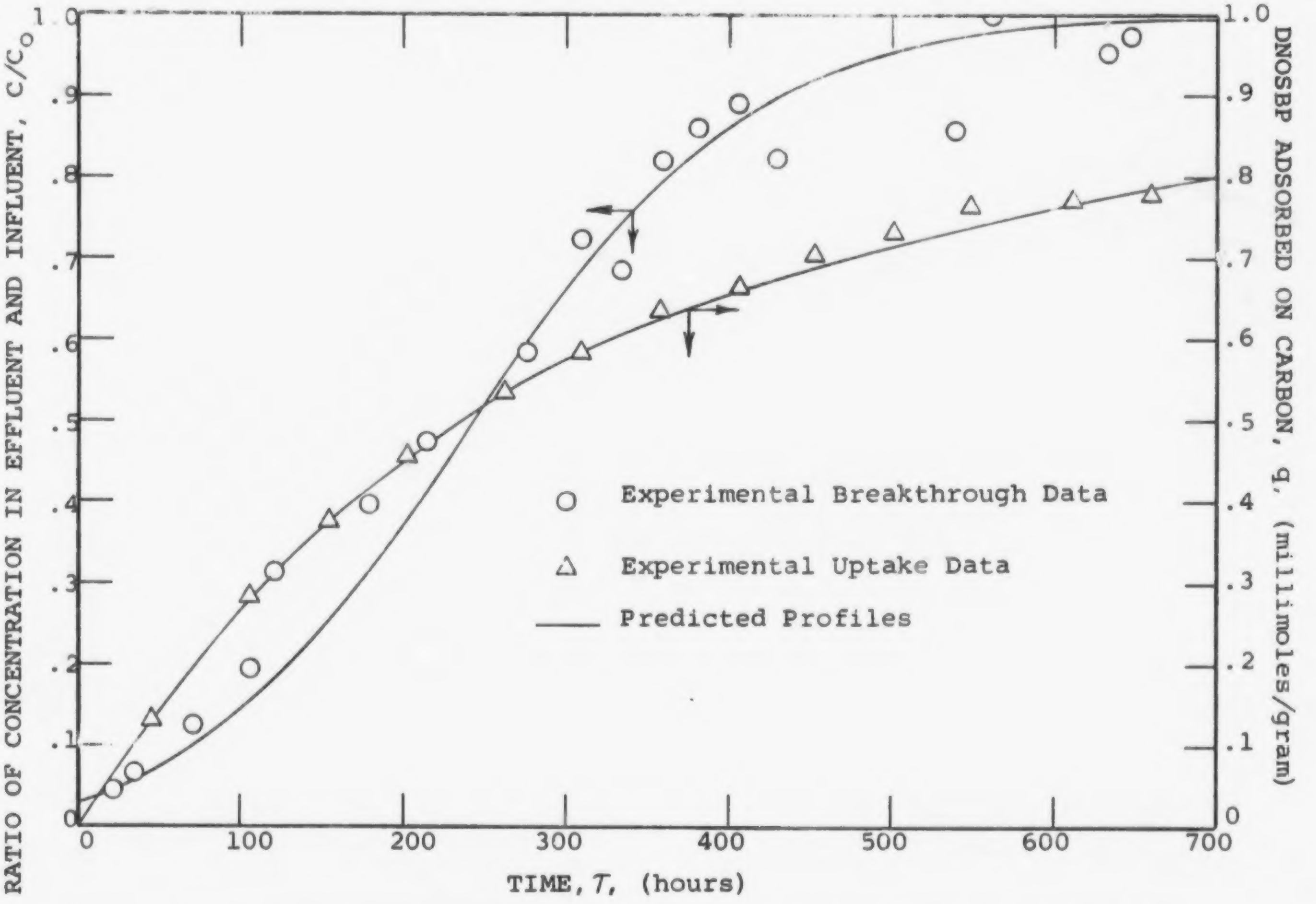

FIGURE 6-9. CONCENTRATION- AND UPTAKE-TIME PROFILES FOR A FLOW RATE OF 10 GPM/SQ. FT. IN A 250-GRAM FLUID-BED OF 0.503-MM CARBON

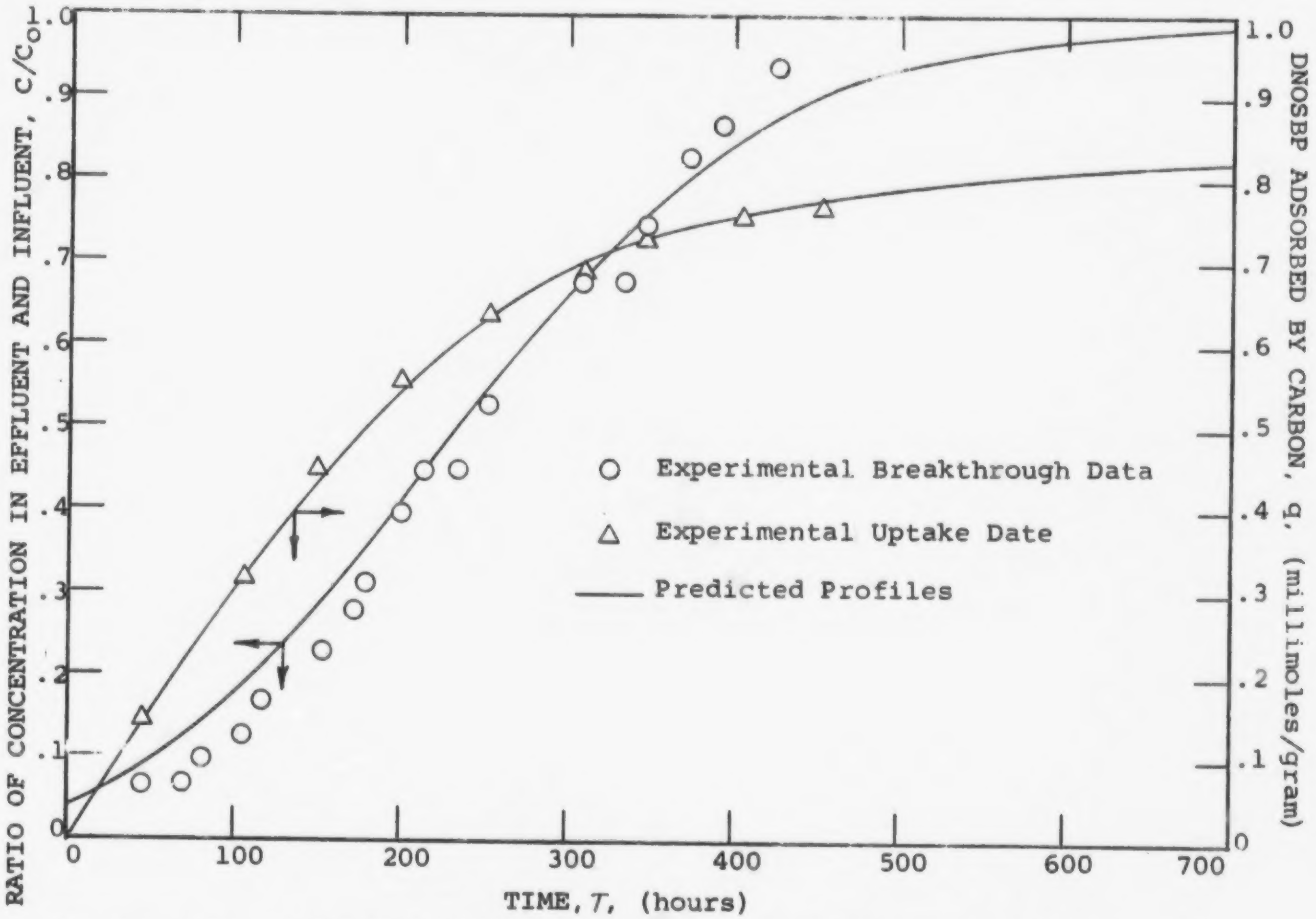

FIGURE 6-10. CONCENTRATION- AND UPTAKE-TIME PROFILES FOR A FLOW RATE OF 10 GPM/SQ. FT. IN A 250-GRAM FLUID-BED OF 0.356-MM CARBON

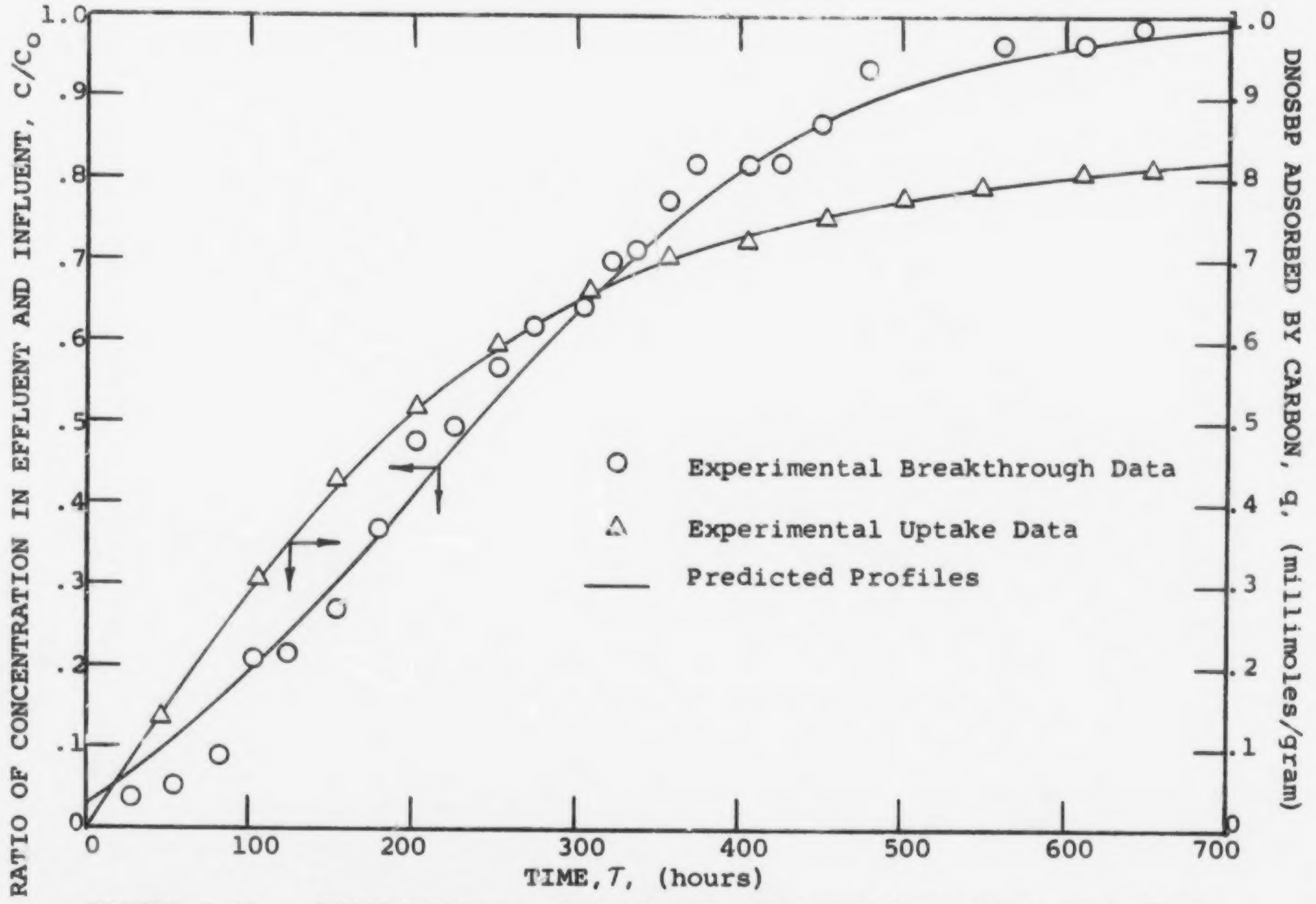

FIGURE 6-11. CONCENTRATION- AND UPTAKE-TIME PROFILES FOR A FLOW RATE OF 10 GPM/SQ. FT. IN A 250-GRAM FLUID-BED OF 0.273-MM CARBON

is again observed. Figure 6-12, a summary plot of the calculated curves, shows rather minor differences between the concentration-time profiles over the experimental range of particle size. This result is expected, however, as both the equilibrium relationships and the initial film-diffusion limited rates have been found to be essentially the same for different particle sizes (63). Because, as previously indicated, film diffusion is the primary rate mechanism for the experimental fluid-bed systems, the overall mass transfer rates should be relatively independent of particle size, and the breakthrough curves should therefore be similar.

Weber and Morris (66) have found considerable differences in fluid-bed concentration-history curves for different particle sizes of a small-pore coconut carbon. The differences, however, were primarily in displacement along the time axis, with the slopes of the breakthrough portions of the curves showing insignificant differences. Thus the data of Weber and Morris also indicate that mass transport rates are similar for different particle sizes, and concur with the data from the current studies. Conversely, values for the equilibrium uptake, q_∞ , in the systems studied by Weber and Morris varied considerably for different sizes, thus accounting for the observed

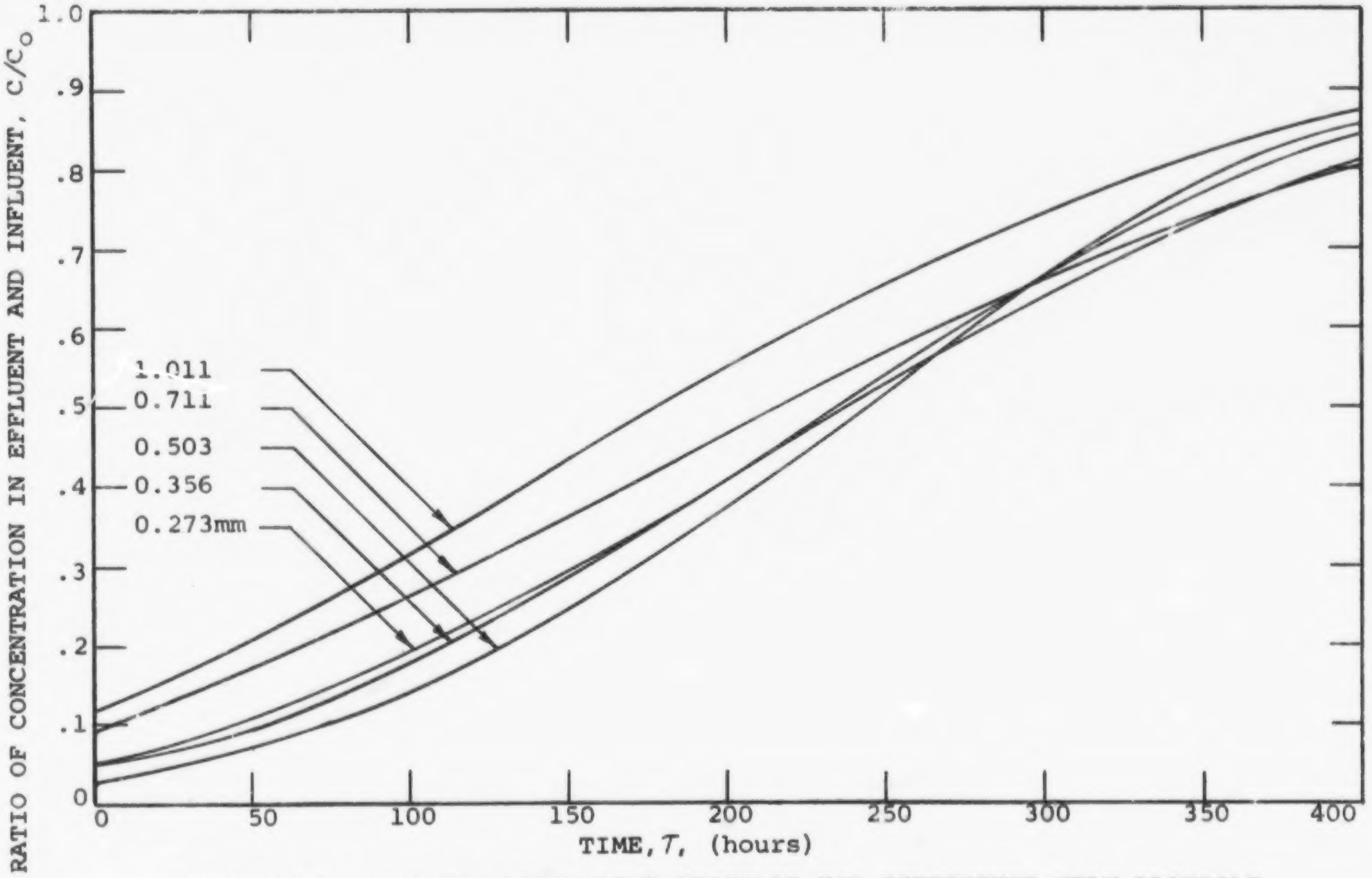

FIGURE 6-12. CONCENTRATION-TIME PROFILES FOR DIFFERENCE MEAN PARTICLE DIAMETERS (250-GRAMS OF CARBON; 10 GPM/SQ.FT. FLOW RATE)

systematic displacement of the breakthrough curves. The variation of q_∞ with particle size for the small-pore carbon used by Weber and Morris has been supported by separate measurements of adsorption isotherms for this carbon, which have indicated that the equilibrium capacity varies with the square of the reciprocal of the diameter of the carbon particle (65). A possible explanation for the observed dependence was advanced earlier; it more than likely may be attributed to the method of preparation of the adsorbent.

Thus, the results for batch and fluid-bed systems presented herein and by Weber and Morris (66) are internally consistent, even though differences in particle size dependence have been noted between the two independent sets of data. Further studies designed to evaluate the specific particle-size effects for the several types of active carbon prepared by different procedures should resolve the observed differences.

Effect of Expanded Bed Depth

Figures 6-6 and 6-13 through 6-16 show breakthrough curves for fluid-bed systems 6 and 11 through 14, in which expanded bed depth was studied as a control variable. Each column in this series was charged with a different quantity (250, 350, 450, 550, and 650 grams, respectively) of 0.711-mm

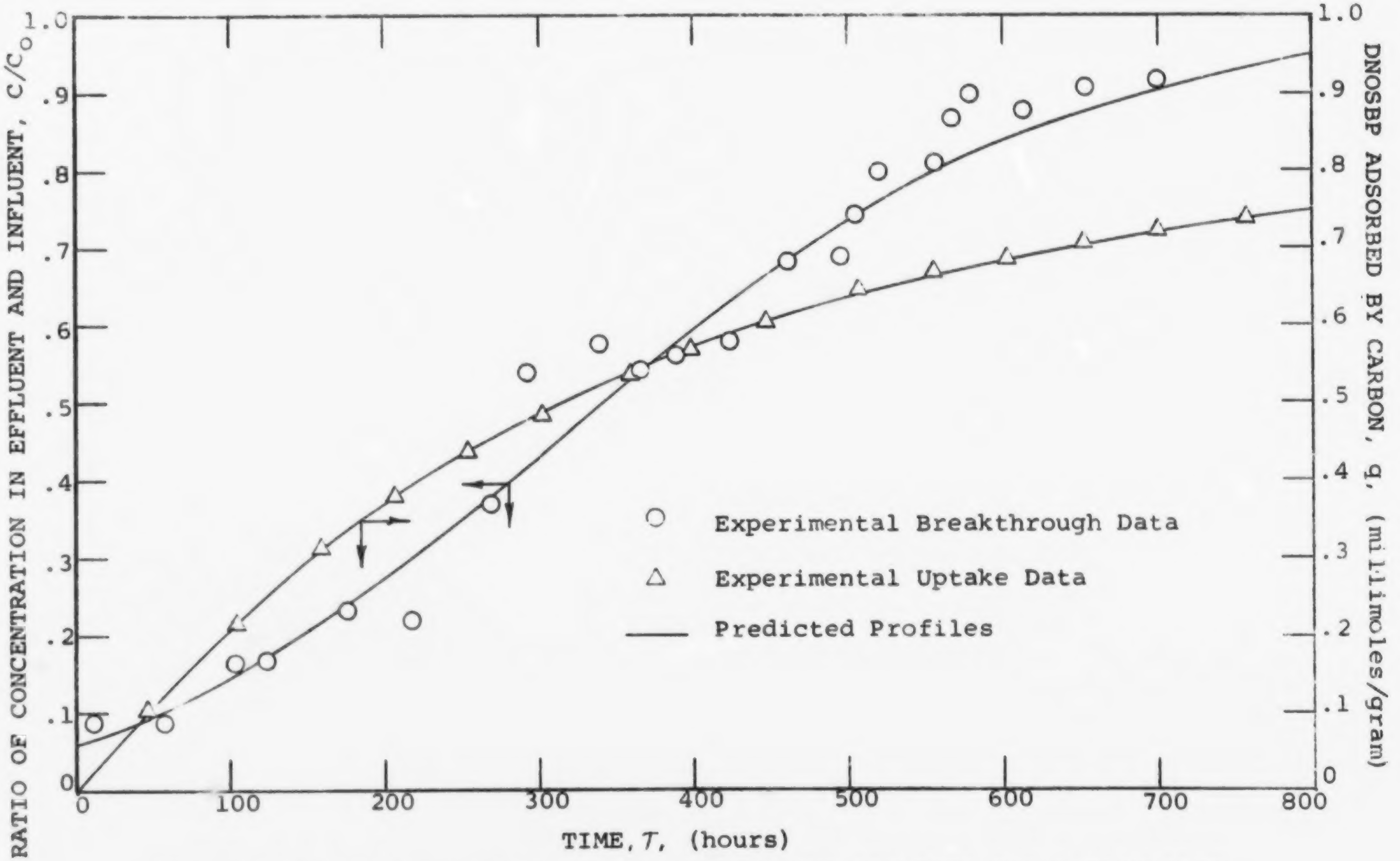

FIGURE 6-13. CONCENTRATION- AND UPTAKE-TIME PROFILES FOR A FLOW RATE OF 10 GPM/SQ. FT. IN A 350-GRAM FLUID-BED OF 0.711 -MM CARBON

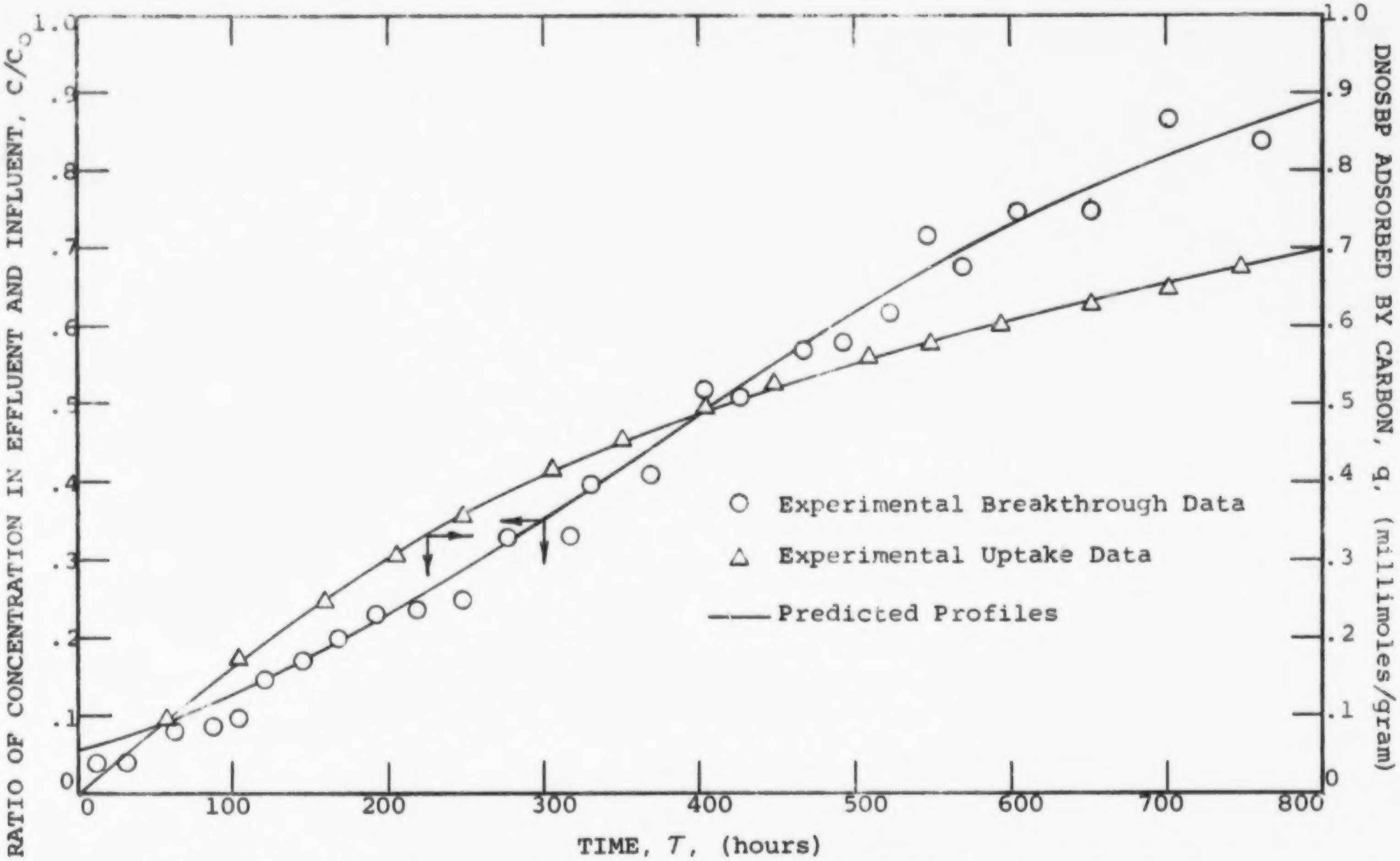

FIGURE 6-14. CONCENTRATION- AND UPTAKE-TIME PROFILES FOR A FLOW RATE OF 10 GPM/SQ. FT. IN A 450-GRAM FLUID-BED OF 0.711-MM CARBON

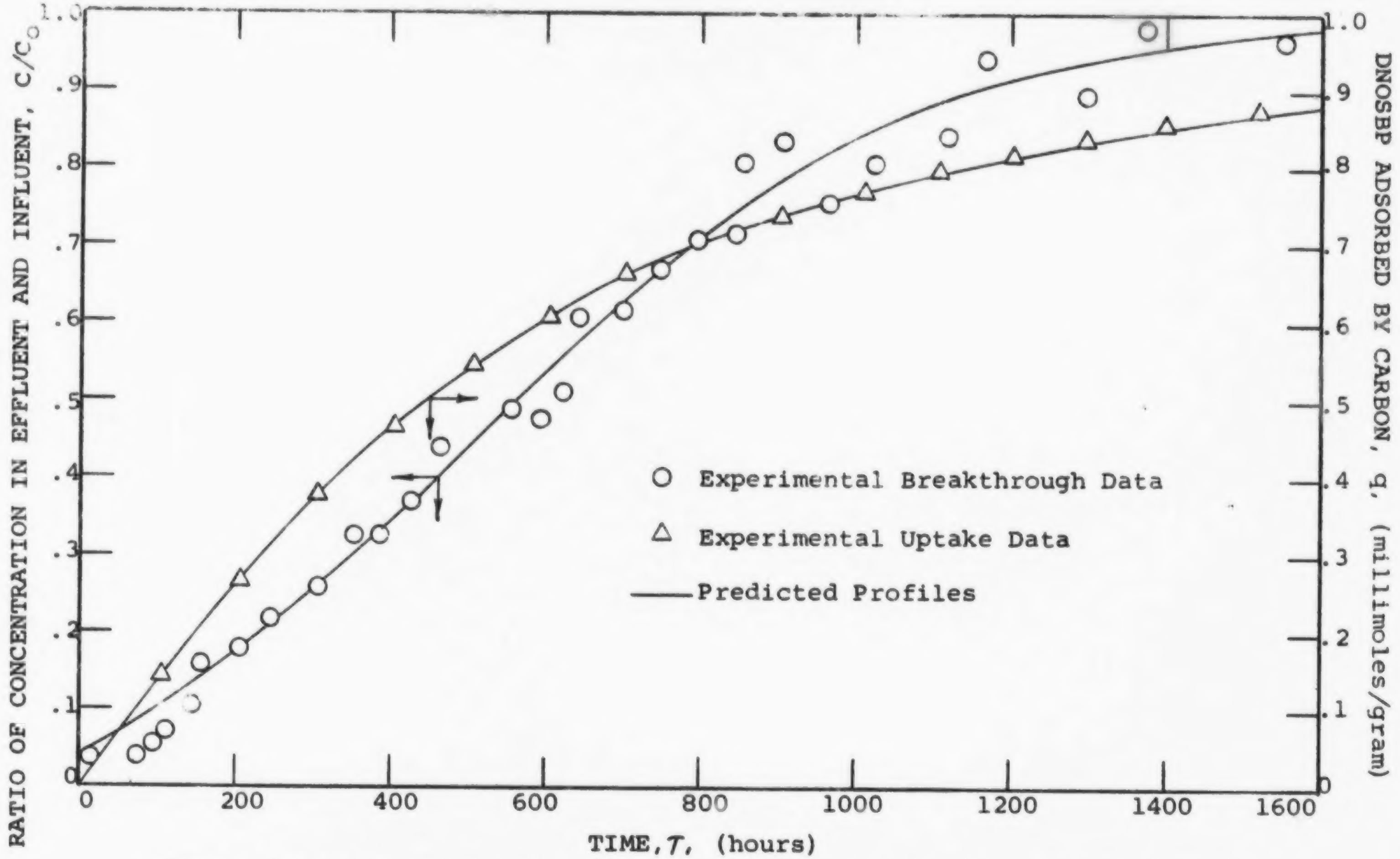

FIGURE 6-15. CONCENTRATION- AND UPTAKE-TIME PROFILES FOR A FLOW RATE OF 10 GPM/SQ. FT. IN A 550-GRAM FLUID-BED OF 0.711-MM CARBON

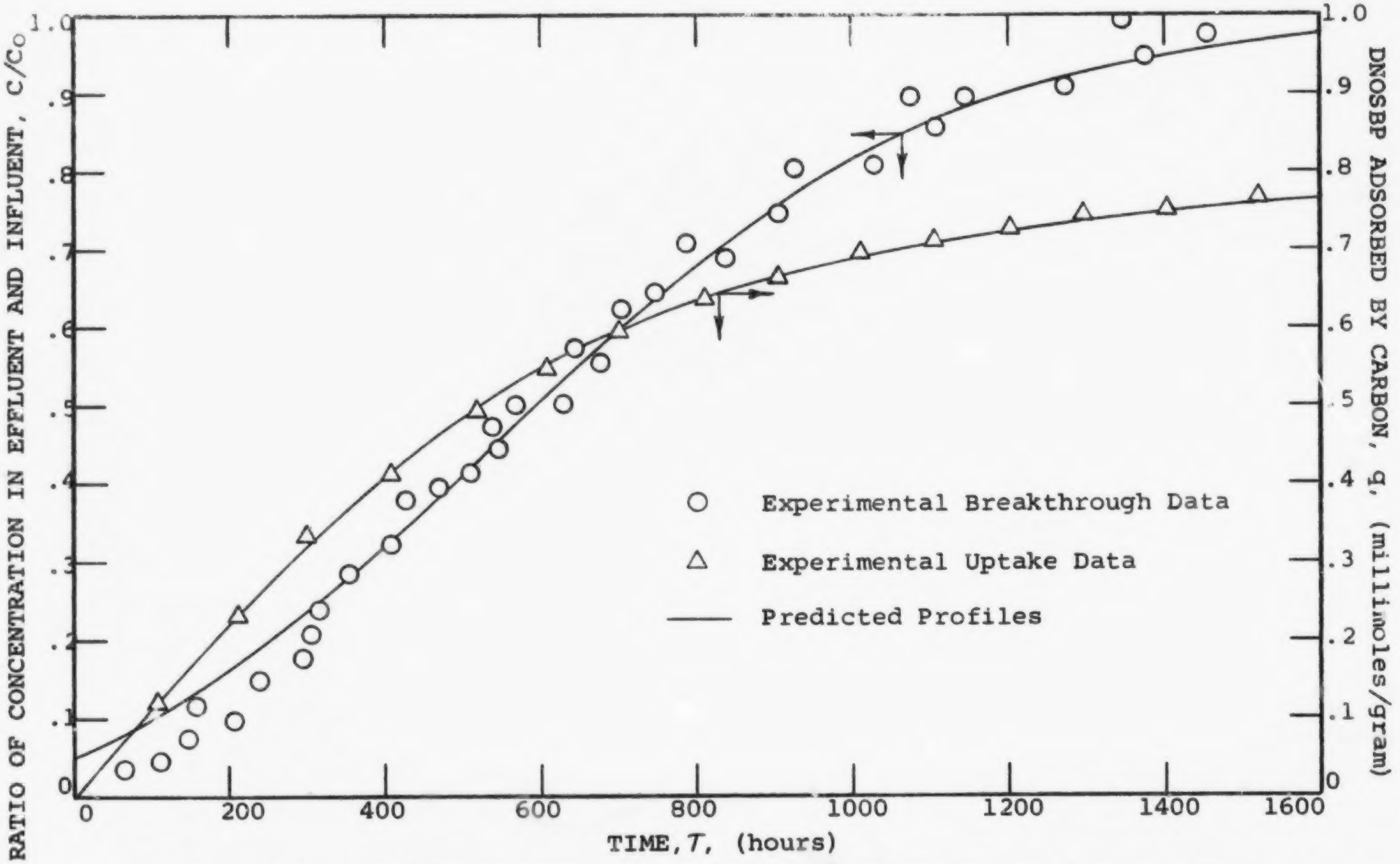

FIGURE 6-16. CONCENTRATION- AND UPTAKE-TIME PROFILES FOR A FLOW RATE OF 10 GPM/SQ. FT. IN A 650-GRAM FLUID-BED OF 0.711-MM CARBON

carbon to yield different expanded bed depths (44.8, 62.6, 81.0, 99.0 and 117.0 centimeters, respectively). The flow rate for each experiment was 10 gallons/minute/square foot, while influent concentrations of DNOSBP were maintained at 16.0 ± 0.4 micromoles/liter.

Reasonable correlation of the predicted curves with the experimental data for the various systems may be observed in the figures. Even though the spread of the experimental data is considerable in several instances, the calculated curves describe, rather well, the general shape of the profiles defined by the experimental data. Figure 6-17 illustrates the relationship of the concentration-time profile to the depth of expanded bed. It may be noted that between 5 and 10 percent of the influent solute is leaking through the column into the effluent from the very outset of each experiment. If the rate coefficient were independent of bed depth, as was anticipated, one would expect that initial breakthrough of solute would be delayed somewhat for the deeper beds. Thus, the observation of approximately the same amount of initial leakage in each case tends to confirm the fact that higher rate coefficients result for shallower beds. The explanation for the observed dependence, forwarded in Chapter 5, appears the most probable, even though further experimentation is neces-

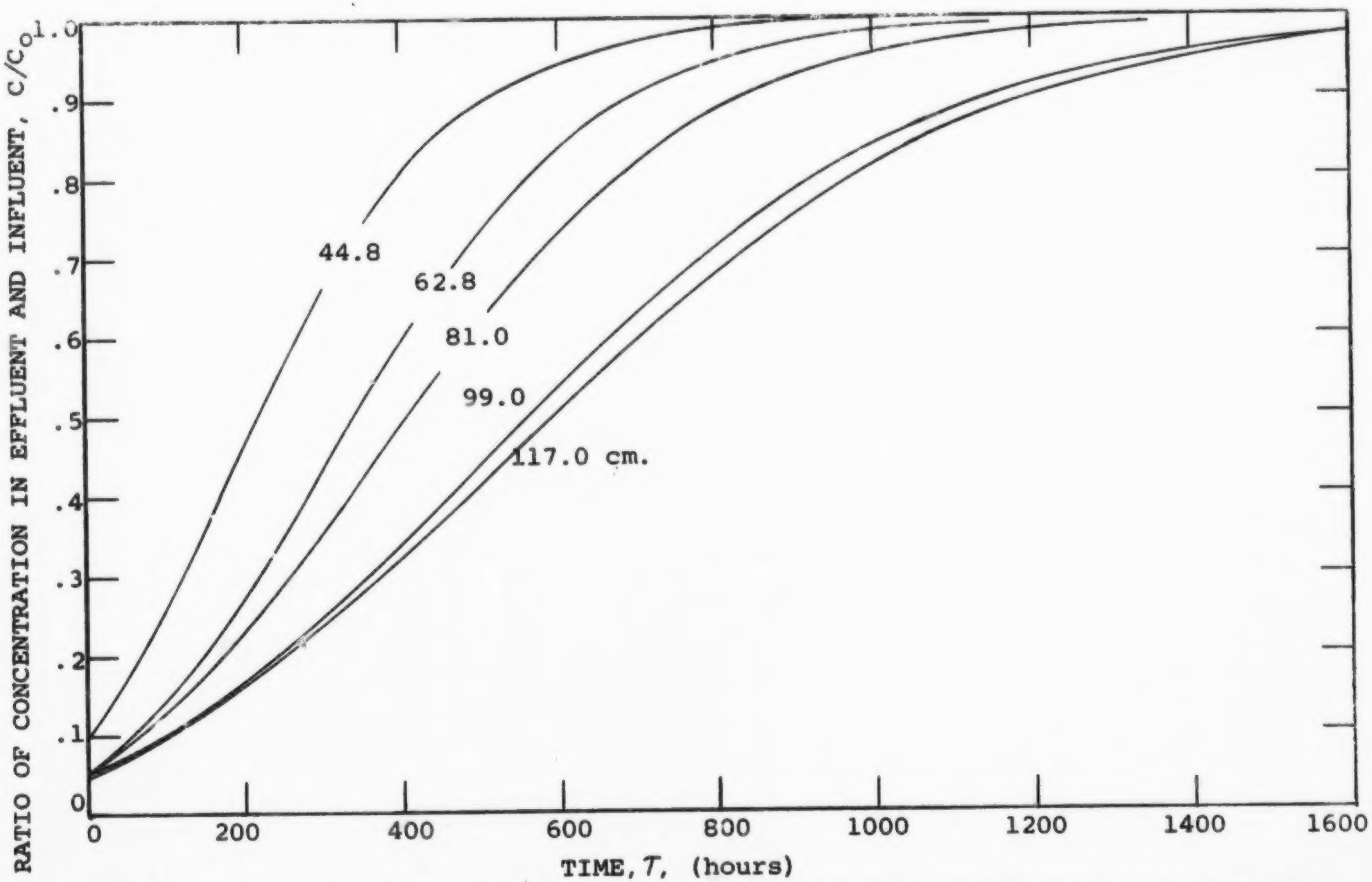

FIGURE 6-17. CONCENTRATION-TIME PROFILES FOR DIFFERENT DEPTHS OF EXPANDED BED (0.711-MM CARBON; 10 GPM/SQ. FT. FLOW RATE)

sary to fully delineate the specific and effects involved.

Solute Concentration as a Variable

The effect of the influent concentration of solute on breakthrough was studied in systems 6 and 15 through 18. Each of the experimental columns contained 250 grams of 0.711-mm carbon. Flow rates were maintained at 10 gal/min/sq.ft., and, because rate of flow and particle size were held constant from system to system, the expanded bed depth for each column was 44.8 centimeters.

Data for these systems in which influent concentrations were maintained at 16.0, 25.8, 35.1, 46.3 and 56.8 micromoles/liter is plotted in Figures 6-6, and 6-18 through 6-21, respectively. The corresponding curves calculated by use of Equation 3-51 are included on these plots for comparison purposes. The agreement between the data and the calculated curve again illustrates the adequacy of the mathematical model for predicting concentration-time profiles.

A summary plot for all columns in which solute concentration was studied as a control variable is presented in Figure 6-22. It is apparent that the sharpness of breakthrough increases with increasing initial concentration of solute. This type of behavior is expected, in that the film diffusion coefficients for the experimental columns

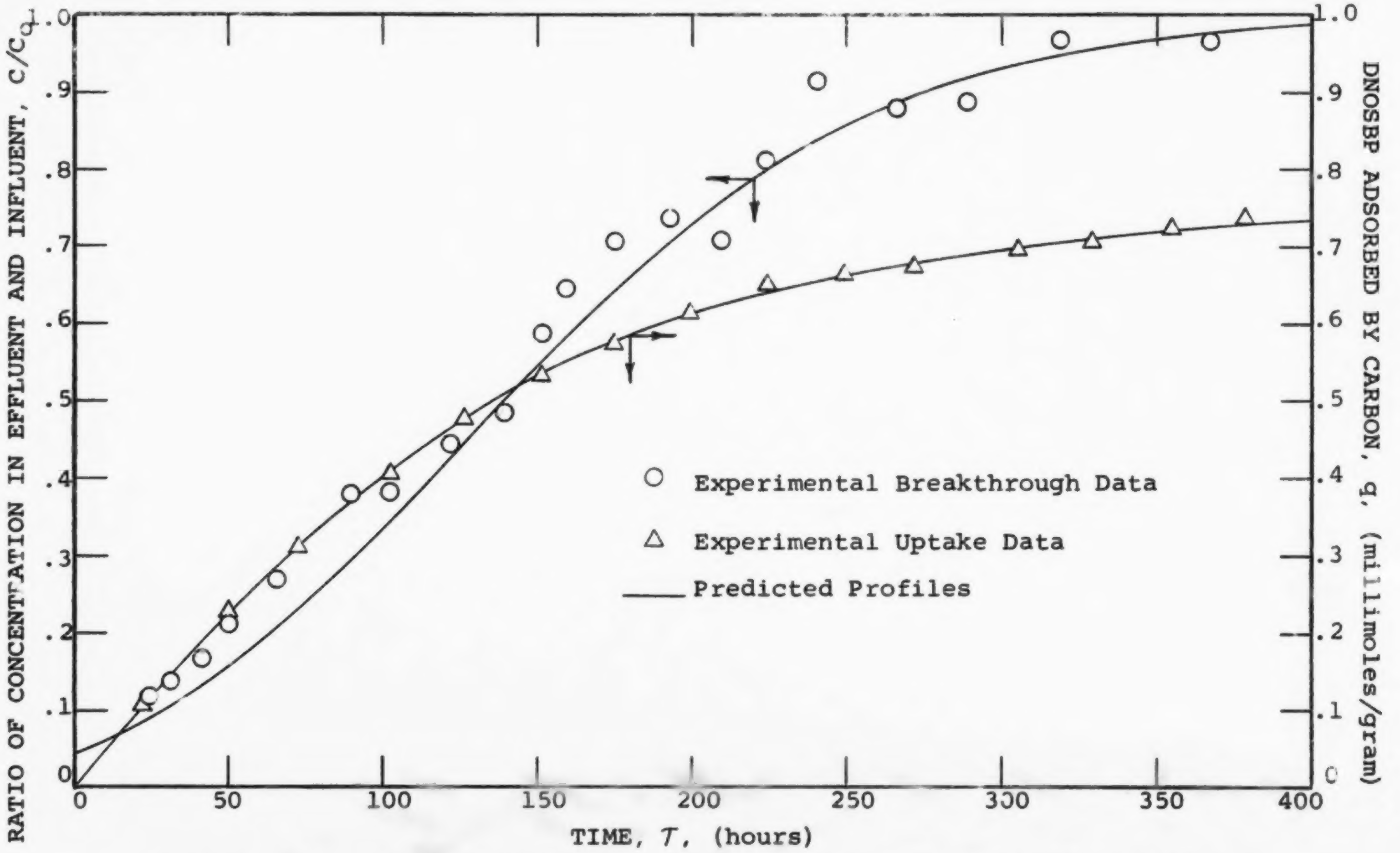

FIGURE 6-18. CONCENTRATION- AND UPTAKE-TIME PROFILES FOR AN INFLUENT CONCENTRATION OF 25.8 μMOLES/LITER (250-GRAMS OF 0.711-MM CARBON; 10 GPM/SQ.FT.)

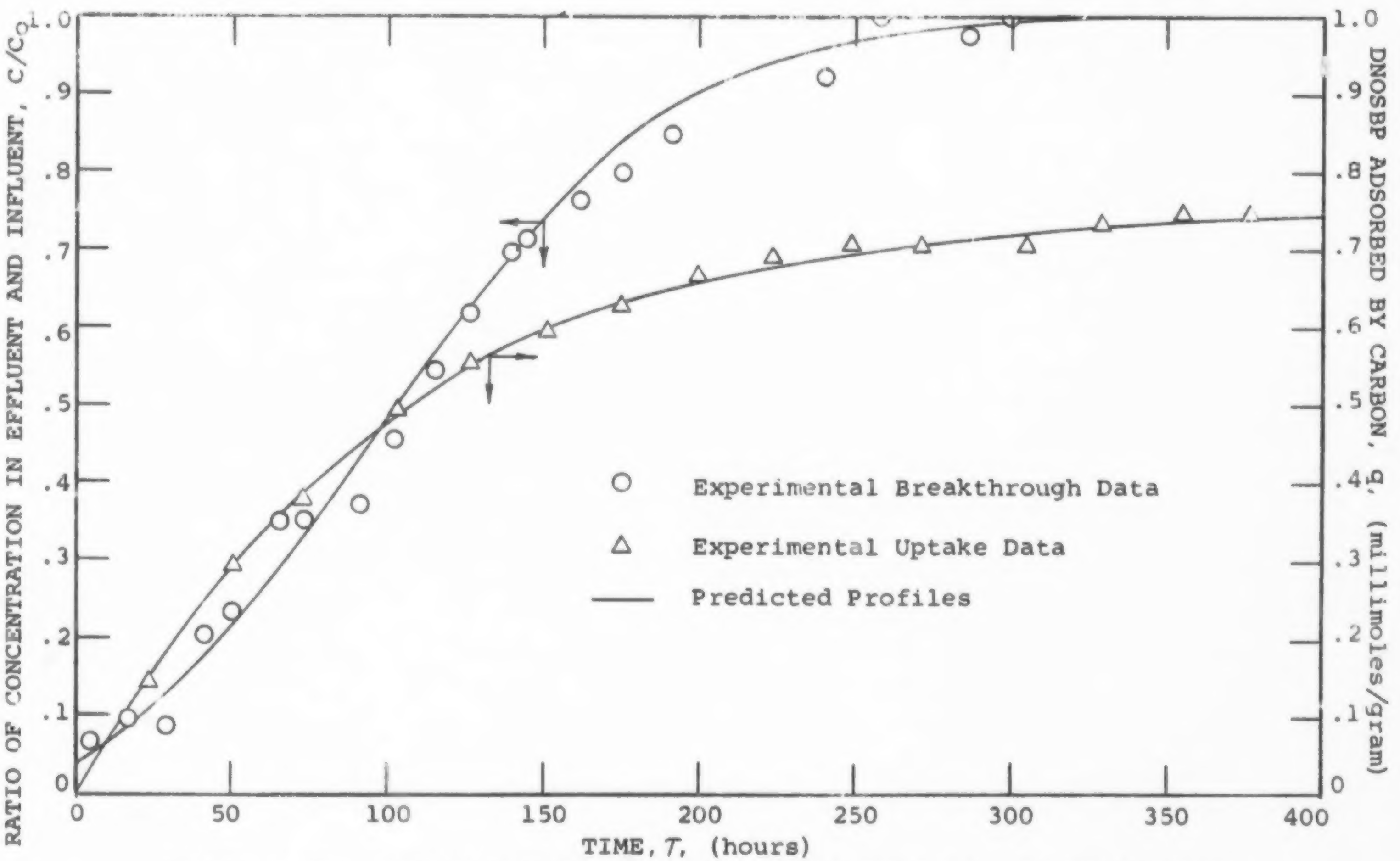

FIGURE 6-19. CONCENTRATION- AND UPTAKE-TIME PROFILES FOR AN INFLUENT CONCENTRATION OF 35.1 μMOLES/LITER (250-GRAMS OF 0.711-MM CARBON; 10 GPM/SQ.FT.)

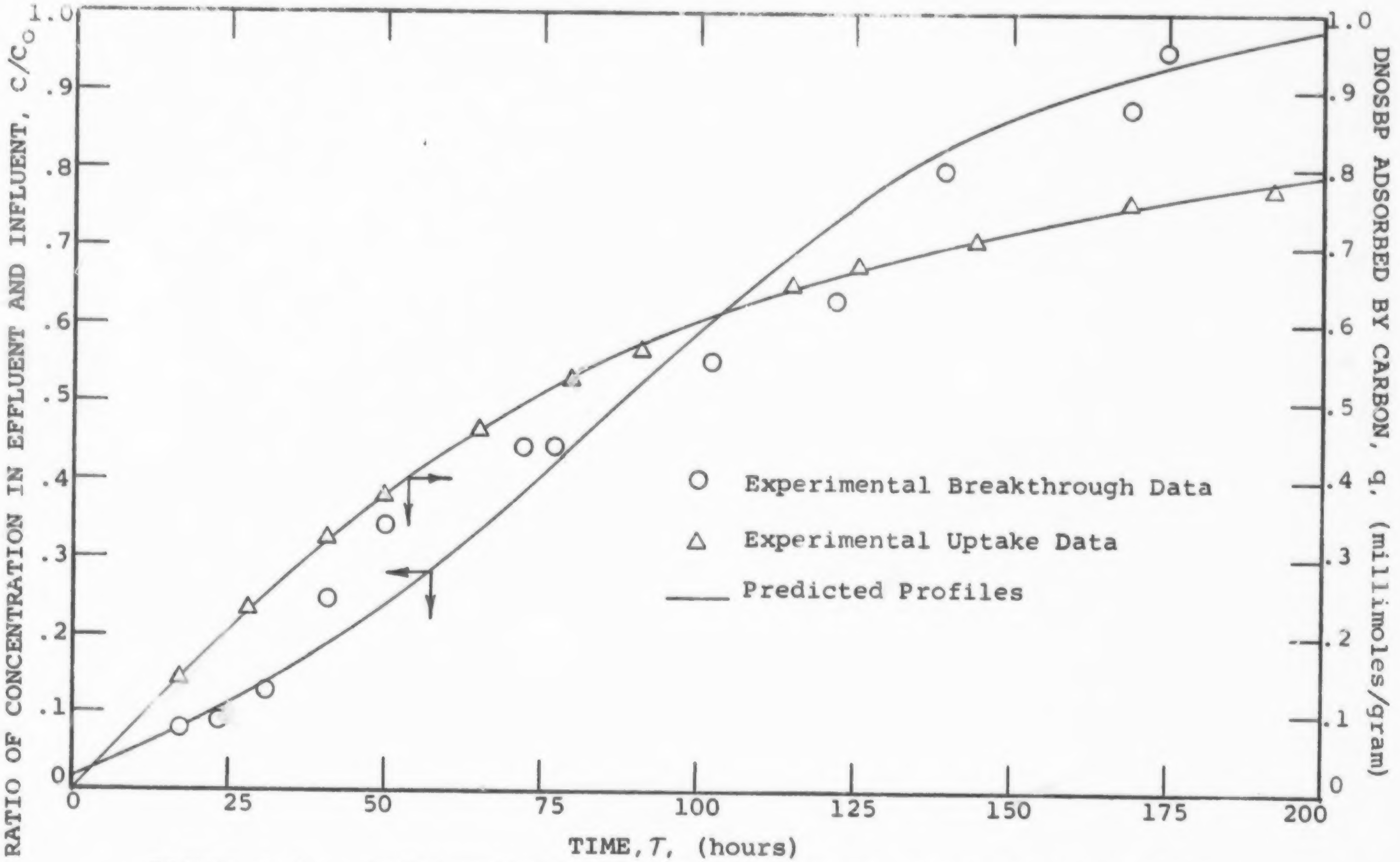

FIGURE 6-20. CONCENTRATION- AND UPTAKE-TIME PROFILES FOR AN INFLUENT CONCENTRATION OF 46.3 μMOLES/LITER (250-GRAMS OF 0.711-MM CARBON; 10 GPM/SQ.FT.)

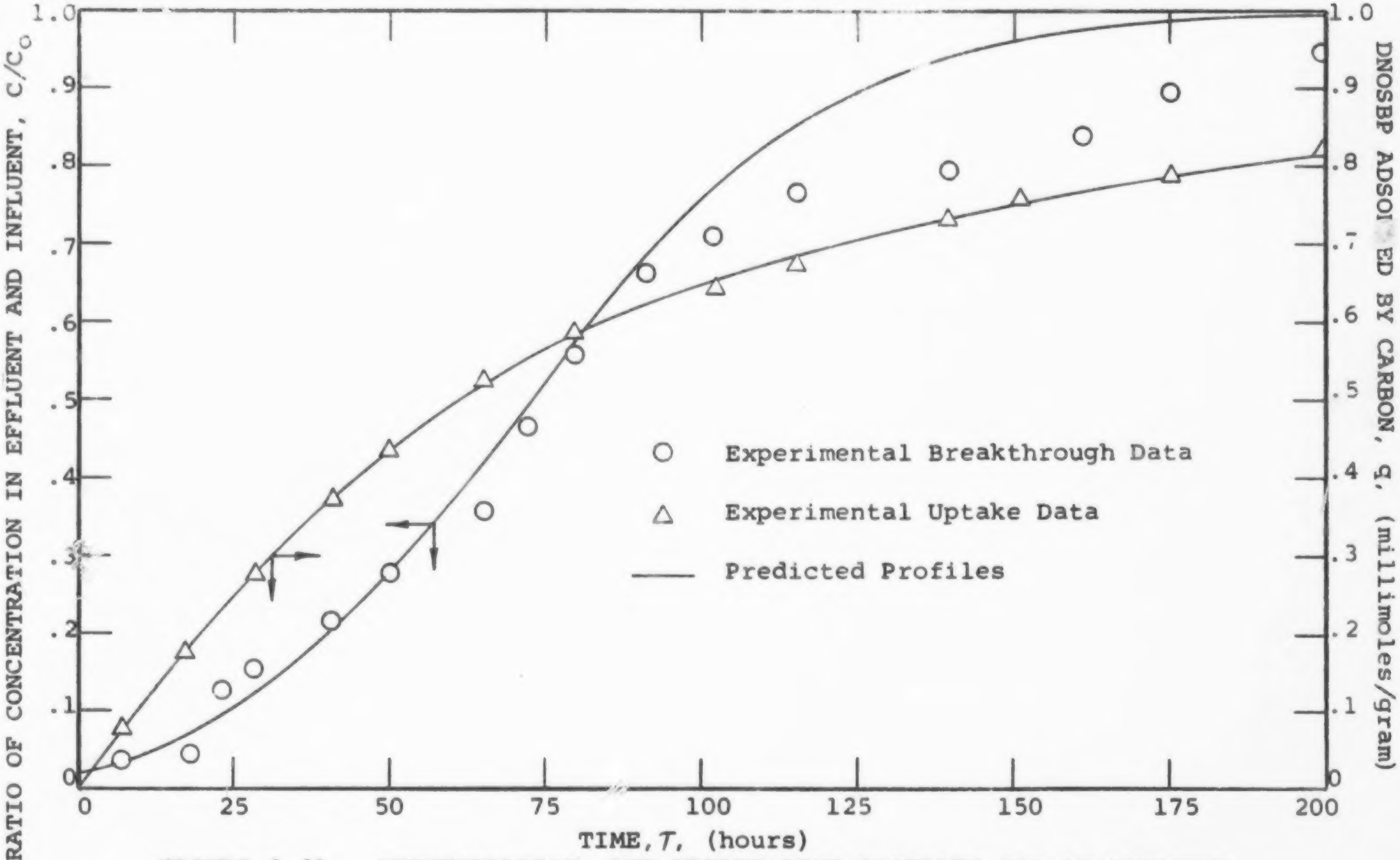

FIGURE 6-21. CONCENTRATION- AND UPTAKE-TIME PROFILES FOR AN INFLUENT CONCENTRATION OF 56.8 μMOLES/LITER (250-GRAMS OF 0.711-MM CARBON; 10 GPM/SQ.FT.)

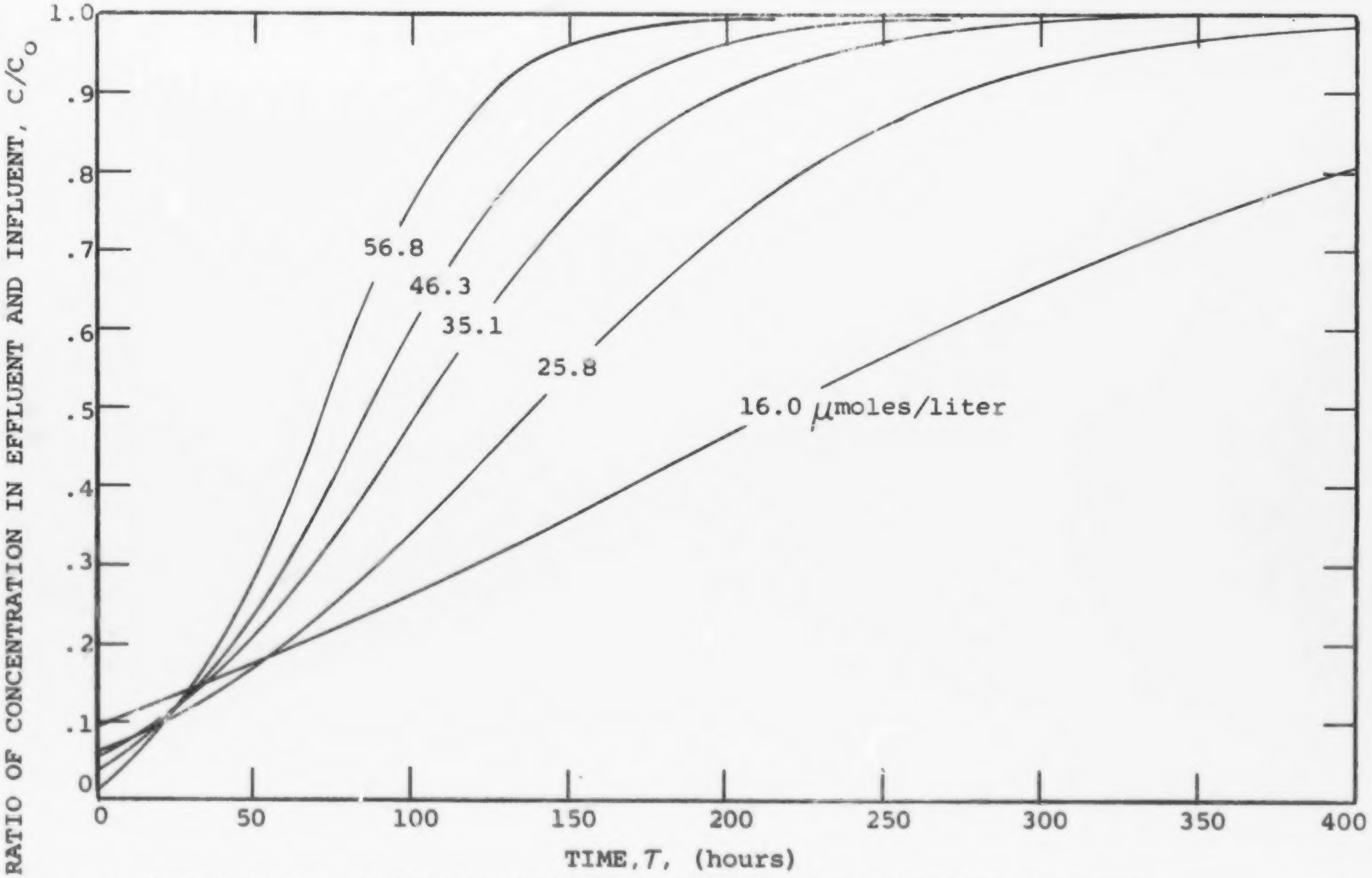

FIGURE 6-22. CONCENTRATION-TIME PROFILES FOR DIFFERENT INFLUENT CONCENTRATIONS (250-GRAMS OF 0.711-MM CARBON; 10 GPM/SQ. FT. FLOW RATE)

(tabulated in Table 5-2) are very nearly equivalent. The rate of transfer of solute through the film surrounding the external surfaces of the carbon is therefore directly proportional to the solute concentration. Thus, rates of uptake are higher for greater influent concentrations, causing the adsorbent to approach equilibrium more rapidly; in turn, an earlier and more rapid breakthrough pattern is expected.

Reversibility

In order to determine the degree of reversibility for the present systems an experimental column was devised in which tap water was passed through a fluid-bed of carbon saturated with DNOSBP. The 0.711-mm active carbon was obtained from System 5 after it was terminated. It had adsorbed 740.67 micromoles/gram in that experiment in which flow rate, maintained at 8 GPM/SQ.FT., was studied as a variable. For the present system the rate of flow was also set at 8 gal/min/sq.ft. Figure 6-23 is a plot of the desorption profile for this experimental column. It is apparent that approximately 145 micromoles/gram (19%) had been desorbed at a time of 1000 hours, at which point the concentration in the effluent became less than minimum detectable levels. It appears, however, that, although the concentration of DNOSBP was no longer detect-

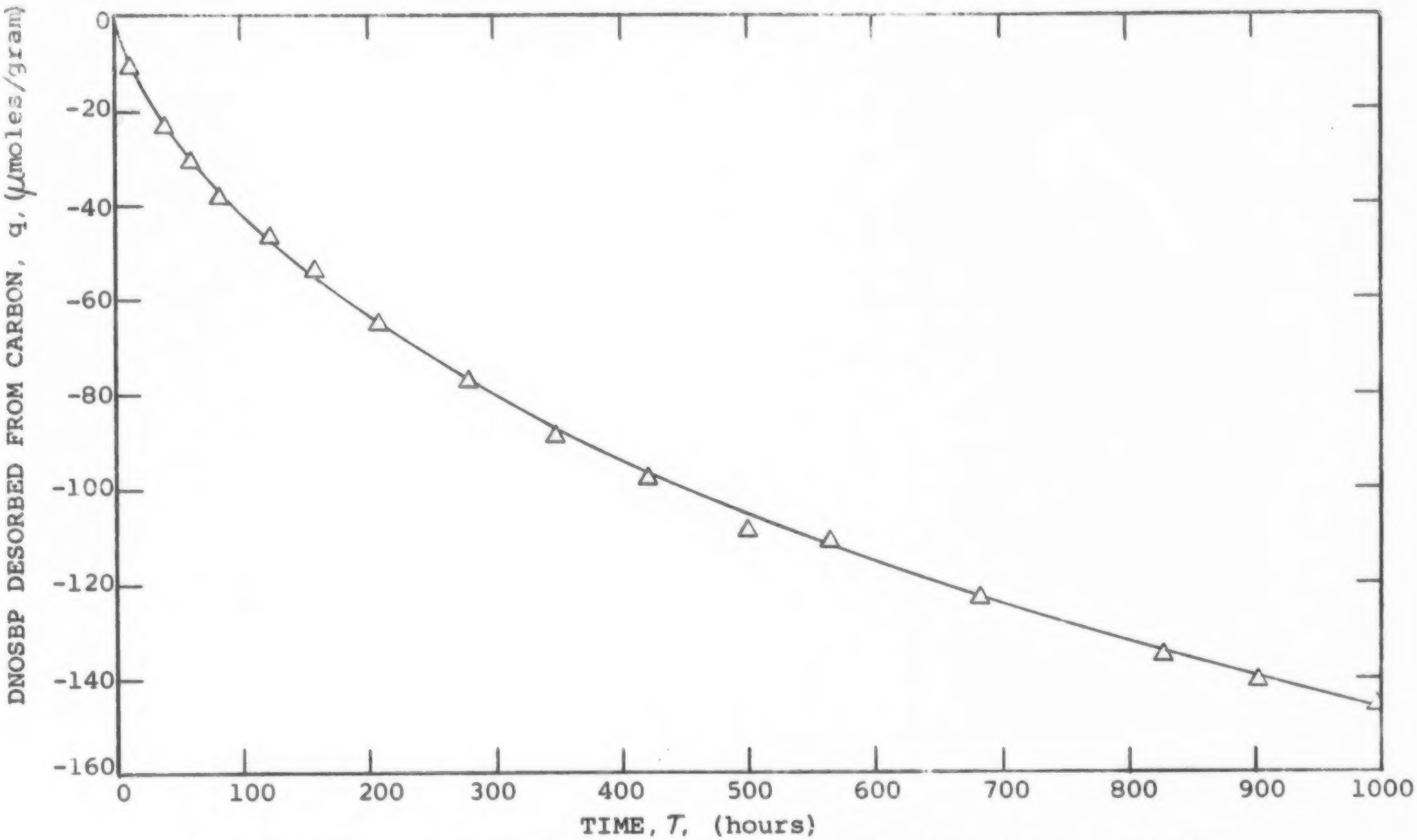

FIGURE 6-23. DESORPTION-TIME PROFILE FOR 250-GRAMS OF 0.711-MM CARBON SATURATED WITH 185.2 MILLIMOLES DNOSBP (8 GPM/SQ.FT. FLOW RATE)

able, trace quantities of the solute were leaching into the effluent, since the desorption profile had not achieved an equilibrium position. The degree of reversibility may, therefore, be somewhat greater than 19 percent, as determined in this study. Unfortunately, the full extent of reversibility can not be determined with the present experimental system. For practical purposes, though, one may conclude that the carbon-solute system is only partially reversible and that the adsorbed solute cannot be fully eluted.

CHAPTER 7

SUMMARY AND PROJECTIONS

Direct and deliberate reuse of surface waters has resulted in the buildup of organic materials that are not readily degraded biologically in conventional waste treatment facilities, or, subsequently in receiving waters. Successive reuse of water will ultimately lead to the concentration of these refractory organics to such an extent that they become aesthetically distasteful or, in the limit, injurious to public health. Further, since various species of aquatic biota have been noted to accumulate pesticides to extreme levels, it has become imperative that the concentrations of such materials in surface waters must not exceed levels which ensure protection of the consumer from the risk of encountering toxic doses.

Because these refractory contaminants are surface active in some degree, the use of adsorptive processes employing materials such as activated carbon appears especially promising as a solution to the problem. Previous investigators have demonstrated the feasibility of separating such persistent solutes from aqueous solution by means of granular active carbon. The adsorption technique has generally been related to columns of either fluidized or packed beds of the sorbent material. Studies which have focused on the development of adsorption technology for wastewater-treatment applications, however, have clearly demonstrated the marked advantages for a fluid bed mode of operation. Successful design of fluidized solids separation processes requires prediction of the concentration-time profile for the effluent. The objective of the current investigation, therefore, has been to provide a mathematical model for predicting effluent concentration-time profiles for continuous-flow fluidized systems from measurement of selected adsorption parameters in critically designed, but much more readily accomplished, non-flow system experiments.

The predictive mathematical model presented in this analysis is patterned after Hiester and Vermeulen's adaptation of Thomas' reaction-kinetics solution for packed beds. Unlike other models describing the mass transfer processes in continuous-flow columnar systems, Thomas' second-order kinetics approach allows the use of a generalized isotherm of the Langmuir type, which may be utilized for accurate description of any favorable type of isotherm. Thomas' solution is based on a reaction scheme in which the sorbate in some manner combines with the sorbent to form a sorbate-sorbent association. This kinetic model then is incorporated in the material-balance relationship and a solution for the breakthrough profiles is obtained in terms of three dimensionless parameters which are a function of the kinetic and equilibrium variables for the system.

The overall rate of adsorption of solute from an aqueous stream flowing through a fluidized bed of porous, activated carbon represents the combined effects of: diffusion through the stagnant layer of fluid surrounding the particle (film diffusion); diffusion within the voids of the particle (fluid-phase pore diffusion); pore-surface diffusion; and adsorption on the internal pore surfaces. For the purpose of this analysis, adsorption at the surface of the adsorbent was assumed extremely rapid and, therefore, the resistance due to this rate step was neglected. Further, an analysis of the relative magnitude of the fluid-phase and solid-phase pore diffusion controlled mass transfer coefficients indicated that the latter is somewhat more rapid than the former. Because they occur in parallel, solid-phase pore diffusion is, therefore, the controlling internal resistance. Previous investigations have indicated that film diffusion is the primary rate-limiting mechanism in fluid-bed systems of this type. Both resistances (solid-phase pore diffusion and film diffusion), since they occur in series, were then combined into one effective step with a single rate parameter. Moreover, it was demonstrated that the diffusion equations for mass transfer are closely related to Thomas' kinetic equations, and that numerical results suitable for design calculations can be obtained by way of this close relationship.

No practicable method for determination of film diffusion coefficients in rapidly-agitated non-flow systems is available. Fortunately, however, a correlational technique, first proposed by Chilton and Colburn, is applicable. A modification of this correlation, advanced by Resnick and White, adapts it for application to systems in which particulate matter less than 0.1 centimeters in diameter is used. This correlation, ln j_d vs. $\ln(N'_{Re}/N_{Ga})$, was shown to adequately describe the relationship between the mass transfer factor, j_d and the Reynolds-Galileo group for systems in which flow rate, particle size, or solute concentration were studied as control variables. One, therefore, need only calculate the factor, N'_{Re}/N_{Ga}, which may be determined from the physical and hydrodynamic characteristics of the system, to obtain a value for j_d and, subsequently, for the external mass-transfer coefficient.

Mass transfer factors for experimental columns in which depth of bed was studied as a variable, however, were not correlated by the j_d - N'_{Re}/N_{Ga} relationship. Instead, j_d decreased regularly with increasing depths of expanded bed for constant values of N'_{Re}/N_{Ga}. The effect is doubtlessly associated with the end effects at the influent section of the cylindrical column. An empirical equation relating the reciprocal of the bed depth to the mass transfer factor was found to adequately correlate the two parameters over the experimental range of interest. No definite projections to larger-scale columnar systems, based on this empirical relation, should be advanced, however, until the nature of the specific end effect has been more fully delineated.

Because previous investigators indicated that pore transport is the rate-limiting step for removal of organic solutes from dilute aqueous solution by porous active carbon in rapidly agitated non-flow systems, measurements of addorption in such systems provide a means for determination of pore diffusion coefficients and values for the corresponding transfer coefficients required for numerical solution of the concentration-time profile equations. Numerous kinetic experiments with batch systems were therefore carried out to define the effect of particle size and initial solute concentration, as control variables, on rates of uptake. Plots of the square of the quantity adsorbed as a function of time were used for normalization of the data; apparent adsorption rates were then obtained from the slopes of such plots. An empirical equation shows the rate of adsorption to be a function of $2.08\ C_o/d_p^{1.4}$ This correlated relation was then used in conjunction with the corresponding reaction-kinetic equations for determination of the appropriate pore diffusion controlled mass transfer coefficients.

Equilibrium as well as kinetic parameters are required for solution of the design equations. Accordingly, an experimental isotherm was determined for each of the particle sizes of granular carbon used in the columnar systems. Interestingly enough, no significant effect of particle size on equilibrium capacities for adsorption was discernable. This result contrasts rather markedly with an earlier study of Weber and Morris, who found that the ultimate uptake of adsorbate per unit weight of adsorbent varied as the reciprocal of the particle diameter squared. The observed differences, nevertheless, can be explained by considering the different methods employed in preparing the carbon for study. Also, the adsorbent used by Weber and Morris was a small-pore gas-phase carbon.

Several variables, including the density, porosity, and volume of the adsorbent bed in the expanded or fluidized state, relate to the hydrodynamic characteristics of the fluid-particle system. These must also be specified to enable numerical solution of the equations describing the concentration-time profiles. In order to determine the required parameters, it is necessary to be able to predict the degree of expansion for any fluidized system. This was accomplished through a consideration of the drag forces acting on each constituent particle in a multi-particle system. The semi-empirical relationship which was derived relates the ratio of the superficial fluid velocity and the terminal particle velocity to the porosity of the fluidized bed. The resultant equation, $\bar{V}/v_{po} = \epsilon^{3.90}$, was then utilized for prediction of bed expansions, given various physical parameters for the fluid-particle system. In addition, an expression was obtained for the minimum fluidization velocity through a pressure drop analysis for the entire bed. This relation was required so that one is able to predict flow velocities at incipient fluidization, such that flow through the adsorbent bed may be maintained high enough for full fluidization to ensure that particulate matter suspended in the fluid stream will not be entrained in the bed and subsequently cause high head losses.

Adequate testing of the mathematical model was accomplished by conducting eighteen fluid-bed experiments. Although the spread of the experimental data is considerable in several distances, rather good correspondence was found between the profiles predicted by use of the kinetic model and the general shape of the profiles defined by the experimental data for selected variables including flow rate, particle size, influent concentration of solute, and depth of the expanded bed. The agreement between the data and calculated curves aptly illustrates the adequacy of the proposed mathematical model for prediction of concentration-time profiles.

Because competitive interactions for multisolute systems may be characterized in batch-type experiments, application of the predictive model to multicomponent systems should be possible. Qualitatively, it would be necessary to specify for each component the four parameters relating to interphase transfer of solute, as well as the influent concentration. An adsorption isotherm for each component in the system may be described mathematically by the Langmuir equation for multiple-solute systems, which takes into account competitive interactions at equilibrium (59). Similarly, individual mass transfer coefficients for the pore diffusion step may be determined from competitive rate experiments in non-flow rapidly-agitated systems; these coefficients should reflect steric effects, sorbent-sorbate, and sorbate-sorbate interactions which may be operative within the porous structure of the granular adsorbent. Film-diffusion controlled mass transfer coefficients, which apparently account for the primary resistance to interphase transfer in fluidized beds of active carbon, may be determined by the j_d - (N'_{Re}/N_{Ga}) correlation, since film-diffusion controlled rates of mass transfer are not subject to competitive interactions. Only the Reynolds-Galileo group and the Schmidt group must be specified to determine appropriate film-diffusion mass transfer coefficients. Formulation of these mass transfer parameters for multicomponent systems, in the manner indicated, should allow one to sol numerically for the concentration-time profile for each solute in the system. Verification of the suggested procedure for projection of the predictive model to multiple-solute systems will be required. This, however, shall remain for the future.

If the proposed procedure for prediction of concentration-time profiles for multiple-solute systems is indeed confirmed, the engineer will have at his disposal a useful method for the design and operation of adsorption systems. Pilot plant-scale preliminary investigations will then no longer be necessary or required for determination of significant process parameters.

LIST OF REFERENCES

1. Acrivos, A., "On the Combined Effect of Longitudinal Diffusion and External Mass Transfer Resistance in Fixed Bed Operations", Chem. Eng. Sci. 13, 1 (1960).

2. Amundson, N. R., "Solid-Fluid Interactions in Fixed and Moving Beds-Fixed Beds with Large Particles", Ind. Eng. Chem. 48, 35 (1956).

3. Aris, R., and Amundson, N. R., "Some Remarks on Longitudinal Mixing or Diffusion in Fixed Beds", AIChE J., 3, 280 (1957).

4. Bird, R. B., Stewart, W. E., and Lightfoot, E. N., "Transport Phenomena", John Wiley and Sons, Inc., New York. (1960).

5. Butler, P. A., "Commercial Fishery Investigations", Effects of Pesticides on Fish and Wildlife, (1965), Circular 226, Fish and Wildlife Service.

6. Chu, J. C., Kalil, J., and Wetteroth, W. A., "Mass Transfer in a Fluidized Bed", Chem. Eng. Progr. 49, 141 (1953).

7. Cibrowski, J., and Wlodarski, A., "Electrostatic Effects in Fluidized Beds", Chem. Eng. Sci. 17, 23 (1962).

8. Dedrick, R. L., and Beckman, R. B., "Kinetics of Adsorption by Activated Carbon from Dilute Aqueous Solution", Chem. Eng. Progr., Symp. Ser. 74, 63, 68 1967).

9. Edeskuty, F. J., and Amundson, N. R., "Mathematics of Adsorption. IV. Effect of Intraparticle Diffusion in Agitated Static Systems", J. Phys. Chem. 56, 148 (1952).

10. Ergun, S., "Fluid Flow Through Packed Columns", Chem. Engr. Progr. 48, 89 (1952).

11. Frantz, J. F., "Design for Fluidization", Chem. Eng. Sept. 17, 1962, 161 (1962).

LIST OF REFERENCES (continued)

12. Frantz, J. F., "Minimum Fluidization Velocities and Pressure Drop in Fluidized Beds", Chem. Eng. Progr., Symp. Ser. 62, 62, 21 (1966).

13. Frear, D. E. H., "Pesticide Handbook", College Science Publishers, State College, Pa., (1962).

14. Frear, D. E. H., "Pesticide Index", College Science Publishers, State College, Pa., (1963).

15. Furnas, C. C., "Heat Transfter From a Gas Stream to a Bed of Broken Solids", U. S. Bureau of Mines Bulletin, 361, (1932).

16. Gleuckauf, E., and Coates, J. I., "Theory of Chromatography", J. Chem. Soc., 1315 (1947).

17. Goldstein, S., "The Mathematics of Exchange Processes in Fixed Columns", Proc. Roy. Soc. (London), A219, 151 (1953).

18. Green, R. S., and Love, S. K., "Pesticides in Water-Network to Monitor Hydrologic Environment. Covers Major Drainage Rivers", Pesticides Monitoring Journal 1, 13 (1967).

19. Griffin, R. P., and Dranoff, J. S., "The Rate of Glycerol Absorption by Ion Exchange Resins", AIChE J. 9, 283 (1963).

20. Hall, K. R., Eagleton, L. C., Acrivos, A., and Vermeulen, T., "Pore-and Solid-Diffusion Kinetics in Fixed-Bed Adsorption Under Constant-Pattern Conditions", Ind. Eng. Chem., Fundamentals, 5, 212 (1966).

21. Hanratty, T. J., and Bandukwala, A., "Fluidization and Sedimentation of Spherical Particles", AIChE J. 3, 293 (1957).

22. Hiester, N. K., Radding, S. B., Nelson, R. L., Jr., and Vermeulen, T., "Interpretation and Correlation of Ion Exchange Column Performance Under Nonlinear Equilibria", AIChE J. 2, 405 (1956).

LIST OF REFERENCES (continued)

23. Hiester, N. K., and Vermeulen, T., "Saturation Performance of Ion Exchange and Adsorption Columns", Chem. Eng. Prog. 48, 505 (1952).

24. Kaplan, W., "Advanced Calculus", Addison-Wesley Pub. Co., Inc., Reading, Mass. (1952) p. 86.

25. Kasten, P. R., and Amundson, N. R., "Analytical Solution for Simple Systems in Moving Bed Adsorbers: Effect of Intraparticle Diffusion", Ind. Eng. Chem. 44, 1704 (1952).

26. Kasten, P. R., Lapidus, L., and Amundson, N. R., "Mathematics of Adsorption in Beds. V. Effect of Intraparticle Diffusion in Flow Systems in Fixed Beds", J. Phys. Chem. 56, 683 (1952).

27. King, C. J., "Mass Transfer During Short Surface Exposures in Countercurrent Flow", Ind. Eng. Chem., Fundamentals 4, 125 (1965).

28. Klinkenberg, A., "Heat Transfer in Cross-Flow Heat Exchanges and Packed Beds - Evaulation of Equations for Penetration of Heat or Solutes", Ind. Eng. Chem. 46, 2285 (1954).

29. Kordecki, M. C., and Orr, C., Jr., "Adhesion of Solid Particles to Solid Surfaces", Arch. Environ. Health 1, 1 (1960).

30. Lapidus, L., and Amundson, N. R., "Mathematics of Adsorption in Beds. VI. The Effect of Longitudinal Diffusion in Ion Exchange and Chromatographic Columns", J. Phys. Chem. 56, 984 (1952).

31. Leva, M., "Fluidization", McGraw-Hill Book Co., New York. (1959).

32. Leva, M., "Some Considerations of Dense-Phase Fluidized Bed Correlations. Part I", Brit. Chem. Eng. 5, 703 (1960).

33. Leva, M., "Some Considerations of Dense-Phase Fluidized Bed Correlations. Part II", Brit. Chem. Eng. 5, 766, (1960).

LIST OF REFERENCES (continued)

34. Leva, M., Shirai, T., and Wen, C. Y., "The Prediction of Incipient Fluidization in Beds of Granular Solids", Genie Chimique 75, No. 2, 33 (1956).

35. Levich, V. G., "Physicochemical Hydrodynamics", Translated by Scripta Technica, Inc., Englewood Cliffs, N. J., Prentice-Hall, (1962).

36. Lewis, E. W., and Bowerman, E. W., "Fluidization of Solid Particles in Liquids", Chem. Eng. Progr. 48, 603 (1952).

37. Masamune, S., and Smith, J. M., "Adsorption Rate Studies - Significance of Pore Diffusion", AIChE J. 10, 246 (1964).

38. Masamune, S., and Smith, J. M., "Adsorption Rate Studies - Interaction of Diffusion and Surface Processes", AIChE J. 11, 34 (1965).

39. Meissner, H. P., and Mickley, H. S., "Removal of Mists and Dusts from Air by Beds of Fluidized Solids", Ind. Eng. Chem. 41, 1238 (1940).

40. Michaels, A. S., "Simplified Method of Interpreting Kinetic Data in Fixed-Bed Ion Exchange", Ind. Eng. Chem. 44, 1922 (1952).

41. Orr, C., Jr., "Particulate Technology", The MacMillan Co., New York. (1966).

42. Parker, H. W., and Stevens, W. F., "Effect of Liquid of Interparticle Forces in Gas-Fluidized Beds", AIChE J. 5, 314 (1959).

43. Resnick, W., and White, R. R., "Mass Transfer in Systems of Gas and Fluidized Solids", Chem. Eng. Progr. 45, 377 (1949).

44. Richardson, J. F., and Zaki, W. N., "Sedimentation and Fluidization: Part I", Trans. Inst. Chem. Engrs. 32, 35 (1954).

LIST OF REFERENCES (continued)

45. Rosen, J. B., "Kinetics of a Fixed-Bed System for Solid Diffusion into Spherical Particles", J. Chem. Phys. 20, 387 (1952).

46. Rosen, J. B., "General Numerical Solution for Solid Diffusion into Fixed Beds", Ind. Eng. Chem. 46, 1590 (1954).

47. Schlichting, H. "Boundary Layer Theory", McGraw-Hill Book Co., New York. (1960).

48 Schwartz, H. G., Jr., "Microbial Degradation of Pesticides in Aqueous Solution", J. Water Poll. Control Fed. 39, 1701 (1967).

49. Snoeyink, V. L., and Weber, W. J., Jr., "The Surface Chemistry of Active Carbon - A discussion of Structure and Surface Functional Groups", Environ. Sci. Tech. 1, 228 (1967).

50. Soo, S. L., "Fluid Dynamics of Multiphase Systems", Blaisdell Pub. Co., Waltham, Mass. (1967).

51. Summary Report - The Advanced Waste Research Program, v. 1, HEW, Public Health Service (May, 1962).

52. Thomas, H. C., "Heterogeneous Ion Exchange in a Flowing System", J. Amer. Chem. Soc. 66, 1664 (1944).

53. Thomas, H. C., "Chromatography: A Problem in Kinetics", Ann. N. Y. Acad. Sci. 49, 161 (1948).

54. Thomas, H. C., "Solid Diffusion on Chromatography", J. Chem. Phys. 19, 1213 (1951).

55. Tien, C., "A Simplified Method for Determination of Solid Diffusion Coefficient with Non-Linear Adsorption Isotherm", Can. J. Chem. Engr. 38, 25 (1960).

56. Vassiliou, B., and Dranoff, J. S., "The Kinetics of Ion Exclusion", AIChE J. 8, 248 (1962).

LIST OF REFERENCES (continued)

57. Vermeulen, T., "Theory for Irreversible and Constant-Pattern Solid Diffusion", Ind. Eng. Chem. 45, 1664 (1953).

58. Vermeulen, T., "Seperation by Adsorption Methods", Adv. Chem. Eng. 2, 147 (1958). Academic Press, New York.

59. Weber, W. J., Jr., "Competitive Interactions in Adsorption from Dilute Aqueous Bi-Solute Solutions", J. Appl. Chem. 14, 565 (1964).

60. Weber, W. J., Jr., "Fluid-Carbon Columns for Sorption of Persistent Organic Pollutants", Paper I-12, Proc. Intern. Conf. Water Poll. Res., 3rd, Munich, Germany (1966).

61. Weber, W. J., Jr., and DiGiano, F. A., "Reclamation of Water for Reuse as a Water Resource", Paper presented at the International Conference on Water for Peace, May 23-31, 1967, Washington, D. C.

62. Weber, W. J., Jr., and Gould, J. P., "Sorption of Organic Pesticides from Aqueous Solution", Adv. Chem. Ser. 60, 280 (1966), Amer. Chem. Soc. Publications, Washington, D. C.

63. Weber, W. J., Jr., and Keinath, T. M., "Mass Transfer of Perdurable Pollutants from Dilute Aqueous Solution in Fluidized Adsorbers", Chem. Eng. Progr., Symp. Ser. 74, 63, 79 (1967).

64. Weber, W. J., Jr., and Morris, J. C., "Kinetics of Adsorption on Carbon from Solution", ASCE, SED, SA2, 31 (1963).

65. Weber, W. J., Jr., and Morris, J. C., "Equilibria and Capacities for Adsorption on Carbon", ASCE, SED, SA3, 79 (1964).

66. Weber, W. J., Jr., and Morris, J. C., "Kinetics of Adsorption in Columns of Fluidized Media", J. Water Poll. Control Fed. 37, 425 (1965).

LIST OF REFERENCES (continued)

67. Weber, W. J., Jr., and Rumer, R. R., "Intraparticle Transport of Sulfonated Alkylbenzenes in a Porous Solid: Diffusion with Nonlinear Adsorption", Water Resources Research 1, 361 (1965).

68. Wen, C. Y. and Yu, Y. H., "Mechanics of Fluidization", Chem. Eng. Progr., Symp. Ser. 62, 62, 100 (1966).

69. Westlake, W. E. and Gunther, F. A., "Occurrence and Mode of Introduction of Pesticides in the Environment", Adv. Chem. Ser. 60, 110 (1966), Amer. Chem. Soc. Publications, Washington, D. C.

70. Wilke, C. R. and Chang, P., "Correlation of Diffusion Coefficients in Dilute Solutions", AIChE J. 1, 264 (1965).

71. Zenz, F. A., and Othmer, D. F., "Fluidization and Fluid-Particle Systems", Reinhold Publishing Corp., New York. (1960).